2014

Voltage Sensing Mechanism in the Voltage-gated and Proton (H+)-selective Ion Channel Hv1

Aaron L. Randolph
Virginia Commonwealth University

Voltage Sensing Mechanism in the Voltage-gated and Proton (H^+)-selective Ion Channel Hv1

By

Aaron L. Randolph

B.A./B.S Hampden-Sydney College 1997

Dissertation

Submitted to the Faculty of

Graduate School of Virginia Commonwealth University

in partial fulfillment of the requirements for the degree

DOCTOR OF PHILOSOPHY

in

Integrative Life Sciences

January, 2014

Richmond, Virginia

Approved: Date:

_____

_____

_____

_____

_____

_____

Voltage Sensing Mechanism of Hv1: The Proton (H^+) Selective Ion Channel

Aaron L. Randolph

Dissertation under the direction of Dr. I. Scott Ramsey

Activation of the intrinsic aqueous water-wire proton conductance (G_{AQ}) in Hv1 channels is controlled by changes in membrane potential and the transmembrane pH gradient (ΔpH). The mechanism by which changes in ΔpH affect the apparent voltage dependence of G_{AQ} activation is not understood. In order to measure voltage sensor (VS) activation in Hv1, we mutated a conserved Arg residue in the fourth helical segment (S4) to His and measured H^+ currents under whole-cell voltage clamp in transfected HEK-293 cells. Consistent with previous studies in VS domain containing proteins, we find that Hv1 R205H mediates a robust resting-state H^+ 'shuttle' conductance (G_{SH}) at negative membrane potentials. Voltage-dependent G_{SH} gating is measured at more negative voltages than the activation G_{AQ}, indicating that VS activation is thermodynamically distinct from opening of the intrinsic H^+ permeation pathway. A hallmark biophysical feature of Hv1 channels is a ~-40 mV/pH unit shift in the apparent voltage dependence of G_{AQ} gating. We show here that changes pH_O are sufficient to cause similar shifts in G_{SH} gating, indicating that G_{AQ} inherits its pH dependence from an early step in the Hv1 activation pathway. Furthermore, we show for the first time that Hv1 channels manifest a form of electromechanical coupling VS activation and G_{AQ} pore opening. Second-site mutations of D185 markedly alter G_{AQ} gating without affecting G_{SH} gating, indicating that D185 is required for a late step in the activation pathway that controls opening of the aqueous H^+ permeation pathway. In summary, this work demonstrates that the Hv1 activation pathway contains multiple transitions with distinct voltage and pH dependencies that have not been previously identified. The results reported here novel insight into the mechanism of VS activation in Hv1 and raise fundamental questions about the nature of pH-dependent gating and electromechanical coupling in related VS domain-containing ion channels and phosphatases.

ACKNOWLEGDGMENTS

I would like to extend a special thanks to my advisor, Dr. I. Scott Ramsey for his support, abundance of ideas and mentoring over the course of this project. I would like to thank the members of my committee for helpful suggestions over the course of my PhD training, but also for asking questions that made me think. I would like to thank Carlos Villalba-Galea for his helpful suggestions during my PhD training. I would also like to thank the Department of Physiology and Biophysics for the opportunity to pursue thesis research in an environment that encouraged intellectual and professional growth. The Integrative Life Sciences PhD program provided the flexibility I needed to find a path; I would like to thank Dr. Rob Tombes and Dr. Bill Eggleston for their assistance and suggestions over the course of my PhD training.

This dissertation is dedicated to my daughters Tallulah Douglass Randolph and Drake Francis Randolph, I love you both with all my heart.

LIST OF TABLES

Table **Page**

LIST OF FIGURES

LIST OF ABBREVIATIONS

VGC – Voltage gated ion channel

I-V – Current (I) plotted as a function of voltage (V) steps.

VS – Voltage sensor or Voltage sensing

S4 – The fourth transmembrane helix of the voltage sensing domain (S1-S4)

R1 –The first arginine residue of S4

V_m – The membrane potential or voltage

ΔpH – The pH gradient; pH outside the membrane minus pH inside the membrane (pH_O-pH_I = ΔpH).

EC coupling – Electromechanical coupling

P_{OPEN} – The probability of a channel pore opening 'open probability'.

6-TM channel – Six transmembrane domain ion channel

E_{H^+} – Reversal potential for H^+

G_{SH} – 'shuttle' pathway conductance

G_{AQ} – 'aqueous' pathway conductance

EQUATIONS

BOLTZMANN FITS:

$$I_{TAIL} = \frac{(I_{TAIL\,\max}) - (I_{TAIL\,\min})}{1 + e^{V - V_{0.5}/dx}} + I_{TAIL\,\min} \quad (1)$$

Boltzmann fit to I_{TAIL}-V relations, where $V_{0.5}$ is the voltage at which 50% of the maximum response [$I_{TAILmax}$] is reached and *dx* is a slope factor, and the minimum value is [$I_{TAILmin}$].

$$G_{STEP} = \frac{(G_{STEPmax}) - (G_{STEPmin})}{1 + e^{V - V_{0.5}/dx}} + G_{STEP\,min} \quad (2)$$

Boltzmann fit to G_{STEP}-V relations where $V_{0.5}$ is the voltage at which 50% of the maximum response [$G_{STEPmax}$] is reached and *dx* is a slope factor, and the minimum value is [$G_{STEPmin}$].

$$G_{STEP} = \frac{f\,(G_{STEPmax} - G_{STEPmin})}{1 + e^{V - V_{0.5}(1)/dx(1)}} + \frac{(1 - f\,)(G_{STEPmax} - G_{STEPmin})}{1 + e^{V - V_{0.5}(2)/dx(2)}} + G_{STEP\,min} \quad (3)$$

Double Boltzmann fit to G_{STEP}-V relations to fit 'early'$^{(1)}$ and 'late' $^{(2)}$ transitions in the 'shuttle' conductance only (G_{SH}). For the 'early' transition, where f is the fractional contribution of 'early' transition to the G_{STEP}-V, $V_{0.5(1)}$ is the voltage at which 50% of the maximum response [($G_{STEPmax}$)] is reached, $dx^{(1)}$ is a slope factor, and the minimum value is [($G_{STEPmin}$)f]. For the 'late' transition, where (1-f) is the fractional contribution of the'late' transition to the G_{STEP}-V, $V_{0.5(2)}$ is the voltage at which 50% of the maximum response [($G_{STEPmax}$) (1-f)] is reached, $dx^{(2)}$ is a slope factor, and the minimum value is [$G_{STEPmin}$].

EQUATIONS

BOLTZMANN FITS:

$$dG_{STEP}/dV = \frac{(dG_{STEP}/dV)_{MAX}}{1+e^{V-V_{0.5-PEAK}/dx}} \quad (4)$$

Boltzmann fit to $d\mathrm{G}_{\mathrm{STEP}}/d\mathrm{V}$-V relations where $V_{0.5\text{-}PEAK}$ is the voltage at which 50% of the maximum response $[(d\mathrm{G}_{\mathrm{STEP}}/d\mathrm{V})_{\mathrm{MAX}}]$ is reached and dx is a slope factor, and the minimum value of $d\mathrm{G}_{\mathrm{STEP}}/d\mathrm{V}$ is zero.

GAUSSIAN FITS:

$$dG_{STEP}/dV = \frac{A}{w\sqrt{\pi/2}} e^{-2\frac{(V-V_{PEAK})^2}{w^2}} \quad (5)$$

Gaussian fit to $d\mathrm{G}_{\mathrm{STEP}}/d\mathrm{V}$-V relations where A is area, w is width, V is membrane potential and V_{PEAK} is the center.

TABLE OF CONTENTS

Voltage Sensing Mechanism of Hv1: The Proton (H+) Selective Ion Channel

By

Aaron L. Randolph

B.A./B.S Hampden-Sydney College 1997

Dissertation

Submitted to the Faculty of

Graduate School of Virginia Commonwealth University

in partial fulfillment of the requirements for the degree

DOCTOR OF PHILOSOPHY

in

Integrative Life Sciences

January, 2013

Richmond, Virginia

Approved

I. Scott Ramsey, PhD Thesis Advisor

Louis J. DeFelice, PhD Committee Chair

Diomedes E. Logothetis, PhD

Hamid I. Akbarali, PhD

A. Rory McQuiston, PhD

Summary

The aim of this dissertation is to describe the mechanism by which changes in membrane voltage lead to activation of the voltage-gated and proton (H^+)-selective ion channel Hv1. Hv1 gating is evidently unique in its sensitivity to changes in both the transmembrane proton concentration gradient (ΔpH) and membrane potential. Although the biophysical properties for Hv1 have been well characterized and some structural features of the protein have been obtained by experimental methods and homology modeling, the mechanism by which changes in ΔpH and membrane potential coordinately control Hv1 gating remains mysterious. Results presented here clearly demonstrate that in Hv1, voltage-sensing and opening of the H^+ conducting pathway occur in two kinetically separate steps. The work indicates that in resting state Hv1, the electric field is focused in a narrow area similar to that shown for voltage sensing domains of other canonical voltage-gated channels, and that the resting-state structure likely contains a hydrated crevice through the hydrophobic core of the protein. In addition, this work demonstrates for the first time that early voltage-dependent transitions have a distinct sensitivity to the transmembrane $[H^+]$ gradient.

Chapter I. Introduction

1. Discovery of voltage H^+ conductances

Voltage-gated proton currents were first measured in a study of Ca^{2+} activated K^+ currents and were considered to be a non-specific residual current[1]. In his earliest efforts to clarify the nature of this residual current, Roger Meech was struck by reports of Kostyuk, et al.[2] that described a non-selective current recorded in nerve cells dialyzed with K^+-free solution which exhibited marked changes in both the position of the conductance-voltage (G-V) curve and the time course of activation and deactivation kinetics upon changes in extracellular pH (pH_O). Meech, together with Roger Thomas, found a similar residual conductance in snail neurons and these researchers were the first to discover that the residual conductance is actually a voltage-dependent and H^+ selective conductance[3]. In their experiments, neurons isolated from *Helix aspersa* were injected with HCl, and pH_I was measured under voltage clamp[3]. The authors showed that recovery from intracellular acidification to pH 6.23 was faster when the membrane potential was clamped at more depolarized potentials, indicating that there is a voltage-dependent pathway for H^+ efflux in *Helix* neurons[3]. Meech and Thomas also showed that voltage-dependent H^+ currents were blocked by heavy metals: Cd^{2+}, Ln^{3+}, Co^{2+} and Zn^{2+} [3].

A study of voltage-gated H^+ conductances (G_{vH^+}) in immature oocytes of the urodele amphibian *Ambystoma* conducted by Barish and Baud (1984) showed that the reversal potential for proton current (I_{H^+}) shifted 54 mV per unit change in external pH, but was not affected by changes in external Cl^- or K^+ concentrations[4]. Because a similar H^+-selective conductance was previously found in snail neuron [3], an important conclusion from the Barish and Baud experiments was that H^+-selective conductance was not species or tissue specific and could possibly be explained by the existence of a voltage-gated H^+ channel orthologue. The steady-state G_{vH^+}-V relationship was sigmoidal over a voltage range with a half-maximal

conductance ($V_{0.5}$) at +15 mV and the time constants for I_{H^+} activation (τ_{act}) and deactivation (τ_{deact}) are bell-shaped with peaks near $V_{0.5}$ for the G_{vH^+}-V relation, consistent with the behavior of G_{vH^+} in other studies[4,5,6]. An important finding by Barish and Baud (1984) was that the G_{vH^+}-V relation was also shifted along the voltage axis following changes in extracellular (pH_O)[4]. The seminal studies of voltage-gated proton conductances in invertebrate neurons revealed most of hallmark biophysical properties of G_{vH^+},and subsequent studies have largely confirmed these findings in other cell types.

Pursuant of findings that G_{vH^+} was not unique to a specific species or tissue, Henderson et al., (1987) proposed a physiological role for H^+ channels in mammalian immune cells[7]. They hypothesized that large H^+ currents would be necessary to compensate the efflux of negative charge associated with outward electron transport that is mediated by the NADPH oxisase, and thereby support sustained superoxide production in human neutrophils, Thus G_{vH^+} was proposed to exist in mammalian physiology before it had actually been measured in any mammalian cell[7]. G_{vH^+} in mammalian cells was first reported by DeCoursey in 1991[8]. Whole cell voltage clamp of rat alveolar epithelial cells was performed with recording solutions composed of large organic ions such as N-methyl-D-glucamine (NMG^+) and methanesulfonate ($MeSO_3^-$), which are presumed to be impermeant to most ion channels, as substitutes for Na^+ and Cl^-, respectively[8]. Using pipettes filled with recording solution buffered to pH 5.5, DeCoursey and colleagues demonstrated that reversal potentials in alveolar epithelial cells changed as expected for a H^+-selective conductance when pH_O was altered[8]. The voltage dependence of channel activation was also reported to shift with changing pH_O, and is thus remarkably similar to G_{vH^+} in *Ambystoma*[4]. The results made a clear and important distinction: it is the transmembrane pH gradient, rather than the absolute value of extracellular pH, that modulates the steady-state position of the G_{vH^+}-V relationship[8]. DeCoursey and colleagues also confirmed that heavy metals such as Cd^{2+} also block G_{vH^+} in rat alveolar epithelial cells[8].

Soon after the discovery of H^+ currents in lung epithelia, G_{vH^+} was identified in immune cells and this has since been the most widely studied cell type for measuring the activity of H^+ channels[9]. Several types of leukocytes express voltage-gated H^+ current at remarkably high current density (measured in pA/pF) in mammalian granulocytes[10]: neutrophils[11], eosinophils[12] and basophils[10,14] each exhibit robust G_{vH^+}. The relative expression levels of G_{vH^+} are important in the context of the developing hypothesis that a large amplitude voltage- and pH-dependent H^+ conductance is required for superoxide production during respiratory burst. Later studies expanded the list of leukocytes, both innate and acquired, that express G_{vH^+} to include macrophages[15], microglia[16], T-cells[13] and B-cells[13]. Other cell types, including skeletal myocytubes[10,17], osteoclasts[18], and renal proximal tubule cells[10,19] were also reported to express G_{vH^+}. The observation that G_{vH^+} with similar biophysical properties is measurable in multiple different cell types from a variety of species suggested that a conserved gene encoding the voltage-gated H^+ channel protein could be identified, but the identity of such genes remained elusive until 2006.

Ramsey, et al. (2006) identified a human gene (HVCN1) using a bioinformatics approach based on the sequences of known voltage-gated cation channels[20]. The protein product of the HVCN1 gene, referred to here as Hv1, is 273 amino acids in length with a predicted mass of 31.7 kDa[20]. A portion of the Hv1 primary amino acid sequence is homologous to the voltage-sensitive phosphatase from *Ciona intestinalis* (Ci-VSP) and the voltage sensor (VS) domain of voltage-gated cation channels such as Kv1.2[20], suggesting that Hv1 might encode a voltage-sensitive protein[20] .A simultaneous report from the Okamura laboratory identified the mouse and *Ciona intestinalis* HVCN1 genes and named the product Voltage Sensor Only Protein (VSOP)[21]. In both reports, HVCN1 and VSOP sequences were conserved among vertebrate and invertebrate orthologues[20,21]. The surprising finding reported by both groups was that despite the fact that Hv1 lacks amino acid sequence encoding an ion channel pore-forming domain, heterologous expression in mammalian cells was found to be sufficient to reconstitute the biophysical properties of native G_{vH^+} [20,21]. Hv1 was quickly accepted as the long-sought *bona fide* voltage-gated ion

channel protein[20,21], and the new availability of cDNAs encoding Hv1 enabled a new wave of molecular investigation into the structural and function of voltage-gated proton channels.

2. Biophysical properties of G_{vH^+}

The identification of HVCN1 genes allowed for the direct characterization of Hv1 as a bona fide voltage gated ion channel. The hallmark characteristics of G_{vH^+} are similar for both native tissue and heterologous expression in cultured cells[8,20–23]. The biophysical properties of G_{vH^+} mediated by native and expressed Hv1 are summarized below.

1. Hv1 exhibits time- and voltage-dependent kinetics for activation and deactivation of the ionic current[8,20,21,24,25]. Voltage steps from negative potentials (where Hv1 channels are closed) to depolarized membrane potentials elicits a time-dependent activation of current (I_{STEP})[8,20,21,24,25]. After an initial delay during which no current is measured, ionic current begins to rise and eventually reaches an apparent steady-state level[8,20,21,24,25]. Activation time constants derived from single exponential fits to the time course of current activation indicate that the activation kinetics of heterologously expressed Hv1 measured in whole-cell mode are strongly voltage-dependent [8,20,21,24,25] (i.e., τ_{ACT} = 715 ± 124 ms at +80 mV[20]). As expected from studies of native G_{vH^+}, the voltage dependence of τ_{ACT} for expressed Hv1 channels is sensitive to changes in both pH and temperature[10,20,22,24]. τ_{ACT} is smaller at elevated temperatures and activation kinetics are slower under conditions of net extracellular acidification (i.e., $pH_O < pH_I$)[20,24,26]. The effects of changes in pH and temperature on voltage-dependent activation kinetics are characteristic of G_{vH^+} [10,20,22,24]. Deactivation kinetics are determined from single exponential fits to tail currents (I_{TAIL}) measured at a negative membrane potential (while channels are closing) immediately after a depolarizing step to a voltage that is sufficient to elicit channel activation[20,25,27]. Deactivation of Hv1 is typically much faster than activation[20,25,27] (i.e., τ_{DEACT} = 65 ± 12 ms at -80 mV[20]). Also, tail currents

decay more quickly at more negative potentials, indicating that the rate of deactivation is voltage-dependent[25].

2. The gating of G_{vH^+} in Hv1 is pH-dependent and this pH-sensitivity is characterized by a ~40 mV shift in the apparent threshold for voltage-dependent activation of tail current (V_{THR}) for each pH unit change in the transmembrane [H^+] gradient[20,21,23]. V_{THR} here is defined as the most negative potential where channels begin to open[10,28]. A more detailed description of pH-dependent gating will be presented in section 6.0.

3. Hv1 exhibits exquisite selectivity for permeation of H^+ over other monovalent cations[10,20,21,23]. The estimated permeability ratio for H^+ vs. Na^+ (P_H/P_{Na}) is >1 x 10^6 [26,29]. The reversal potential (V_{REV}) for instantaneous H^+ current, follows the Nernst equation prediction for a H^+-selective conductance: V_{REV} changes roughly 54.7 mV (at ~22°C) per pH unit change in the transmembrane [H^+] gradient[20].

4. The unitary conductance of Hv1 is extremely small. Estimates of the single channel conductance are in the range of 10-50 fS at pH_I 6.5[10,30,31]. Reports have suggested that unitary conductance in Hv1 increases two- to four-fold (90-250 fS at pH_I 5.5) when the driving force for H^+ is altered by changing pH_O[17,30].

5. Heavy metal ions potently affect Hv1 gating. The divalent metal ions Zn^{2+} and Cd^{2+} are used frequently to decrease H^+ current amplitude in studies of G_{vH^+}[3,4,8,10,12,15,18,20,28,32]. Hv1 gating is sensitive to micromolar concentrations of Zn^{2+}, and the half-maximal inhibitory concentration (IC_{50}) is estimated to be ~2 μM[20]. Hv1 gating is also sensitive to micromolar concentrations of other divalent metals with rank order of potency Cu^{2+} > Zn^{2+} > Ni^{2+} >Cd^{2+} >Co^{2+} >Mn^{2+} [10]. The consensus of many studies is that Zn^{2+} affects Hv1 by shifting the voltage dependence of channel activation to more positive potentials; Zn^{2+} also slows the opening rate and speeds deactivation[4,10,12,32–34]. Simultaneous mutation of two extracellularly-

accessible residues (H140 and H193) in human Hv1 abolishes the effect of micromolar Zn^{2+}, suggesting that these two residues may directly coordinate Zn^{2+} binding[20].

6. Hv1 exhibits channel-like gating and H^+ permeation. Although the unitary conductance of Hv1 is small at physiological pH, it does not behave like an exchanger or pump[27,35]. A variety of membrane proteins, including bacteriorhodopsin[36], H^+-ATPases[37], F_0F_1-ATPases[37] and M2 viral channels[38,39] contain proton transfer pathways. Hv1 is not gated by a ligand (i.e., photoisomerized retinal or ATP) and its time-dependent current activation produces a robust efflux of H^+ current flowing down its electrochemical gradient that is both voltage- and pH-dependent.

7. Subtle but distinct differences in the biophysical properties of native vs. heterologously expressed Hv1 are reported[23]. Hv1 channels expressed in either HEK-293 or COS-7 cells differs from native proton channels in that V_{THR} is ~30mV more negative than native Hv1 channels at all ΔpH[23]. As a result, inward I_{STEP} can be elicited in heterologously expressed Hv1 because the channels begin to open at voltages that are negative to V_{REV}[23]. There is also a difference in the τ_{ACT}-V relationship measured in heterologous expression: wereas τ_{ACT}-V for Hv1 expressed in HEK-293 cells is bell-shaped, τ_{ACT}-V decreases monotonically with increasing depolarization for native channels[23]. Despite the relatively minor differences in V_{THR} and τ_{ACT}-V relations, the sensitivity of the G_{vH^+}-V relationship to changes in both pH_O and pH_I is similar in both native and heterologously expressed Hv1 channels[23].

8. The timecourse of Hv1 activation is sigmoidal, and thus similar to the activation kinetics seen for both Na^+ and K^+ currents activation in nerve membrane[6,40]. The rise in Hv1 current after depolarization is delayed when increasingly negative prepulses are applied[40], suggesting that Hv1 exhibits a Cole-Moore type activation delay similar to that which was originally described for K^+ channels in the squid axon[41]. A Cole-Moore activation delay suggests that the channel visits multiple closed states prior to opening[41]. An Hv1 gating model proposed by Cherny et al. (1995), hypothesizes at least two distinct transitions and three or more states in the pathway from Closed (C_1, C_2) to Open (O) channels (i.e., $C_1 \leftrightarrow C_2 \leftrightarrow O$)[24,40].

3. Physiological roles for Hv1

The identification of G_{vH^+} in innate immune cells was preceded by the hypothesis that G_{vH+} is required for superoxide ($O_2{\cdot}^-$) production in neutrophils[7,42,43]. In the years following Henderson's 'charge compensation' hypothesis for voltage-gated H^+ channels in neutrophils, the role of Hv1 to support sustained superoxide production by NADPH oxidase during the phagocyte respiratory burst has been carefully investigated[10,28,44–47]. The functional interdependence of Hv1 and NADPH oxidase is supported by the following findings: (1) The active NADPH oxidase enzyme complex translocates electrons across the phagosomal membrane from the cytosol into the organelle lumen and is therefore electrogenic[10,48]. (2) H^+ flux into the phagosome lumen occurs when the NADPH oxidase enzyme complex is active[7,43,46]. (3) H^+ current is thought to electrically compensate the large electron current generated by NADPH oxidase, providing a balance of charge to prevent a large depolarization that would otherwise inhibit NADPH oxidase activity[7,42,49]. (4) H^+ efflux is generated by a voltage-gated H^+ channel that is activated by the depolarizing NADPH oxidase electron current[43,48,49].

During the respiratory burst in phagocytic leukocytes, NADPH oxidase-mediated electron transport catalyzes redox reactions that reduce extracellular or intraphagosomal O_2 to $O_2{\cdot}^-$ [10,28,50,51]. The NADPH oxidase complex consists of $p22^{phox,}$ Rac, $p67^{phox,}$, $p40^{phox,}$, $p47^{phox,}$, and $gp91^{phox}$ proteins[50,51]. The product of the NOX2 allele, $gp91^{phox}$, is the predominant Nox isoform expressed in phagocytic leukocytes[50,51]. Two protein components in the NADPH complex ($gp91^{phox}$ and $p22^{phox}$) are integral membrane proteins and the other subunits are membrane-bound via their association with $gp91^{phox}$ or $p22^{phox}$ [10,28,50,51]. The NADPH oxidase complex catalyzes the following reaction to generate free electrons:

Reaction 1: $NADPH + 2\ O_2 \leftrightarrow NADP^+ + 2\ O_2{\cdot}^- + H^+$

The free electrons are translocated across the plasma or phagosomal membrane by the $gp91^{phox}/p22^{phox}$ heterodimer, creating an electron current (I_e) that results in depolarization of the phagocyte membrane potential by +100 mV or more in human neutrophils and eosinophils[10,52]. The calculated rates of depolarization caused by I_e in human eosinophils is 1.1 kV/min, which represents a rapid change in

membrane potential, and the predicted E_{REV} for electron is near +200mV[10,52]. The resulting positive shifts in membrane potential will effectively deactivate the NADPH oxidase complex[53]. Hence, there is a critical need for a compensating charge flow to repolarize the cell membrane potential and maintain continuous function of the activated NADPH oxidase[10,52]. Hv1 channels appear to mediate most of the charge compensation that is required for sustained high-level $O_2^{\cdot -}$ production during the respiratory burst[10,52].

Proton efflux across the phagocyte membrane has an additional function during the respiratory burst in phagocytes that is distinct from charge compensation *per se*. As shown in Reaction 1 above, one H^+ is liberated in the cytoplasm for each electron produced by the NADPH oxidase, causing pH_I to fall. H^+ efflux is needed to balance cytoplasmic pH to neutral levels, and proton efflux is thus required for optimal NADPH oxidase activity[40]. Experimental findings from many studies have provided both direct and indirect evidence for the role of Hv1 in supporting the respiratory burst[7,11,16,28,43–45,53–59]. A study measuring voltage gated proton efflux under conditions in which NADPH oxidase is actively transporting electrons concluded that H^+ flux is sufficient to compensate the large depolarizations caused by electron current, and demonstrated that Cd^{2+} or Zn^{2+} inhibit both H^+ current and $O_2^{\cdot -}$ production[53]**.** *In vitro* experiments using cells isolated from Hv1 knockout mice report ~75% lower $O_2^{\cdot -}$ production in bone marrow cells[45] and 50% less $O_2^{\cdot -}$ production in eosinophils[59]. These studies indicate an important role G_{vH^+} in production of ROS during respiratory burst and illustrate the need for a clearer understanding of how G_{vH^+} gating is modulated by voltage and pH.

Hv1 has also been studied for its role in the acquired immune system, due to its involvement in the production of reactive oxygen species (ROS) such as $O_2^{\cdot -}$ by lymphocytes. G_{vH^+} was discovered in both human B-cells and T-cells, but expression levels are markedly higher in B-cells[13]. ROS are produced in B-cells by the same NADPH complex as in granulocytes (Nox 2); however, the amount of ROS produced in B-cells is ~10% of that in phagocytic cells[60,61]. Antigen-activation of the B-cell receptor (BCR) initiates an signaling cascade that controls B-cell differentiation and proliferation[60,61]. BCR can

signal only when the enzymatic activity of the tyrosine phosphatase SHP-1 is inhibited[60,61]. SHP-1 inhibition is mediated by the oxidation of its catalytic site by ROS, and this is achieved by local ROS production in the vicinity of the BCR receptor[60,61]. Capasso et al., (2010) demonstrated that Hv1 co-localizes with BCR, and studies with Hv1-null cells concluded that Hv1 modulates the amount of ROS produced in B-cells subsequent to BCR activation; loss of Hv1 thus profoundly affects antigen-dependent B-cell activation and proliferation responses[60].

G_{vH^+} in primary cultures of rat alveolar lung type II cells is proposed to have a very different role in the lung than in phagocytic cells[8]. Airway epithelia express distinct DUOX isoforms[62,63] of NADPH oxidases, and in contrast to Nox2, DUOX proteins do not necessarily require a compensating H^+ channel activity for function because lung epithelia are able to independently regulate the intracellular pH and the membrane potentials[64]. In contrast to the large depolarization caused by I_e in during NADPH oxidase activity in phagocytes, the membrane potential in airways is relatively stable at ~-20mV[65] and does not increase substantially when DUOX proteins are active[64].

A study performed in the Fischer laboratory proposed that Hv1 helps to maintain an acidic pH on the lumenal surface of the lung; evidence in support of this hypothesis is reported in a study that discovered the first naturally-occurring human mutation in Hv1, M91T[65,66]. The study examined the contribution of G_{vH^+} to maintain stable pH of the airway surface liquid (ASL) [64]. Acid secretion from airway epithelia when the ASL is acidic ($pH_O \approx 6.0$), is thought to be mediated by an ATP-dependent transport process because H^+ secretion occurs against the $[H^+]$ gradient ($pH_O < pH_I$)[64]. When ASL is alkalinized, H^+ secretion flows down the $[H^+]$ gradient and is Zn^{2+}-sensitive, consistent with a potential role for H^+ channels to mediate proton efflux[64]. The M91T mutation alters the position of the G_{vH^+}-V relationship in Hv1, shifting activation +30mV, thus decreasing channel open probability (P_{OPEN}) at the typical resting membrane potential[64]. The authors observed that H^+ secretion required a larger extracellular alkalization in cells expressing Hv1 M91T, supporting the idea that Hv1 is responsible for H^+ secretion under when $pH_I < pH_O$ and that the M91T mutant impedes normal H^+ secretion[64,66].

Hv1 has been identified in human spermatozoa and is hypothesized to play an important role in sperm capacitation, a maturation process that sperm undergo within the female reproductive tract[49,67,68]. One hypothesis suggests that Hv1 is necessary for capacitation because the normally low pH_I in sperm that inhibits metabolic processes, tends to increase Hv1 P_{OPEN}, but high levels of Zn^{2+} in seminal fluid (~2.2 mM), prohibit Hv1 activation[49,67,69]. The removal or diffusion of Zn^{2+} in the female reproductive tract promotes Hv1 mediated H^+ efflux[49,67,69]. The mechanism by which Hv1 promotes sperm capacitation remains to be elucidated but the hypothesis suggests that H^+ efflux mediated by Hv1 activation would remove high intracellular $[H^+]$ concentrations and promote metabolic processes needed for sperm maturation[49,67,69].

Interestingly, Hv1 has been identified in two types of marine phytoplankton: coccolithophores (*Coccolithus pelagicus ssp. braarudii* and *Emiliania huxleyi*)[70,71], and dinoflagellates (*Karlodinium veneficu*)[72]. Hv1 is proposed to be involved in the conversion of HCO_3^- to $CaCO_3$, which is necessary to produce the calcified scales in coccolithophores[70,71]. Hv1 channels could therefore play a role in carbon sequestering and ocean acidification on a global scale[70,71].

In summary, the physiological necessity for Hv1 in the phagocyte respiratory burst and acid secretion in the lung are contingent upon membrane depolarization and/or intracellular acidification, each of which promotes increased G_{vH^+}. The involvement of Hv1 in important biological processes warrants a clearer understanding of G_{vH^+} gating mechanisms. The following sections will highlight structural and functional characteristics of Hv1 and contextualize our chosen experimental approach.

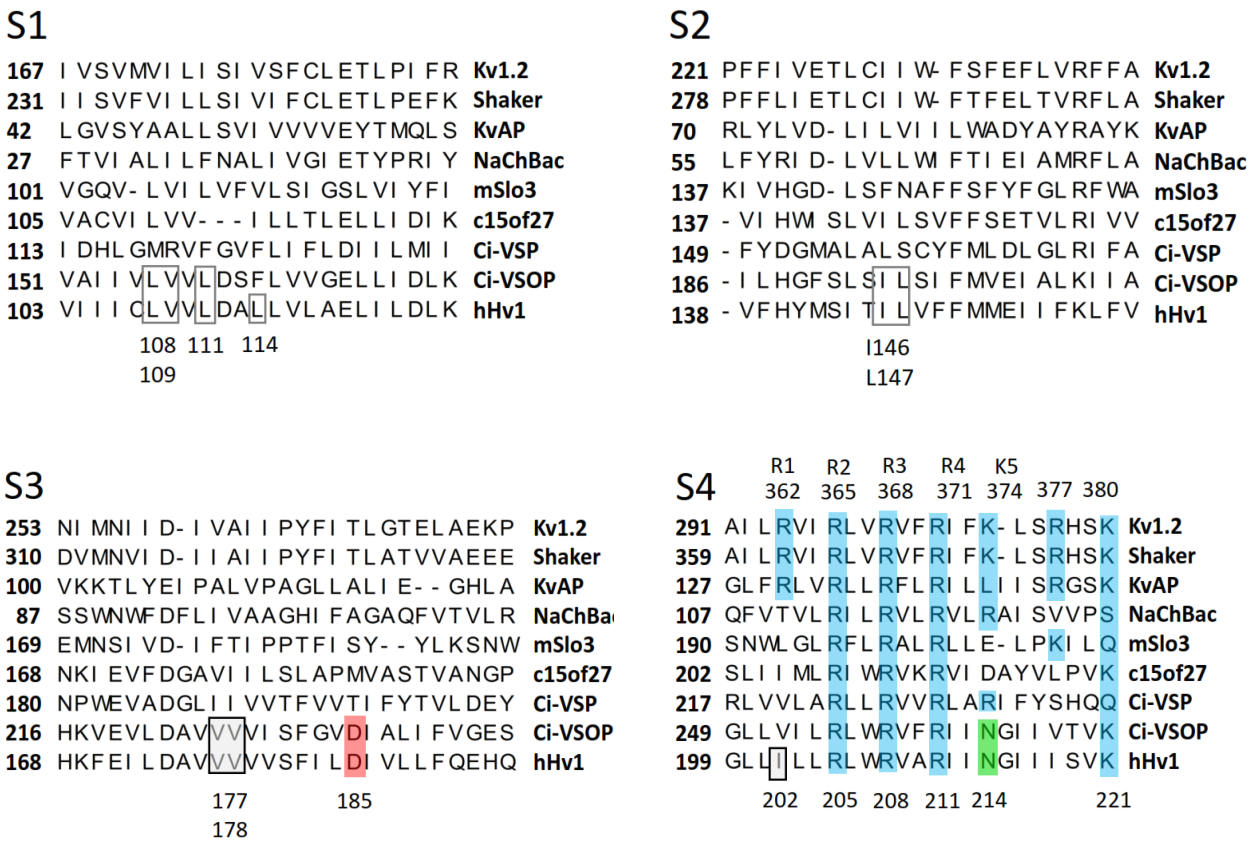

Figure 1. Amino acid sequence of Hv1 species orthologues and voltage sensor domains of ion channel proteins.

Alignment of amino acid sequence in VS domain S1-S4 segments from *H. sapiens* Kv1.2 (NP_004965), *D. melanogaster* Shaker (CAA29917), *A. pernix* KvAP (Q9YDF8), *B. halodurans* NaChBac (NP_242367), *M. musculus* mSlo3 (AAB99742), *H. sapiens* c15orf27 (NM_152335), *C. intestinalis* Ci-VSP (BAD98733), *C. intestinalis* Ci-VSOP/Hv1 (NP_001071937) and *H. sapiens* Hv1 (NP_115745). Colored boxes indicate locations of selected acidic (red), basic (blue), polar (green) and hydrophobic (white or gray) residues. Numbers above alignments (Shaker) and numbers below alignments (Hv1) refer to amino acid positions.

4. Structure of the voltage sensor (VS) domain

Hv1 was identified based on sequence homology to other voltage gated ion channels[20,21], and exhibits distinct amino acid sequence homology to the voltage sensor (VS) domains of these ion channels[20]. The superfamily of voltage-gated cation ion channels (VGCs) is composed of integral membrane proteins with a shared secondary (six putative transmembrane-spanning helical segments) and tertiary (two distinct protein domains) structure[73–77]. The first 4 helices (S1-S4) form the VS domain, while S5-S6 compose the pore domain[73–77]. VGCs function to permit gated and selective transmembrane movement of ions down their electrochemical gradients[78–81]. VGCs are classified into Na^+, K^+, and Ca^{2+} channels based on ionic selectivity, which is determined by the pore domain selectivity filter[35,74,75,79,81–83]. In voltage-gated Na^+ and Ca^{2+} channels, the primary amino acid sequence contains four homologous domains that are concatenated to encode a single protein with pseudo four-fold symmetry about the central ion-conducting pore[75,80,81]. Several members of the VGC superfamily, including Ci-VSP, TPTE/TPTE2, c15of27 and Hv1, have VS domains but lack the S5-S6 pore domain[20,21,78,84–87]. In Ci-VSP, the N-terminal VS domain is covalently attached to a C-terminal lipid phosphatase catalytic domain that selectively dephosphorylates $PI(4,5)P_2$ and $PI(3,4,5)P_3$ [84,85,88]. Hv1 lacks the pore domain seen in other VGCs, but retains voltage-sensitive and H^+-selective ion channel activity[20,21]

Structural and functional characteristics of VS domains are discussed in the following section. In VGCs, the VS domain undergoes conformational changes in response to changes in membrane potential, and structural changes in the VS domain are coupled to opening or closing of the pore domain[77,80,81,89,90]. In the case of Ci-VSP, the VS domain alters the activity of the catalytic phosphatase domain[84,85,88]. The 4^{th} helix in the VS domain (S4) exhibits a conserved stretch of 2 to 7 positively charged basic (arginine or lysine) residues at every third position along the helix, and these conserved basic residues are separated by hydrophobic residues[73,81,82,91]. Charged residues in the S4 segment are proposed to form salt bridges with negatively charged acidic residues located in the neighboring S1, S2 and/or S3 segments[81,82,92–94], and salt bridges between and among basic and acidic groups in the VS domain are likely to be broken and

re-formed during voltage-dependent VS activation and deactivation. The primary amino acid sequence of selected VGCs is shown in Figure 1, and illustrates similarity between VS domains, VSPs and the functionally uncharacterized c15orf27 (NM_152335) proteins. The three strongly-conserved arginine residues in S4 of Hv1 are aligned with the 'gating charge' residues of VGCs[73,77,82,90,95–103], suggesting that these residues share a common role in the VS mechanism (Fig. 1). Recent studies that support this hypothesis will be summarized later (Section 6.0). The VS domain proteins shown in Fig. 1 also exhibit a number of conserved acidic residues in S1-S3 that contribute to electrostatic networks that stabilize the activated or deactivated state of the VS[73,83,93,95,104–109].

The X-ray crystal structure of a voltage gated K^+ channel offered the first 3-dimensional view of a voltage gated channel tertiary structure[75,76,83,110]. As predicted from earlier biochemical and functional studies, the X-ray crystal structures of K^+ channels are homotetramers assembled from four identical protomers (Fig. 2A)[75,76,83,110]. Each subunit has an S1-S4 VS domain that is located peripherally and a central pore domain that forms the selectivity filter structure which coordinates the permeating K^+ ion (green sphere in Fig. 2A) [75,76,83,110,77].

A side view of the K^+ channel VS domain highlights the organization of S1-S4 helices in the membrane and suggests possible structural differences between the activated-state X-ray crystal structure (Fig. 2B, *left panel*) and a hypothetical resting-state model structure (Fig. 2B, *right panel*)[76]. The precise nature of conformational rearrangement is still debated, but it is commonly accepted that VS activation consists of the movement of the S4 Arg residues across the membrane[73,76,80–82,91,111,112].

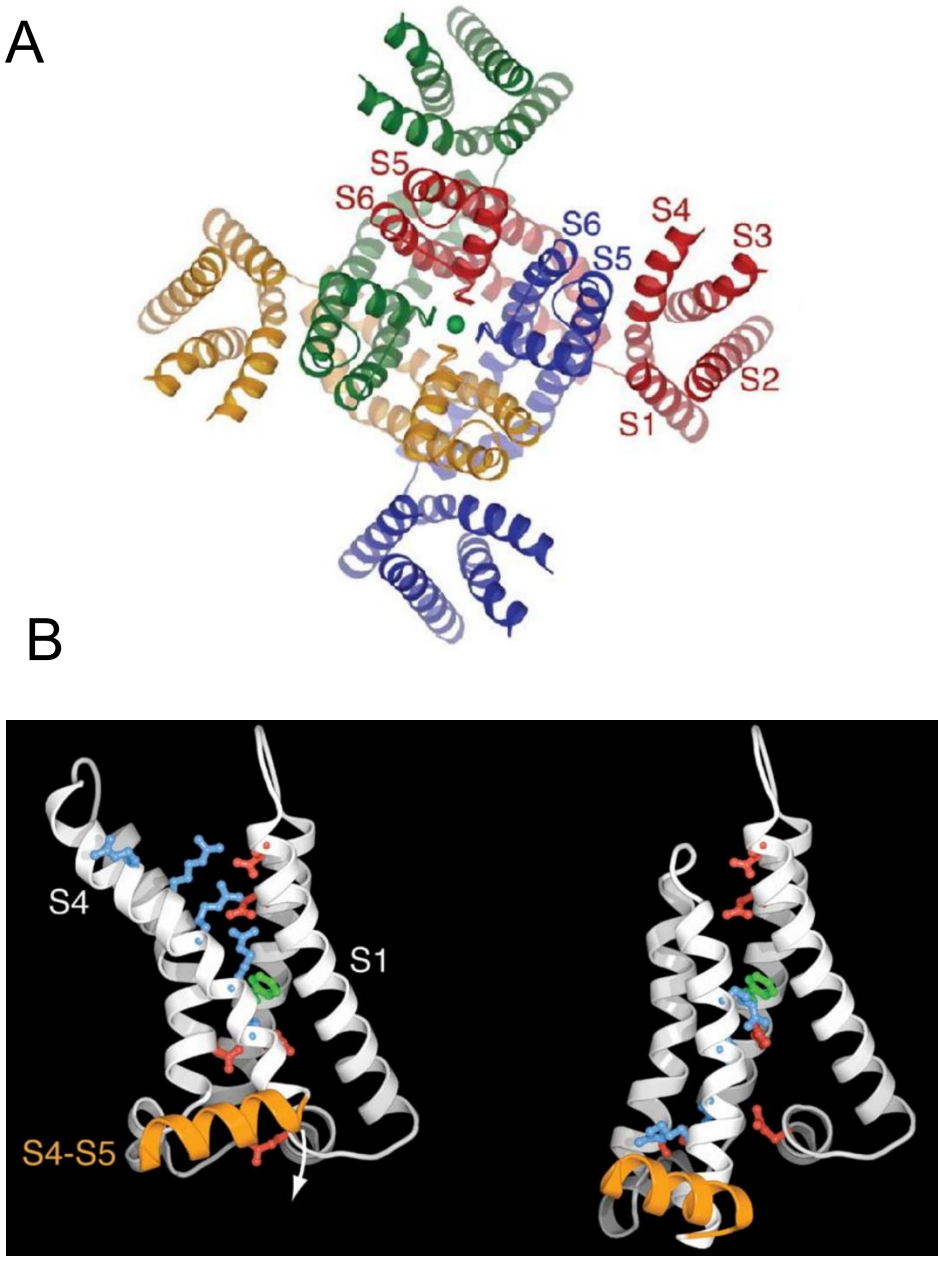

Figure 2. K^+ channel structure and hypothetical gating in VS domain structure.
A. Kv1.2 X-ray crystal structure (2.9Å resolution; shows the tetrameric channel complex viewed from the extracellular solution. Each of the four subunits is colored uniquely and helices are shown as ribbons. The central pore is open and contains a permeating K^+ ion (green sphere). The transmembrane helices S1 to S6 are labeled. Each S4 helix is nearest to the S5 helix of a neighboring subunit. Reproduced from Long et al. (2005).
B. *Left panel*, Kv1.2-2.1 chimera X-ray crystal structure (2.4Å resolution; Long, et al. 2007) viewed from the pore domain within the membrane. VS domain S1-S4 helices are shown as white ribbons and the S4-S5 linker is shown as orange ribbon. Conserved S4 basic residues (R1 to K5) are shown as blue sticks. Negatively charged residues are red and phenylalanine is green. *Right panel*, a hypothetical resting state structure of the VS domain. Reproduced from Long et al. (2007).

In the MacKinnon model illustrated in Figure 2B, the movement of structural elements in the VS domain, particularly S4, is coupled to S6 in the pore domain by the S4-S5 linker[76]. The primary gating charges are thought to be Arg and Lys residues in the S4 segment[82,98,113–115]. The highly conserved Arg residues in the S4 segment are depicted on the VS crystal structure (Fig. 2B) along with conserved acidic residues that are proposed to stabilize charged Arg during VS gating and outward movement of S4[82,94,99.76]. The X-ray crystal structure of the bacterial voltage-gated Na^+ channel NavAb from *Arcobacter butzleri* (a member of the NaChBac family) was resolved by Payandeh et al. (2011) and exhibits strong structural similarity to K^+ channels[99]. Consistent with K^+ channel X-ray structures, the NavAb structure also contains S4 charged arginines and conserved acidic residues in the S2 segment[99]. Hv1 exhibits sequence homology to the VS domains in Kv1.2-2.1, NaChBac and many other VGCs, thus it is proposed to have structural homology as well[116–118].

An important structural feature of the VS domain is that it spans the thickness of the lipid bilayer, and contains a hydrophilic constriction within the central portion of the four helix bundle referred to as the 'hydrophobic gap', that effectively separates the intracellular and extracellular milleux[80,81,91,106,111]. A portion of the S4 segment is hypothesized to translocate through the hydrophobic gap during VS activation[80,81,91,106,111]. The first clear evidence that S4 arginines move through an aqueous pore-like region in the VS domain was reported from cysteine accessibility studies on a voltage-dependent Na^+ channel conducted by Yang and Horn[119,120]. In this approach charged arginine residues in S4 were substituted with cysteine. The cysteine thiol side chains could then be chemically labeled with a membrane impermeable, thiol-specific MTS reagent (2-(trimethylammonium) ethyl) methanethiosulfonate (MTSET)[119,120]. The cysteines were assayed for their ability to react with MTS reagents in both open and closed channel conformations during voltage clamp experiments[119,120]. The main finding was that the reactive thiol becomes more accessible to labeling from the extracellular side at depolarized potentials, while at hyperpolarized potentials the thiols are more accessible to intracellular labeling[81,82,119,120]. Assuming that S4 remains helical in the resting state[73,76,112], the results suggest that the internal- and

external-facing residues are separated by a hydrophobic barrier of ~10 Å[80–82,119,120]. The effective thickness of the hydrophobic gap is therefore much thinner than that of the lipid bilayer (~28 Å)[80–82,119,120]. A consensus view of the VS structure has begun to emerge: the S4 segment is lined by intra- and extracellular water-accessible crevices that are interrupted by a thin hydrophobic gap; the S4 segment slides through the hydrophobic gap between aqueous crevices during VS activation and deactivation in response to changes in membrane potential[80–82,119,120].

Other experimental approaches have provided strong evidence for aqueous crevices within the VS domain. In one approach, streptavidin was used to label Arg to Cys substituted residues in the VS domain of a bacterial Kv channel from *Aeropyrum pernix* (KvAP). The bound streptavidin was then chemically labeled with biotin and revealed state and voltage-dependent access[80,110]. The conclusion from these experiments was that charged residues in S4 undergo voltage-dependent changes in accessibility to aqueous compartments[80,110]. Histidine scanning mutagenesis also illustrated aqueous compartments in the VS domain structure. In this approach Arg to His substitutions in the Shaker K^+ channel S4[106,121–123] were made because the pK_a of His (6.0) allows it to readily exchange H^+ with water at neutral pH, whereas Arg (pK_a 12.48) is essentially trapped in the ionized form at physiological pH. It was found that a substituted His in S4 could facilitate voltage-dependent H^+ transfer by alternating accessibility to intra- and extracellular water[80]. This approach will be described in greater detail in a later (Section 5), but is important to note that His substitutions elicited voltage-dependent channel- and transporter-like H^+ currents (referred to as 'shuttle' currents)[121–123]. The histidine mutagenesis results indicate that residues in S4 have alternating access to intracellular and extracellular water vestibules and can make excursions through the 'hydrophobic gap' during VS activation and deactivation[121–123].

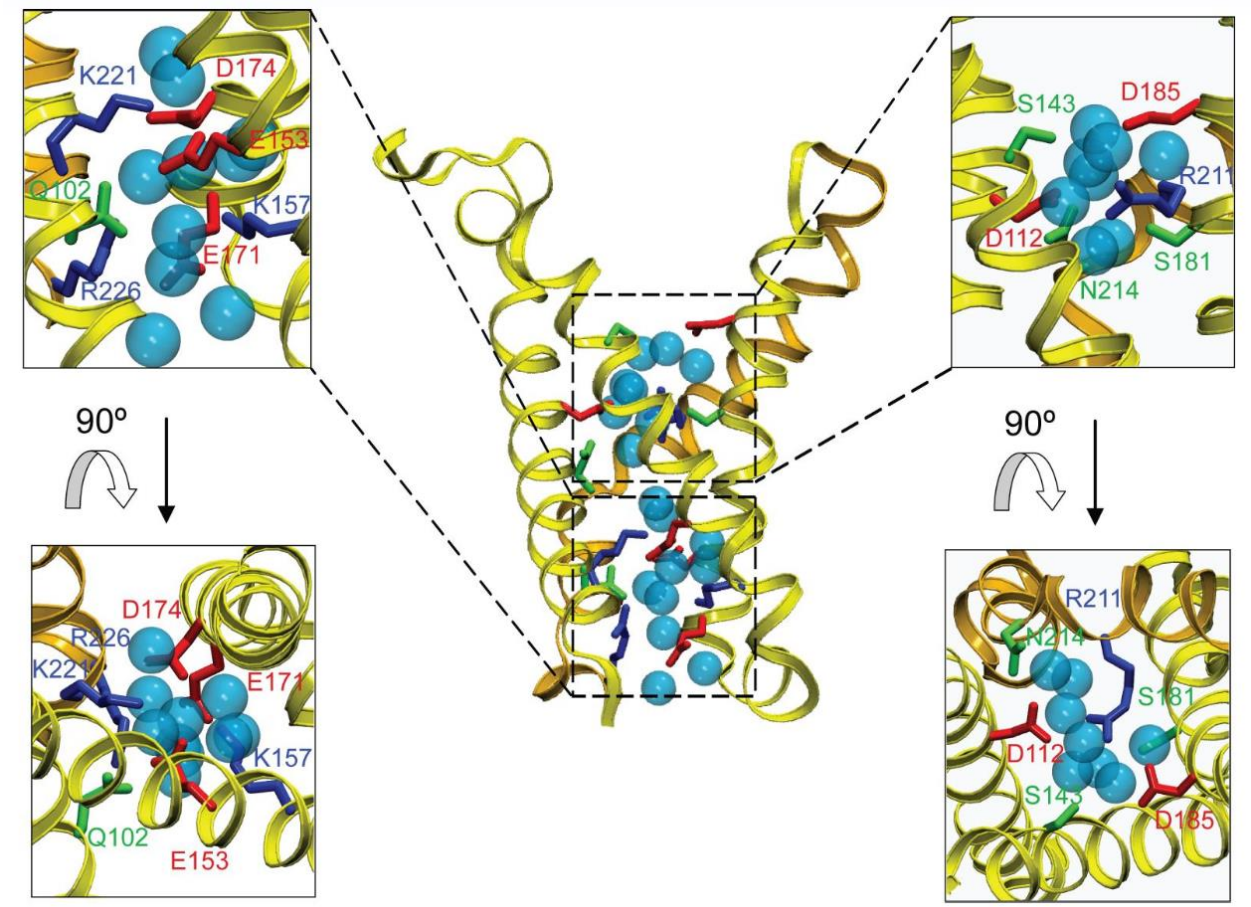

Figure 3. Hv1 channel activated state model structure showing the aqueous crevice.
Homology model of Hv1A (based on KvAP X-ray structure). The final snapshot of an atomistic molecular dynamics simulation (t = 20 ns) showing water molecules along the central axis of the S1–S4 bundle is shown. Insets show water coordination at the internal and external clusters of charged and polar residues. Residue side chains found to form extensive hydrogen bond interactions with water are highlighted in blue (basic), red (acidic) or green (polar uncharged). Water molecules, light blue spheres. For simplicity, only oxygen atoms of waters are shown. S1–S3 segments are represented by yellow ribbons and S4 by orange ribbon. Figure is reproduced from Ramsey, et al. (2010).

In the absence of an Hv1 X-ray crystal structure, several groups have used *in silico* approaches to visualize the architecture of the Hv1 VS domain. Ramsey et al. (2010) constructed homology models for human Hv1 (Fig. 3) based on the KvAP[83] and Kv1.2-2.1chimera[76] X-ray crystal structures[94]. Hv1 model structures were subjected to sequential coarse-grained and atomistic Molecular Dynamics (MD) simulations in the presence of water and ions (Fig. 3). As expected, the Hv1 model structures are defined by S1-S4 segments packed into the typical VS bundle[94]. MD simulations revealed a central aqueous crevice within the Hv1 VS, and the authors indicate that an aqueous proton wire could form if waters effectively bridge the intra- and extracellular facing aqueous compartments[94]. Water molecules in the central crevice were well coordinated by hydrogen bonding with multiple partner residues in the putative Hv1 open state model structure during MD simulation (Fig. 3)[94]. Water density calculations reveal a continuous column of water molecules in the Hv1 central crevice. Unlike Hv1, water densities measured during MD simulations of the Kv1.2-2.1 chimera and KvAP VS domain X-ray structures exhibit large discontinuities in water residence of the central crevice[94]. A snapshot of the MD-equilibrated open-state Hv1 model structure (Fig. 3) features networks of polar and charged residue side chains organized into external (Asp112, Ser143, Ser181, Asp185, Arg211) and internal (Glu153, Lys157, Glu171, Asp174 and Lys221) clusters[94]. MD simulations revealed that side chains in these clusters face the central crevice and participate in electrostatic interactions with one another and hydrogen bonds between and among side chains and water molecules[94].

Wood, et al. (2012) also constructed an Hv1 homology model based on Kv1.2-2.1 chimera X-ray structure[124,76]. Consistent with the previous report[94], atomistic simulations showed that a fully hydrated pathway connects the intracellular and extracellular sides of the VS domain[124]. Wood, et al. (2012) observed that a constriction point is formed by a cluster of hydrophobic side chains (V116, I146 and L147) at the center of protein close to the intracellular side, and that R211 (the 3rd Arg in S4 of Hv1), occupies the extracellular side of this constriction point[124]. A previous report showed that intracellular cysteine modification of the N214C mutant is sufficient to abolish H^+ current in Hv1[125]. In order to determine whether that the previously proposed hydrogen-bonded chain of water molecules[124] maintains

its connectivity through the VS central crevice is an artifact of homology modeling and MD simulation, Wood, et al. (2010) simulated Hv1 N214R and found that water wire formation was only sporadic during the time scale of the simulation trajectory, and that the configuration of the water molecules in Hv1 aqueous crevice resembled that of non-conducting VS domains[124] . In essence the two simulation studies agree that Hv1 contains an water-filled crevice that may function as a water-wire for H^+-selective conduction[124,94].

Kulleperuma, et al. (2013) constructed three Hv1 homology models based on the VS domains of KvAP, Kv1.2-2.1 chimera and NavAb channel X-ray crystal structures[126]. As with previous homology modeling and simulation results, the authors report the presence of a central hourglass-shaped water crevice that is constricted by salt bridge interaction between D112 (in S1) and R211 (in S4)[126]. The amino acid sequence alignment used to create one of the initial homology models is distinct from previous reports due to changes they imposed in the register of conserved S4 arginine residues[126]. Atomistic MD simulations confirm the presence of an aqueous vestibule but conclude that a 'water wire' may not be favorable for H^+ permeation[126], and suggest instead that titratable residues, such as D112, which is found near the hourglass constriction point in their simulations, is likely to be required for selective proton transport[126]. Although homology modeling and MD simulations are useful tools for determining possible structural conformations of Hv1 based on similarity to other VGCs, interpretation of the resultant structures depends on many assumptions that must subsequently be experimentally tested.

All three studies of Hv1 model structures mentioned previously are in agreement with the hypothesis that Hv1 contains a continuous aqueous transmembrane crevice across the VS domain in the putative activated or open state[124,94,126]. Electrostatic interactions and hydrogen bond networks formed between and among centrally located residue side chains and waters are a common feature of Hv1 model structures[124,94,126]. Although the specific details of the central aqueous crevice constriction architecture vary from model to model, the studies agree that S4 in Hv1 is likely to undergo conformational rearrangement during VS domain activation to open the H^+ permeation pathway[94,126,127].

A recent study by Chamberlin, et al. (2013) addresses the structure of Hv1 in its resting state using homology modeling and MD simulation in both open and closed states[118]. Using the Kv1.2-2.1 chimera VS domain as a template, an open state Hv1 model was constructed for *Ci*Hv1[76]. A closed state Hv1 model was based on the Pathak, et al (2007) closed-state model of Kv1.2[128,129]. Thus the closed-state model proposed by Chamberlin, et al. (2013) is a model of a model. Nevertheless, the closed-state model is useful for defining residues that participate in the formation of the hydrophobic gap in a non-conducting state of Hv1. Based on the comparison of open- and closed-state model structures, the authors conclude that S4 adopts a position that is accessible to the intracellular solution in the closed state[118], as suggested by previous cysteine accessibility data[130]. The closed-state model also suggests that there are two centrally located hydrophobic plugs in Hv1[118]. The first and most extracellularly located plug consists of hydrophobic residues on S1 (Val157 in *Ci*Hv1; V109 in hHv1) and S4 (V252 in *Ci*Hv1; I202 in hHv1), and is proposed to prevent waters from penetrating deep into the central crevice from the extracellular side[118]. The second plug, located beneath the first plug (i.e., on the intracellular side), is proposed to consist of salt bridge interactions between S4 arginines and acidic glutamate residues on S2 (Glu201 in *Ci*Hv1; E153 in hHv1) and S3 (Asp222 in *Ci*Hv1; G174 in hHv1)[118]. The authors conclude that S4 undergoes a conformational rearrangement, and that the central crevice of the protein is largely dehydrated in the closed state conformation[118].

Experimental data reinforce the notion that Hv1 undergoes substantial conformational rearrangements during activation gating. Gonzalez et al. (2013)[116] used a cysteine scanning assay in conjunction with voltage clamp fluorimetry[130] to study conformational rearrangements in Hv1, and concluded that the voltage sensing mechanism in Hv1 is likely to be grossly similar to that in other VGCs[130]. Cysteine accessibility performed under voltage clamp was used to determine the state dependence of accessibility in S4 of Ci-Hv1. A group of residues, including L256C through V259 (L206 to V209 in hHv1), are inaccessible in either closed or open states. In the closed state, the range of inaccessible residues spans from A246 to V259 (E196 toV209 in hHv1), while in the open state the region that is inaccessible is located in a different part of S4: from L256 through N264 (L206 to N214 in

hHv1)[116]. The authors conclude S4 movement in Hv1 VS domain is measurable, but the amplitude of the vertical translation during activation gating may not be as extensive as in other VGCs[116] . Gonzalez, et al. (2013) suggest that S4 moves enough to translate the equivalent of 2–3*e* through the electrical field, and that charge translocation associated with S4 movement could occur in three ways: 1) due to a movement of a rigid S4 helix; 2) due to changes in aqueous crevices around S4 that expose or shield gating charges; or 3) due to a change in the secondary structure of S4[130].

Unlike tetrameric voltage gated K^+ and Na^+ channels, Hv1, exists as a dimer[130–134]. In the Hv1 dimer, the two VS domain subunits are tethered together by a C-terminal coiled coil motif[131,132,135]. Heterologously expressed Hv1 forms puncta that are consistent with the existence of primarily dimeric channel complexes configuration under TIRF microscopy[135,136]. Western blots of Hv1 protein from the same preparation reveal both monomeric and dimeric protein[135]. Nonetheless, removal of the C-terminal coiled coil region, either by premature truncation (ΔC)[131,137–139] or by substitution with the C-terminal phosphatase domain from Ci-VSP[135], is sufficient to increase the proportion of monomeric Hv1 channels in both biochemical and fluorescence assays[135,136] H^+ currents elicited by Hv1-ΔC suggest that monomeric Hv1 channels are gated similarly to wild-type dimers[130], but channel opening in the Hv1 monomer is faster in monomers than dimers[131,133–135,139]. Although C-terminal truncation is thought to monomerize Hv1, there is evidence for inter-subunit interactions in Hv1-ΔC[140]. Lee, et al. (2009) used a substituted cysteine crosslinking assay to map residues that participate in the dimer interface[140]. They found that cysteine substitution of residues at the outer end of the S1 segment (I126 and I127 in hHv1) formed covalent crosslinks with residues of the adjacent subunit, leading to a proposal that two S1 helices face each other at the dimer interface[140]. The existence of multiple interaction interfaces is consistent with the experimental evidence that ΔC channels remain capable of forming dimers[133]. The X-ray crystal structure of the Hv1 C-terminal fragment from mouse[139] and human[138] channels was solved and was found to be ~55 amino acids in length beginning ~10 residues C-terminal to the end of S4. The structure was shown to adopt a coiled-coil domain structure with a distinctive heptad repeat pattern[139]. Subtle mutations (i.e.,

Leu to Ile) in the coiled-coil alter channel assembly, and can cause trimer or tetramer formation[141]. This suggests the possibility that other, subtly different coiled-coil interactions between Hv1 VS protomers are possible, but the that the optimal architecture of the coiled-coil core in WT Hv1 is dimeric[139,141].

The ~100 residues that are located N-terminally to S1 are intracellular, but only a few residues have been assigned specific functions. A phosphorylation site at Thr29 in hHv1 is thought to be responsible for enhanced gating of proton channels in activated phagocytes[142]. Also located on the intracellular N-terminus is the Met91, which was identified as the locus of a spontaneous human mutation (M91T)[66]. As discussed earlier, M91T alters the position of the G_{vH+}-V relation at all ΔpH tested[66]. Although both T29 and M91 mutations are sufficient to alter the voltage-dependent of gating, no specific mechanism for the observed effects has been proposed.

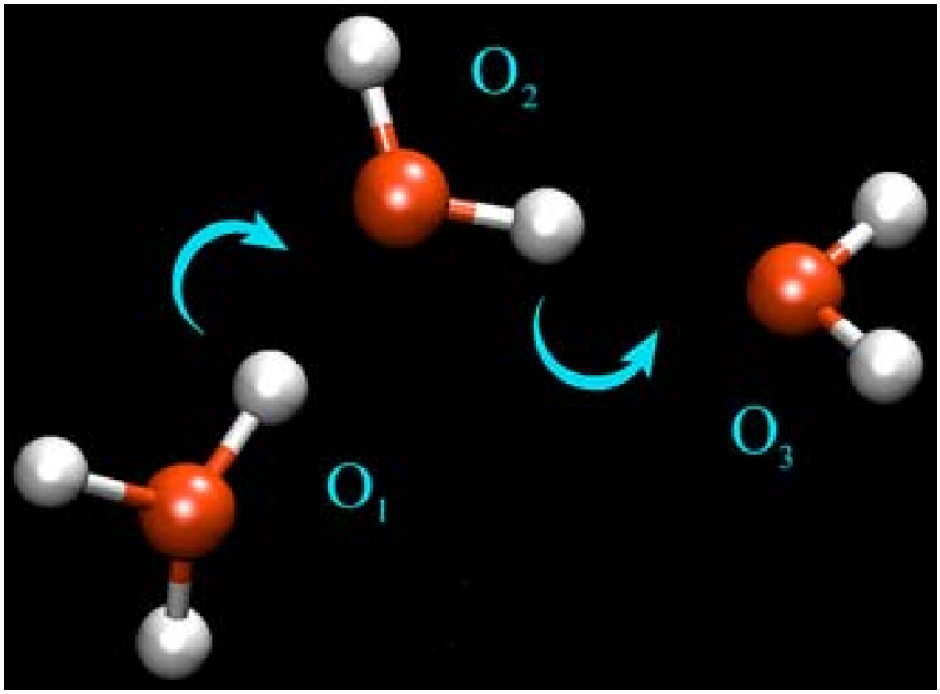

Figure 4. Grotthuss H^+ 'shuttling'
The Grotthuss proton shuttling process in water. One H_3O^+ molecule and two H_2O molecules are shown. Red ball represents oxygen and white balls are hydrogen. Blue arrows indicate direction of H^+ shuttling across single file chain of water (i.e., a "water wire). Figure is reproduced from Voth (2003).

5. Proton permeation

Examples of proton transport through a narrow aqueous or proteinaceous channel by a hydrogen-bonded chain (HBC) transfer or the Grotthuss mechanism are plentiful in biology[10,27,94,143–145]. In an HBC, protons 'hop' from the donor such as hydronium ion (H_3O^+) to an acceptor such as water as depicted in Figure 4. The principal requirement for Grotthuss H^+ transfer is that the donor and acceptor groups form a hydrogen bond[9,22,143,144]. Thus, vectorial Grotthuss-type proton transfer in an HBC can thus be faster than Brownian diffusion of the protonated donor alone, which explains the 'anomalously high mobility' of H^+ in aqueous solution[10,22,94,143,144,146,147]. In addition H^+ permeation rates through membranes were found to be 5-6 orders of magnitude larger other monovalent cations[10,148–150]. Protons can 'hop' by the Grotthuss mechanism in a chain of water molecules without requiring displacement of the oxygen atoms, and HBC transfer is thus observed even in ice; a similar mechanism likely explains the ability of H^+ to hop between side chain atoms in proteins with rigid backbone structure[10,22,94,143,144].

One important difference between proton permeation in voltage-gated H^+ channels and the permeation of other physiologically important inorganic cations in VGCs is that $[H^+]$ is $>10^5$ times lower than the plasma concentrations of Na^+, K^+ and Ca^{2+} [10]. The free concentrations of several membrane-permeable ions in mammalian skeletal muscle are (in mM): $[K^+]_{in} = 150$; $[K^+]_{out} = 4$; $[Na^+]_{in} = 12$; $[Na^+]_{out} = 145$; $[Cl^-]_{in} = 4$; ; $[Cl^-]_{out} = 123$; $[Ca^{2+}]_{in} = 0.0001$; $[Ca^{2+}]_{out} = 1.5$[35]. At pH 7.4, $[H^+] = 450$ nM, or 4.5×10^{-4} mM. The net result of high mobility but low concentrations of H^+ in biological systems can be explained by the Grotthuss mechanism of rapid proton migration, where H^+ move by hopping from one water to the next. The extremely high selectivity in Hv1 channels for H^+ over other more readily available cations suggests that Hv1 is likely to have a Grotthuss type conduction mechanism for H^+ transport that does not support permeation of other cations[10,148–150].

Cells selectively transport ions across the membrane using a variety of different proteins[35]. The major groups of ion-transporting proteins include channels, carriers, and pumps; among these, channels

typically mediate faster rates of ion flux[35]. The number of ions moved per protein per unit of time (turnover number) is analogous to the unitary conductance of a single ion channel protein, because ionic current requires the binding and unbinding of the permeant ion[35]. Unlike ion channels, which catalyze high rates of ion flux in the open state, the turnover number of pumps and some carriers is thought to be limited by conformational changes that occur during each transport cycle[35,151–154]. In the alternating access model of pump function, no continuously accessible pathway for ion movement across the membrane is established[35,151–154]. Typical rates of ion flux in channels range from 10^5-10^8 s^{-1} (millions of ions per second), whereas carrier- and pump-mediated rates are typically in the range of 10^1-10^4 s^{-1} [10,35]. The difference between pump-like ion transport and channel-like flux is evident in electrophysiological measurements of macroscopic current[35,91,151,152]. A pump-like alternating access ion transport mechanism generates maximal current amplitude when cycling rate is highest, and a plot of current vs. stimulus over the full range of activity can be bell-shaped[35,91,151,152,155]. In channels, open probability (P_{OPEN}) depends on stimulus strength, and is observed to rise monotonically toward its intrinsic maximum[6,35,80]. The shapes of the current vs. voltage relations (I-V) for voltage-dependent pumps and channels is thus distinct[35,151,152]. Differences in the shapes and positions of the I-V relations can be used to investigate gating and permeation mechanisms in mutant ion transport proteins. We will next review a series of studies in which His-substitution mutant voltage-gated Shaker K^+ channel are reported to manifest pump- or channel-like mechanisms depending on the location of the mutation. The His mutagenesis approach is the cornerstone of the experimental strategy employed for Hv1 in our studies.

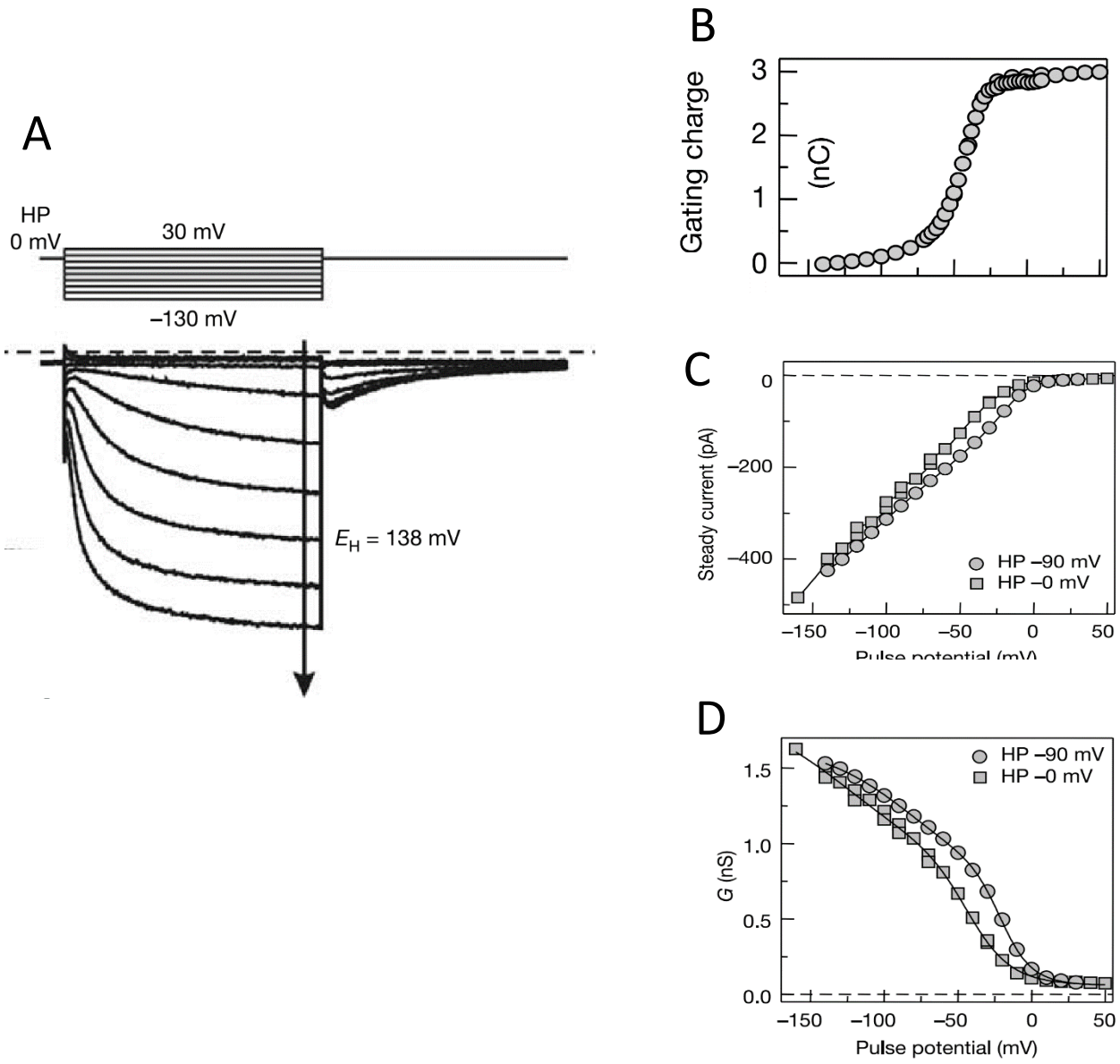

Figure 5. Shaker K^+ channel R362H and double Boltzmann fits.
A. Proton currents from the R362H Shaker channel were measured from a cell-attached macropatch on a perforated oocyte in $pH_O5/pH_I7.4$ solutions. Voltage protocol above figure. Steady-state current measured for I-V plot indicated by arrow. **B.** Voltage dependence of the gating-charge (Q-V) for Shaker R365H. **C.** Voltage dependence of the steady-state current (I-V) from Shaker R365H. Currents elicited from holding potential of -90mV (circles) and 0mV (squares) **D**. Voltage dependence of conductance (G-V), calculated ($G= I /V- E_{H^+}$) from steady-state currents elicited from holding of -90mV (circles) and 0mV (squares) in Shaker R365H. Figures are reproduced from Starace, et al. (2004).

Starace, et al. (1994, 2001, 2004) replaced S4 arginine residues with histidine and found that the mutant channels exhibited several different voltage-dependent H^+ transport gain of function phenotypes[121–123]. One effect of an Arg to His mutation is lowering of the pK_a from ~12 (Arg) to ~6 (His), making the protein mode readily ionizable at physiological pH[121–123]. When His replaces S4 Arg residues that are fully translocated across the hydrophobic gap (i.e., fron intracellular- to extracellular-accessible compartments) during VS activation (see Section 4), the His imidazole side chain facilitates a H^+ conductance with a bell-shaped I-V curve[121–123]. The voltage at which the maximum H^+ transport is measured corresponds to the midpoint of the gating charge vs. voltage relation, suggesting that Shaker Arg to His VS mutants behave like an alternating access voltage-dependent ion pump whose maximum cycling rate is observed when the probability of VS activation is 0.5[121–123].

Histidine scanning mutagenesis has advantages over other similar cysteine scanning mutagenesis for S4 movement because replacement of arginine with histidine is a less disruptive charge neutralization and proton binding of histidine is occurs at rates much faster than the rate constants of gating transitions [121–123,156]. Histidine substitutions of gating charges R362H, R365H, R368H, and R371H in the Shaker S4 segment were made in the background of the non-conducting mutant (W434F)[157], non-inactivating (IR, Δ6–46)[158], because the W434F mutation effectively disables intrinsic K^+ conducting pore, and allows for measurement of histidine mediated H^+ transport in the absence of large K^+ ionic currents[121–123,156].

A channel-like proton current was measured in Shaker R362H demonstrating that histidine is simultaneously accessible to protons in both the intra- and extracellular milieux[121–123,156]. Because Grotthuss-type proton transfer or proton shuttling occurs over the distance of a hydrogen bond, the results suggest that the maximum distance from internal to external waters in the resting state is focused across a rather narrow hydrophobic gap that is short-circuited by protons via the histidine mutation[121–123,156]. We define this channel-like resting-state proton ‘shuttle’ conductance as G_{SH} and distinguish it from the transporter-like proton fluxes associated with the R365H, R368H, and R371H mutations in Shaker. Voltage sensor activation turns off histidine mediated proton ‘shuttle’ conductance (G_{SH}) because voltage-

dependent S4 movement causes the histidine at position 362 to adopt a conformation that is not permissive for Grotthuss-type proton shuttling[121–123,156]. The authors further showed that the G_{SH} -V relation for this proton shuttle pathway in mutant Shaker channels occurred over a similar voltage range as the movement of gating charge (Fig. 5B,C,D) suggesting that resting-state proton shuttle conductances might be a generally applicable proxy for the measurement of gating current per se in other VS domain containing proteins[121–123,156].

The pump-like proton transport associated with R365H, R368H, and R371H mutations in Shaker, represents a situation where histidine is exposed to water on one side of the membrane but S4 makes excursions across the membrane between the resting and activated positions, thus transporting is based on histidine binding and unbinding of H^{+}[121–123,156]. A pH gradient applied across the membrane means that the histidine will pick up a proton when exposed to the high [H^{+}] side and release it when exposed to the low [H^{+}] side, producing a net proton current in the direction of the pH gradient. Net transport will be maximum at potentials where the voltage sensor has an equal probability of being in the resting or the active states and reflect a bell-shaped I-V relation, corresponding to the midpoint of the gating charge-voltage relation (Q-V)[121–123,152,156]. Unlike R362H, which has simultaneous access to outside and the inside solutions in the resting state, R365H, R368H, and R371H create an H^{+} transport mechanism that is based on voltage dependent conformational rearrangements of S4[121–123,156].

Two biophysical properties reported for R362H were an estimated unitary H^{+} conductance and block of the H^{+} transport by divalent metal[122]. Estimates of single proton channel conductance, was done with non-stationary variance analysis of R362H channel currents[122]. Analysis was based on a set of current traces that were elicited by repetitive test pulses to a negative potential (-100mv) under pH conditions pH_{Out}5.0 and pH_{In}9.2 to create a large inwardly directed [H^{+}] gradient[122]. Estimates of unitary channel current 9fA and unitary conductance 40fS, corresponded to a flow rate of ~10^{4} s^{-1} [122]. The authors note that single-channel conductance of each of the four R362H proton channels in the Shaker tetramer is about one-quarter that of that estimated for proton channels found in eosinophils[30,122]. The R362H H^{+}

currents are blocked by histidine binding to nickel. Addition of 5 mM $NiSO_4$ to the external solution at pH_O7.4 resulted in a significant reduction of the proton current, which indicates direct binding of nickel to an externally facing histidine residue[122]. The nickel block could be relieved only by washing with an external solution of pH_O5.0, so that high $[H^+]$ was needed to compete for the histidine nickel binding site[122]. These properties of histidine mediated H^+ conduction in the VS domain of Shaker K^+ channel are important in the context of our research and serve as a guide for histidine scanning mutagenesis approach in Hv1 and other VGCs.

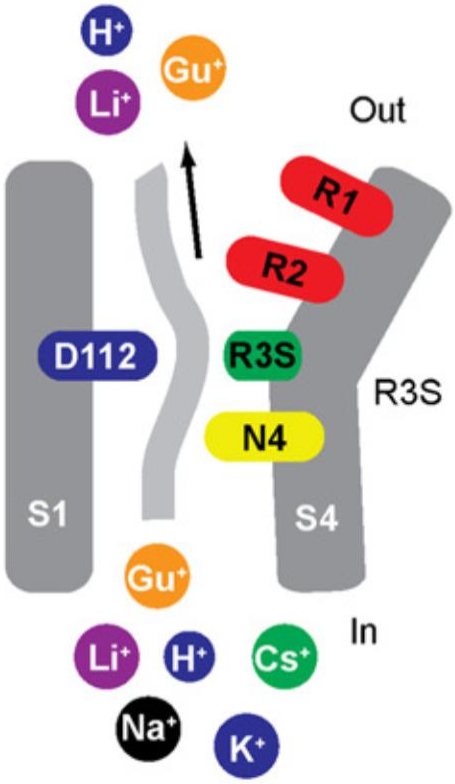

Figure 6. Hv1 model for R211S mutation and altered selectivity.
A proposed model for an altered selectivity filter in hHv1 consisting of the acidic residue D112 on S1 and the R3S substitution on S4. D112 (blue) and R3S (red). Model based on data for selectivity changes with R211S mutation, and shows lithium, guanidinium and hydrogen permeation. Inferred from experimental data of inside-out patches from *Xenopus* oocytes and bath solutions 100 mM Li^+ and Gu^+ at pH 8. Figure is reproduced from Berger et al. (2013).

The mechanism for proton permeation in Hv1 is proposed to consist of a Grotthuss type H^+ transfer along a continuous hydrogen bonded chain (HBC) of water ions that compose an aqueous 'water wire' within the central aqueous crevice of the Hv1 VS domain. Thus the aqueous 'water wire' H^+ conducting pathway is an HBC that facilitates proton transport from the intracellular side to the extracellular side, down an electrochemical [H^+] gradient[23,29,94,127,146,159]. The water here is considered protein-associated because it interacts with the side chains of residues that protrude into the aqueous crevice within the VS domain[94,126,127]. The water wire hypothesis is inherent upon hydrogen bonds between and among waters and specific residue side chains, with the side chain hydrogen bonds serving to restrict water mobility[10,94,127,143,144,159–161]. A membrane-spanning chain would need to be ~20 water molecules long[10,159]. Molecular dynamics simulations of HBCs through the lipid bilayer suggest that a narrow hydrophobic pore can effectively immobilize the waters and inhibit water or other ion flux, while still permitting protons to hop across the waters[144]. The HBC mechanism of proton transport also takes into account that protons in aqueous solution almost always exist in hydrated form as hydronium ions (H_3O^+), and in larger protonated water clusters such as Zundel cations ($H_5O_2^+$) and Eigen cations ($H_9O_4^+$)[10,162]. Theoretical studies propose that water networks containing an excess protons may consist of these large protonated water clusters[143,160,162–164]. Protons can also be transported by ionizable amino acid side chains. It is known that titratable amino acids with low enough p*K*a (aspartate, glutamate, and histidine) do relay protons in several H^+ transport proteins, including M2 viral channel[38], K^+ channel mutants (Shaker R362H) [121–123,156], H-ATPase[37] and bacteriorhodopsin[36]. However, H^+ transport in these proteins is accomplished by transient protonation of residue side chains, which contrasts with the explicit H^+ binding and movement along an HBC of waters. Nonetheless, H^+ conductance via 'water wire' is known to exist in H^+ permeable proteins. The gramicidin channel is known to have a narrow pore containing an HBC of water molecules in single file that support a large H^+ conductance[150,161,164]. Evidence for HBC 'water wire' proton transfer in Hv1 has been reported in theoretical and experimental studies[143,160,162–164]. Homology modeling and atomistic simulations all indicate the existence of water lined crevice within the Hv1 VS domain, and the stability of these water wires is attributed to their

interaction with the protein side chains lining the permeation pathway[94,124,126]. This suggests that formation of a HBC water wire bridging both sides of the membrane relies on the same structural components that are associated with VS domain gating transitions, and both gating and permeation occur through the same structural pathway [94,124,126]. Because ionizable residues are proposed to interact with water in Hv1, the possibility of a H^+ transport mechanism involving titration of side chains was tested. In a study by Ramsey et al. conserved candidate ionizable residues were systematically mutated to nonionizable residues[94]. The study concluded that neutralizing mutagenesis did not abolish Hv1 H^+ current, demonstrating that explicit side chain titration is not required to sustain the aqueous H^+ conductance (G_{AQ}) [94].

The mechanism for nearly perfect H^+ selectivity ($P_{H^+}/P_{Na^+} > 10^6$) in Hv1 is not well understood, but recent studies have implicated structural components that participate in the formation of an ion selective apparatus[27,94]. Within the typical (S1-S6) pore region, the 'selectivity filter'[35,77,82,165], very narrow structural constraints and electrostatic interactions discriminate among free permeable ions. Hv1, without a discernable pore domain, binds H^+ with great fidelity and excludes other readily available cations, evidently by using a selective mechanism contained within the voltage sensing domain[49,126,166–168]. The 'selectivity filter' in Hv1 is proposed to be very narrow region within the VS domain central crevice that is available for H^+ transfer after S4 moves and the VS transitions to an activated state[49,126,166–168]. Reports suggest that R211 on S4 and the acidic D112 residue on S1 participate in forming the 'selectivity filter' in Hv1[166,167]. Musset et al. (2011) transferred residues from an orphan 'silent' homologue c15of27, (see Fig. 1) to corresponding sites in Hv1, and found that one particular substitution (D112V) was sufficient to abolish H^+ channel activity[167].

Other neutralizing substitutions D112 (D112N/K/H/S/F) were found to allow permeation of anion species[167]. It is important to remember the reversal potential for H^+ is always equal to that of OH^- ($E_{H^+} = E_{OH^-}$) and it is technically difficult to distinguish between H^+ selective or OH^- selective conductances. Nonetheless, the study concluded D112 neutralizing substitutions caused V_{REV} to shift away from the Nernst predicted V_{REV} for the imposed $[H^+]$ gradient[167]. The relative permeability for D112 mutants, determined by the Goldman-Hodgkin-Katz equation, was reported as OH^- (or H^+) > Cl^- > $CH_3SO_3^-$, indicating that D112 mutants retain a high level of H^+ selectivity but can also bind and transport anions[167]. Berger et al. found that an R211S substitution on S4 disrupted selectivity (Fig. 6), and allowed for permeation of lithium (Li^+) and a large organic guanidinium cation (Gu^+)[166]. Also, the double mutation D112S-R211S caused even larger disruptions in ion selectivity and this was interpreted by the authors to mean that D112 and R211 form the selective mechanism[166]. They propose that S4 movement during activation positions R211 in a narrow region adjacent to D112 and electrostatic interactions between the two residues contribute to forming the 'selectivity filter'[166]. More studies will be needed to understand Hv1 selectivity, however, an important conclusion from these studies is that the aqueous H^+ permeation pathway in Hv1 runs along the same pathway taken by the S4 arginines[166,167].

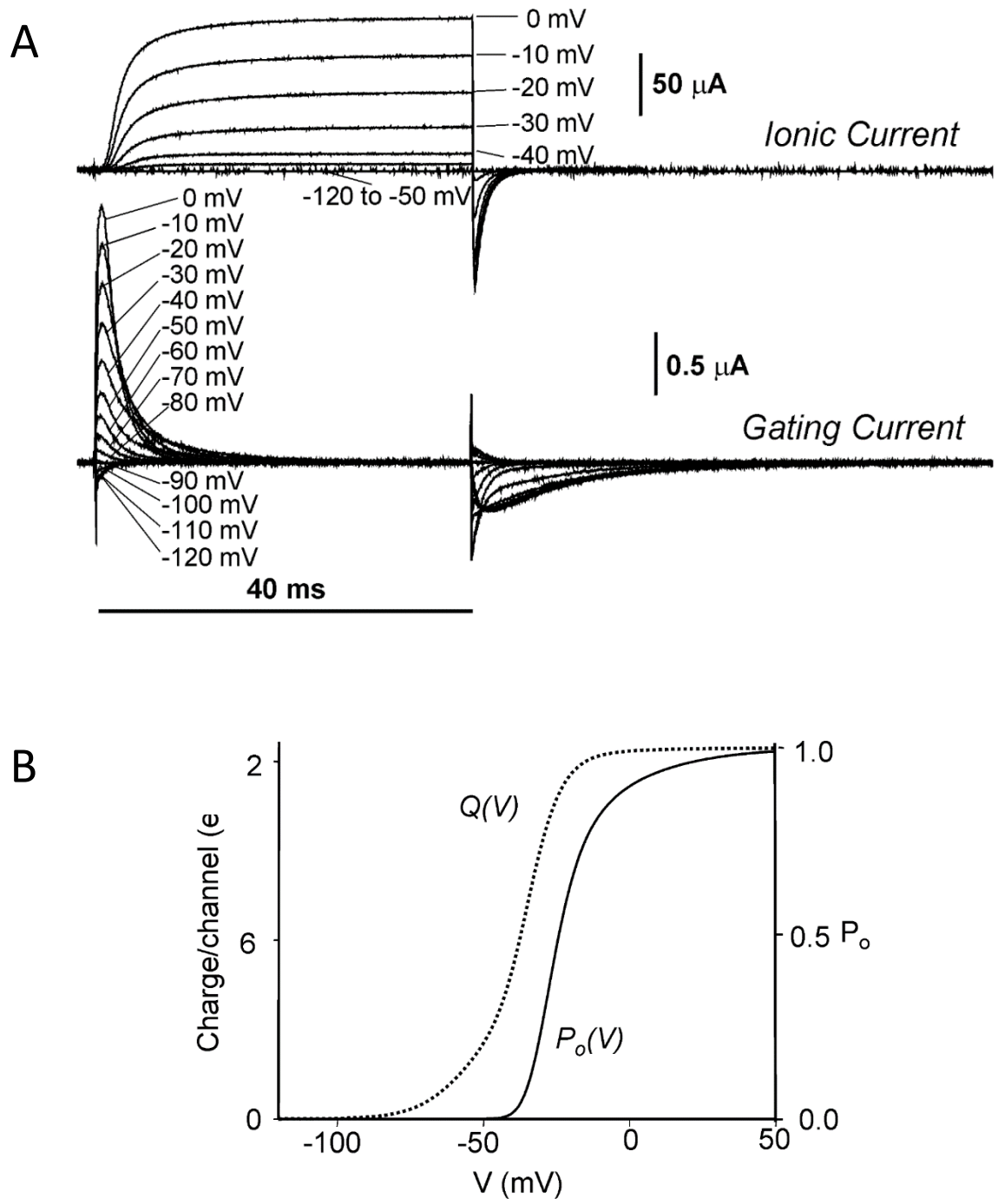

Figure 7. Voltage dependent gating of Shaker K^+ channel: Ionic current and Gating current.
A. Current recorded from Shaker-IR. Top traces: time course of ionic currents for pulses to the indicated potentials starting and returning to -90 mV. Bottom traces: time course of the gating currents for the pulses indicated. Notice the difference in the amplitude calibration for ionic as compared to gating currents. **B.** The voltage dependence of the open probability (P_{OPEN}-V) and voltage dependence of charge moved per channel Q-V. Figures are reproduced from Bezanilla (2005).

6. Voltage-dependent ion channel gating

In voltage gated K^+ channels, the electromechanical coupling of VS domain activation to pore opening can be measured from recording ionic K^+ current (I_{STEP}) elicited by step depolarizations to a range of potentials. Tail current (I_{TAIL}) is measured at a fixed negative voltage where channels close, and when plotted as a function of step potentials, yields an approximate open probability-voltage (P_{OPEN}-V) relationship for channel activity[35,111]. However, if the pore is disabled, either by toxin pore blockers or by mutation, smaller transient gating currents can be detected because the large ionic current is absent[5,93,96,129,169–171]. It is widely accepted that these transient 'capacitive' currents measure movement of protein associated charge in the membrane electric field, rather than ion binding[5,93,96,129,169–171]. The main charges thought to underlie this current are the conserved S4 Arg residues on the VS domain[5,93,96,129,169–171]. Notice in Figure 7A, that ionic current and gating current differ in amplitude by 10 fold. The gating charge (Q) is calculated from the time integral of the gating currents and is plotted as function of step potential to yield the Q-V relation[5,156]. So, VS domain movement gives rise to the Q-V, whereas the P_{OPEN}-V relates concerted opening of channels. Thus voltage sensing and pore opening can be experimentally separated, and when plotted together (Fig. 7) we see that much of the charge moves at voltages that are negative to where the channels open[5,156]. In the case of Ci-VSP, depolarization generates robust gating currents that increase the phosphatase catalytic activity, independent of an interaction with an ion conduction pathway[84,88,100,112]. In channels and in VSPs, gating charge movement represents an early voltage sensitive transition in the activation pathway that is electromechanically coupled to function[78,156,169].

Unlike the transient capacitive gating current that describes S4 associated charge movement, 'gating pore' currents describe a resistive current pathway in mutant VS domains that opens at negative potentials when the VS domain is in the resting state[100,122,129,172–177]. Resting state currents were first described by Starace and Bezanilla (described in Section 5) for the H^+ selective current produced by the Shaker R362H mutant[121–123]. Alternate substitutions of the outer most S4 arginine in Shaker (R362C,

R362V, R362A and R362S) produce, non-specific cation resting-state conductances, termed 'Omega currents'[103,129,174,176,178]. The non-selective cation current is characterized by the permeation of a variety of ions including H^+, Li^+, K^+, Cs^+ and guanidinium[103,129,174,176,178]. Analogous S4 substitutions in the VS domains of Na^+ and Ca^{2+} channels have been found to naturally occur and produce the same voltage dependent non-selective resting-state ('Omega' or gating pore) conductances[172,179–182]. 'Omega' currents indicate ion permeation through a narrow transmembrane VS domain gap that separates water-filled crevices, within a focused membrane electric field. In the VS resting state, the gap is normally occupied by the first charged arginine on S4 (R1) that evidently disrupts aqueous continuity between the intra- and extracellular vestibules[103,129,174,176,178]. Thus resting state conductances are a good proxy for voltage dependent movement of R1, the first gating charge (Q) in VS domains.

In a Q-V relation, exponential increase in charge movement over a voltage range is typically described by a two state (Resting ↔ Activated) model and is characterized by a Bolzmann equation fit to data (Fig. 7)[170,183,184]. However, the voltage dependence of gating pore or 'shuttle' conductance (G_{SH}) may not adhere to this same paradigm. The Boltzmann theory of voltage dependence relates the probability at equilibrium of finding the resting or activated state, and it dictates the ratio of charge movement (or P_{OPEN}) in terms of voltage change[35,80]. The expectation is that a voltage dependent process (measured from I_{TAIL}-V, Q-V or G-V) consisting of a two state equilibrium will fit a sigmoid shaped Boltzmann type function, but most data reported for gating pore currents do not include Boltzmann analysis for P_{OPEN}. Perhaps the only example of such analysis is illustrated in Figure 5D, where Starace and Bezanilla fit the R362H resting state G_{SH} to the sum of two Boltzmann equations[122]. The authors state that G_{SH} is most voltage dependent between -10mV and -100mV and from visual inspection of the data in Figure 5D, one can see that G_{SH} at extreme negative voltages has a very shallow slope and is observed at more negative voltages than that of the Q-V (Fig. 5B)[122]. Two possible explanations for this phenomenon are: (1) The P_{OPEN} of G_{SH} at extreme negative voltages is maximal and independent of voltage-sensitive state transitions; thus it represents a low resistance, passive ionic (H^+) current flowing, such that Ohms law

(I=V/R) could be used to describe it. (2) The shallow G_{SH}-V relation at extreme negative voltages occurs as a result of changes of multiple contributing elements, such as: unitary conductance (selectivity), the number of participating channels, $P_{OPEN,}$ structural or chemical hysteresis, or other more complex biophysical phenomena associated with the imidazole side chain of R362H (i.e. electrostatic H^+ interactions, tautomerization, or 'water wire' formation). Nevertheless, it is important to remember, in context of our research findings presented later, that there is a need for more robust in analytical methods used to describe the G_{SH}-V relation.

Conformational rearrangements of the VS domain involve S4 charge movements, however other late VS domain transitions have been identified, that are depolarization dependent and occur after initial charge movement. Villalba-Galea and collaborators (2008) used voltage clamp fluorimetry of Ci-VSP to reveal a voltage-independent conformational change following the activation of Ci-VSP through a process termed 'relaxation'[112]. Voltage sensor relaxation allows the VS domain structure to adopt a lower energy state following voltage-dependent activation[112] presumably by dissipating energy gained by the voltage sensing domain from the electric work done by the electric field on sensing charges. The study concluded that in the relaxed state VS domain conformation is likely to involve a structural transition of the S4 segment 3_{10}- helix into an α-helix [112]. The study revealed thermodynamically distinct, late transitions that occur during activation of a VS domain without a pore, and these transitions are produced by electromechanical coupling[112]. Interestingly, there is some preliminary evidence for relaxation in H^+ conducting VS domain of Hv1[185]. Relaxation in Hv1 is proposed to consists of a transition that occurs concomitantly with the opening of the H^+ conducting pathway[185] and this suggests that voltage sensor-pore coupling can exists in a channel where the VS domain and pore are contained within the same structural unit.

Gating of the voltage sensitive ion channels is stochastic and follows the laws of probability; however, the probability of a channel being in either a closed or open state is influenced by voltage [35,170,186,187]. Although single-channel recordings contain the most intricate information about channel conductance and probabilistic gating, this information can also be derived from analysis of macroscopic current elicited from a population of ion channels. If we assume that unitary current is voltage independent, the expression below[156,186,187] describes macroscopic current elicited from a population of channels

$$(I = NiP_{OPEN}) \quad (1)$$

where I is the macroscopic current measured; N is the number of channels; *i* is the unitary current; and P_{OPEN} is the probability of being open. The approximate P_{OPEN} can be derived from Boltzmann two state model fits of macroscopic tail currents (I_{TAIL}) or calculated conductance (G). Hodgkin and Huxley indicated in some of the earliest studies of ion channels, that movement of gating particles open channels and this was born out in later studies that measured gating charge movement[35,92,96,169,186]. Thus the transition from closed to open moves a distinct amount of charge. Without the means to accurately measure gating charge movement, the limiting slope method is employed to estimate the gating valence from macroscopic conductance using the Boltzmann theory for voltage dependence[35,170,184]. Because the Boltzmann equation characterizes the ratio of closed to open channels (P_{OPEN}) at equilibrium in terms of energy change, the exponentially rising slope of a Boltzmann fit is used in limiting slope to estimate the charge valence required to alter P_{OPEN}[35,170,184]. It is important to note that the limiting slope method has shortcomings in that, it measures only the range of charge movement which is energetically linked to channel opening (charge movement during activation), ignoring the latent and peripheral charge movements and it fails to accurately measure charge movement at very low P_{OPEN}[170]. The best known method to determine charge movement has been measurement of gating current to derive the Q-V. The Q-V fit to a two state Boltzmann model determines the fraction of charge moved with change in voltage and informs whether small or large changes in voltage are needed to affect function or structural changes

in the protein[93,169,188]. A recent report indicates that two state Boltzmann fits to a Q-V also has limitations, based on the inaccuracy of estimates for total charge that likely moves in multiple transitions[183]. Nevertheless, these methods are reasonable approximations for channel activity and when combined can be used to reveal coordinated mechanisms of electromechanical coupling that link voltage sensing to pore opening.

The ability to experimentally separate the Q-V from the P_{OPEN}-V (Fig 7), led to a few important discoveries that shape our understanding of electromechanical coupling. A classic study by Ledwell and Aldrich uncovered a mechanism for the cooperative coupling of charge movement to pore opening during K^+ channel activation[189]. Two mutant K^+ channels were used that had S4 segments perturbed, either by chimeric substitution (Shaker/Shaw K^+ channel chimera) or by combined site mutations on S4 (Shaker 'ILT'; V369I, I372L and S376T). The 'ILT' and Shaker/Shaw mutants created differential changes in the position of the Q-V relative to P_{OPEN}, demonstrating that the coupling of VS domain activation to pore opening can be disrupted[189]. Coupling is therefore based on a coordinated transition in which all VS domains must be activated, that then act together in one concerted step to open the pore domain[189]. Hv1 lacks the typical pore domain found in K^+ channels, and this raises a fundamental question: Is there a form of electromechanical coupling between initial voltage sensor activation and 'aqueous' channel opening in Hv1?

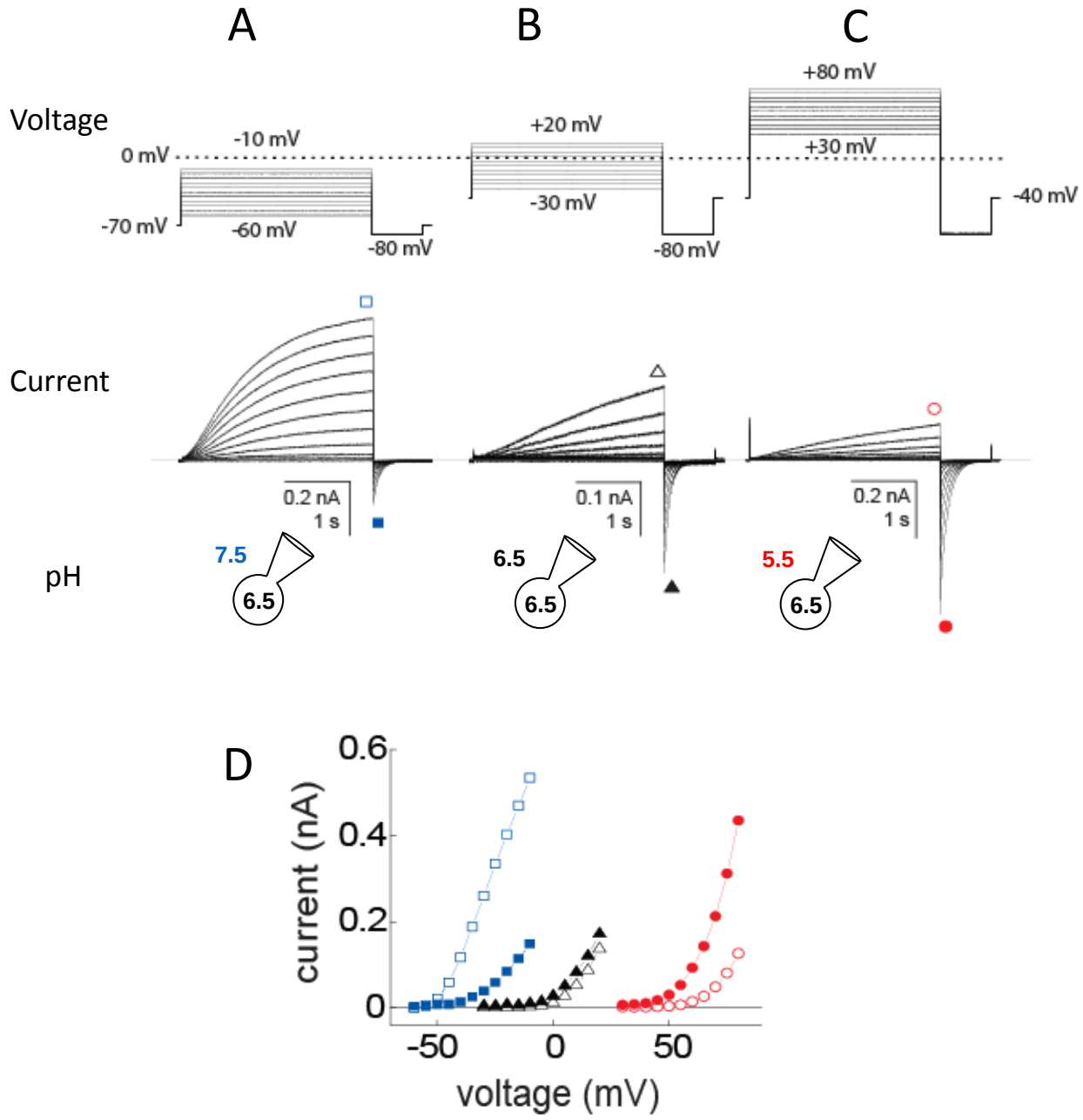

Figure 8. Voltage and pH dependent gating of Hv1.
Depolarizing voltage steps (10mV increments) were applied to an Hv1-transfected HM1 cell to elicit outward currents and deactivating inward tail currents. pH_I5.5 for A-C. Dotted line is zero current level. **A.** pH_O7.5; HP= -70mV (V_{STEP}= -60mV to -10mV); V_{TAIL} = -80mV. **B.** pH_O6.5; HP = -70mV (V_{STEP}= -30mV to +20mV), V_{TAIL}= -80mV. **C.** pH_O5.5; HP =-70mV, (V_{STEP}= +30mV to +80mV), V_{TAIL}=-40mV. **D.** Current voltage relations in 3 pH_O. I_{STEP} (Open symbols) and absolute values of I_{TAIL} (filled symbols) for A-C, current measured at symbol placements on traces. Notice the ~40mV/pH shift in I_{STEP}-V and I_{TAIL}-V with change in pH_O. Figures are reproduced from Ramsey et. al (2006).

Voltage dependent gating in Hv1 is a variable property that depends on transmembrane [H^+] gradient. A Q-V for Hv1 is not reported, creating a major limitation in describing early voltage dependent transitions. Limiting slope analysis of the G_{vH^+}-V relation estimates gating a valence of ~6.0 elementary charges for Hv1[23,49,190]. The P_{OPEN}-V relation in Hv1 is estimated from tail current (I_{TAIL}) analysis and threshold of activation (V_{THR}) approximations[23,49,190]. Visual inspection of current traces is used for estimation of V_{THR}. Because Hv1 can demonstrate a Cole-Moore effect, proposed state models suggest that it visits multiple closed states before transition to the activated state ($C_1 \leftrightarrow C_2 \leftrightarrow O$)[25]. Early transitions that might describe the electromechanical coupling of VS domain activation to opening of the aqueous H^+ conductance G_{AQ}, are not well understood.

The effect of changing pH on Hv1 gating is evidenced by the shift in P_{OPEN}-V in function of transmembrane pH gradient (ΔpH), as seen in Figure 8. This figure, taken from Ramsey, et al. (2006), displays current traces from heterologously expressed in Hv1, where permeant ions such as K^+, Na^+, and Ca^{2+} are removed from pipette and recording solutions to measure relatively pure H^+ currents[20]. Hv1 has slow kinetics of H^+ current activation (Section 2, Fig. 8) and thus lengthy depolarizations are required to reach maximal steady state proton current. The outward rectifying current-voltage relation (I-V) for Hv1 is measured from steady state currents[20]. Steady state proton currents are subject to changes in amplitude due to proton depletion and repletion effects, even with proton buffers as high as 100 – 200 mM in the recording solutions[10,27]. In whole cell patch clamp experiments, depletion is thought to result from Hv1 mediated H^+ efflux from the cell that occurs faster than buffer molecules can diffuse enough H^+ to restore internal pH[10,27]. It is important to note that Hv1 gating kinetics, P_{OPEN}-V and steady state currents are all affected by ΔpH.

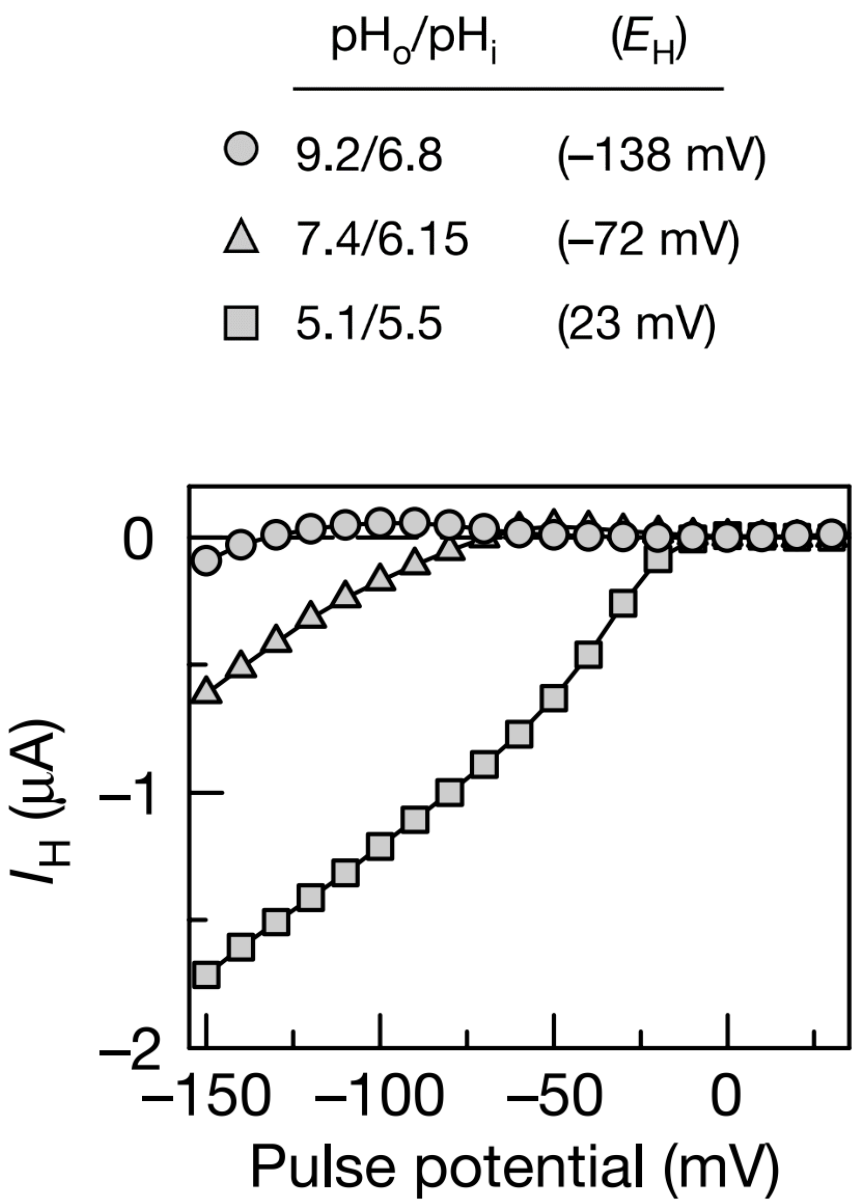

Figure 9. Shaker K^+ channel R362H I-V relations at different pH gradients.
Steady state proton (H^+) currents from the R362H Shaker channel. Currents were measured from a cell-attached macropatch on a perforated oocyte. Holding potential= 0mV (V_{STEP} = +30mV to -150mV). The pH gradient (pH_O/pH_I) and expected reversal potentials are designated above plot. Figures are reproduced from Starace et al. (2004).

Few studies have demonstrated pH sensitivity of early voltage dependent transitions. A few reports demonstrate the effects of extracellular [H^+] on channel opening in voltage gated ion channels such as: Na^+ channels (NaChBac)[191], Ca^{2+} channels (Cav 1.2; and Cav 3.3)[192,193], K^+ channels ('M-current' KCNQ2+KCNQ3[194]; and Slo3[195,196]). However, it is not known if the effects from either high or low extracellular [H^+], are manifested by pH sensitivity of the Q-V relation. pH effect on the Shaker Q-V is illustrated in Figure 9, taken from a Starace and Bezanilla (2004) histidine scanning study[122]. The voltage at which R362H 'shuttle' current turns on, shifts to more positive potentials with decreasing external pH (pH_O)[122]. At pH_O7.4, the R362H proton current turns on at approximately -80mV, whereas at pHo5.1, the currents turn on at approximately -30mV, demonstrating a displacement of about 20mV per pH unit[122]. The authors note a that a small positive shift with low pH_O was observed for the non-mutated Shaker Q-V and a shift of about ~13mV per pH unit was observed for R365H currents[122]. But, it was concluded that the positive shifts along the voltage axis with decreasing pHo result from surface-charge screening by external protons[122]. Charge screening has been described as the ability of ions to influence local electric fields by setting up charges near the membrane-solution interface, thus biasing the electric field[35,197]. Charge screening effects can also result from direct binding of ions to any charged externally exposed residue, thus influencing how a proteins function or sense changes in the field[35,198]. In either case, the net result of charge screening by H^+ or any other ion, is a measurable effect on ion channel voltage gating and none of the effects from multivalent ions or pH changes can be described in full as local potential changes[35]. It seems plausible that the gating effect in Shaker R362H 'shuttle current' and Q-V are relating a pH sensitive mechanism in VS domain activation.

Opening of the aqueous H^+ conductance (G_{AQ}) in Hv1 is unclear because it lacks a discernable pore domain and leaves to question what constitutes the gate. A recent voltage clamp fluorimetry study, suggests that an early voltage dependent transition occurs prior to G_{AQ} activation, but there is yet no report of a Q-V or any proxy of voltage sensing for comparison[199]. Much experimental information about gating has been derived from mutagenesis of S1-S4 residues. Ramsey, et al. (2010) combined homology modeling and mutagenesis to target ionizable residues that might gate or transport H^+ [94].

Modeling and MD simulations revealed organization of conserved polar and charged residue side chains into two clusters within the central crevice[94]. Mutagenesis of residues in the internally exposed cluster shifted V_{THR} negatively, whereas mutagenesis of residues on the externally exposed cluster shifted V_{THR} to positive potentials[94]. MD simulations suggests that network interactions among side chains work in concert to gate the aqueous H^+ pathway[94]. One particularly striking result was seen in current traces elicited from the N214R mutation. Outward current at depolarized potentials was exceedingly small, but robust time dependent tail currents could be seen at a negative potential[94]. Similar results from previous reports were noted[135–137]. The lack of outward current suggests a depolarization dependent pore block that is relieved by voltage step to a negative potential[94]. Interestingly, the voltage dependence and kinetics of H^+ current activation varied widely among the mutant channels, but all retained ΔpH sensitivity[94]. Mutations at R205 and R208 produced only small shifts in V_{THR}, but faster gating kinetics were observed[94]. Other studies demonstrate that individual or combined truncations of the C-terminal and N-terminal domain dramatically speed G_{vH^+} activation but do not shift the G_{vH^+}-V relation[125,137].

In summary, the physiological roles proposed for H^+ channels are distinctly reliant on robust H^+ flux that can be discriminately controlled by either voltage or transmembrane $[H^+]$. Thus the biophysical features of Hv1 are of paramount importance to its function in physiology. Unlike other voltage gated channels, Hv1 lacks an S5-S6 type pore domain, indicating that the highly selective H^+ 'pore' lies within the central aqueous crevice of the voltage sensing domain. Limiting slope analysis estimates a gating valence for G_{vH^+}, however, no Q-V is reported. Hv1 can exhibit a Cole-Moore Effect, indicating that early transitions in the activation pathway must exist. These early transitions in the gating pathway have yet to be elucidated and represents a major gap in our understanding of gating the aqueous H^+ conducting pathway.

7. Major outstanding research questions and experimental strategy

The most important difference between Hv1 and the voltage sensor (VS) domains of other VGCs is the existence of an 'aqueous' H^+ permeation pathway within the VS domain of Hv1[94,124]. Our goal is to understand how voltage sensing controls H^+ channel opening. The lack of a direct method to assay early steps in the Hv1 activation pathway has represented a major obstacle to understanding the mechanisms of VS activation and pH sensitive gating in Hv1. In other VGCs early transitions represent VS activation (Q-V) that is coupled to the opening of a structurally distinct pore domain (P_{OPEN}-V) [5,156]. Early and late transitions can determined by comparing the Q-V with the P_{OPEN}-V (Fig. 7), Thus voltage sensing precedes channel opening but importantly, VS activation is coupled to pore opening[35,170,186,187].

We adopted an experimental strategy that was first developed by Starace and Bezanilla[121–123,156], where the first S4 Arg of Shaker K^+ channel VS domain is replaced by His (R362H) to mediate voltage-dependent H^+ transport that reports VS activation. Because Hv1 shares homology to Shaker VS domain, we hypothesize that a similar Arg>His mutation in Hv1 (R205H) will elicit a resting-state 'shuttle' H^+ current in that will report structural changes correlated with VS activation. We predict that the voltage dependence of R205H resting-state 'shuttle' currents will report early voltage-dependent transitions that occur prior to opening of the 'aqueous' H^+ conducting pathway in Hv1.

The N214 position on the Hv1 S4 is located one helical turn lower than the last Arg of S4 R211 (i.e. R205, R208, and R211 in human Hv1). The N214R substitution has been reported to dramatically reduce outward H^+ current in Hv1[94,116]. Evidently, the block is relieved at negative potentials[94]. We make this mutation in the background of R205H to test whether we can measure resting-state 'shuttle' currents at negative potentials, and observe block of the intrinsic 'aqueous' currents at positive potentials. We expect that outward block of 'aqueous' H^+ conductance will allow 'shuttle' H^+ conductance to be measured in isolation. The Shaker R362H mutation was made in the background of a non-conducting (W434F)[157], non-inactivating (IR, Δ6–46)[158] mutant[121–123,156] and similarly we expect that R205H-N214R will permit resting-state H^+ 'shuttle' currents to flow at negative potentials but exhibit N214R mediated

block of outward 'aqueous' H^+ current at positive potentials. With effective isolation of the resting-state 'shuttle' H^+ current from the 'aqueous' H^+ current, we can further test the hypothesis that the voltage-dependent transition reported by the R205H-N214R is insensitive to changes in the pH gradient.

Aspartate 185 is located in the S3 segment toward the extracellular end. This location appears to correspond to the S3b portion of S3 that contributes to the paddle structure seen in X-ray crystal structures of voltage-gated K^+ channel VS domains solved by the MacKinnon laboratory[75,76,83,110]. However, an Asp at this position is conserved only in Hv1 orthologues (Fig 1). In the background of WT Hv1, the D185A mutation was reported to shift 'aqueous' pathway opening by about +70mV[94]. We combined two different substitutions at this position with the R205H mutation discussed previously, to test if D185 mutations also shift gating in R205H-D185A/H double mutations. We expect that the D185A/H mutations will shift 'aqueous' opening substantially toward more positive potentials but will not affect resting-state 'shuttle' currents at negative potentials. Thus, we can separate 'shuttle' currents gating from 'aqueous' pathway gating but retain the ability to measure both pathways in the same protein.

If the R205H 'shuttle' gating represents early transitions, then we can test whether Hv1 possesses a form of electromechanical coupling that links VS activation with opening of the 'aqueous' pathway. Ledwell and Aldrich[189] demonstrated that by mutating hydrophobic residues V369I, I372L, and S376T (ILT) in S4 of Shaker, they could differentially separate the voltage dependence of charge movement (Q-V) from pore opening (P_{OPEN}-V). Using the R205H-D185A/H double mutant in Hv1, we test whether the early voltage-dependent transition reported by 'shuttle' gating is shifted relative to voltage dependence of D185A/H 'aqueous' pore opening. We expect that VS activation and 'aqueous' pore opening are two separable mechanisms and that voltage sensing precedes channel opening on a voltage axis. We expect that we can further separate 'shuttle' gating (voltage sensing) from the 'aqueous' pathway opening either by changing the pH gradient (Fig. 8d) or adding second-site mutations.

Mutations of a conserved aspartate residue in S1 (D112) were shown to perturb the normally exquisite H^+ selectivity of Hv1[166,167]. D112 mutations also either shift voltage-dependent opening of G_{AQ}

[166,167] or abrogate G_{AQ} entirely (D112V) [166,167]. It remains unclear whether the effects of D112V result from a perturbation of the H^+ conducting G_{AQ} pathway or disruption of a gating transition that is required to open G_{AQ}. We make the R205H mutation in the background of D112V to measure 'shuttle' currents that will distinguish the effects of this mutation as either gating defect or perturbation of the H^+ conducting pathway.

A Hv1 homology model based on the X-ray crystal structure of the Kv1.2-2.1 chimera [94] was used to select candidate residues within the aqueous crevice that line the constriction point of the hydrophobic interior of Hv1. We do histidine scanning mutagenesis on select residues of S1-S4 in Hv1 that we predict. The expectation is that histidine mutagenesis of selected residues will create resting-state H^+ 'shuttle' currents at hyperpolarized membrane potentials, just as His substitutions at positions in S1 and S2 of the Shaker K^+ VSD were found to yield resting-state H^+ 'shuttle' currents[106,121–123,156]. Considering the spatial constraints of H^+ hopping[10,27,94,143–145], the His mediated H^+ shuttle currents allow for improved resolution of structural constraints over other methods[119,120]. Candidate residues S1-S4 listed here are mutated to Histidine for voltage clamp experiments: **S1**: L108, V109, L111, L114; **S2**:I146H, L147; **S3**: V177, V178; **S4**:I202, R205. Estimations of VSD resting state structure as well as gating distances of TMs (S1 ~5Å, S2 (~10Å), S3 (~15Å), S4 (~2-20Å)[119,120], provide useful information but are subject to experimental limitations. We expect the results from His scanning will inform a structural model for Hv1.

c15of27 is an uncharacterized protein that shows distinct sequence homology to Hv1 and homology to VS domains of other proteins in the 6TM family of ion channels. A unique feature of c15of27 is that it appears to have a large C-terminal globular domain attached to a voltage sensor, similar to the voltage activated phosphatase Ci-VSP. The predicted protein c15of27, has homology to Hv1 the human voltage gated proton channel. The proposed experiments will allow us to determine whether c15of27 possesses authentic voltage-sensor function and to compare it to other known VSDs that are predicted to have homologous function (i.e. Shaker, Hv1, Ci-VSP, etc.). We expect that the novel uncharacterized c15of27

functions as a voltage sensor that is homologous to VGCs and other VS domain proteins such as Ci-VSP and Hv1.

By focusing explicitly on the biophysical aspects of VS mechanisms in Hv1 we attempt to separate VS sensing 'shuttle' and 'aqueous' gating into two separate events in the activation of voltage sensing proteins. It is not known if voltage sensing in Hv1 is governed exclusively by membrane potential or involves changes in pH gradient. Gating is thought to be a variable property in Hv1 that is influenced by local proton concentration (pH) but little is known about early transitions that may be voltage- or pH-dependent. This R205H histidine mutagenesis approach will be used to assay the voltage-dependence of two distinct components of S4 movement via proton 'shuttle' conductance and 'aqueous' H^+ pathway opening.

CHAPTER II

EXPERIMENTAL METHODS

1. Molecular biology

For expression in *Xenopus laevis* oocytes, human Hv1 cDNA (Accession No. NP_115745) was subcloned from pQBI25-fC3 (Ramsey, et al. 2006) as a HindIII/NotI fragment into the expression pBSTA plasmid (kind gift of C. A. Villalba-Galea[84] containing a T7 promoter upstream of *Xenopus* β -globin 5'-UTR sequence followed by a Kozak translation initiation site at the 5' ATG for the enhanced green fluorescent protein (EGFP) cDNA and *Xenopus* β-globin 3'-UTR sequence. Overlap-extension PCR was used to construct Ci-VSP (Accession No. BAD98733) N-terminus1-107:88-STOP hHv1 chimeras to improve expression in oocytes. Cycling parameters were 98°C for 1 minute followed by 21 cycles of 98°C for 1 minute, 55°C for 1 minute, and 72°C for 5 minutes. Products were resolved by agarose gel electrophoresis, purified, and ligated into expression vector pBSTA. Constructs were verified by sequencing as described below. Hv1 cDNA constructs were subcloned as SpeI/XbaI fragments 3' and in frame with EGFP for *in vitro* transcription of sense mRNA encoding an N-terminal EGFP-Hv1 fusion protein (subsequently referred to as Hv1). For tetracycline-inducible expression in stable mammalian cell lines, EGFP-Hv1 was subcloned from pBSTA as a HindIII/NotI fragment into pcDNA5/FRT/TO (Life Technologies) in which the expression of N-terminal EGFP fusion (EGFP-hHv1) proteins are regulated by tetracycline. For tetracycline-inducible expression of c15orf27 (NM_152335) EGFP-c15orf27 was subcloned from pBSTA as a HindIII/NotI fragment into pcDNA5/FRT/TO. The pBSTA HindIII/NotI fragment was also subcloned into pQBI25-fC3 for transient expression of an N-terminal GFP-tagged human Hv1 (GFP-hHv1). Site-directed mutagenesis was done with high fidelity PCR kits, (Phusion by Finnzymes). DNA sequencing to confirm mutations was done at VCU Nucleic Acids Research Facilities

(NARF) in ABI 3730xl DNA analyzers. DNA sequences were analyzed with SeqBuilder software (DNASTAR Lasergene 8). The cDNA was transfected using Lipofectamine 2000. Cells were lifted by trypsinization 12-24 hrs after transfection and plated onto glass coverslips in culture medium for whole-cell patch clamp electrophysiology 12-48 hrs later.

2. Expression in Xenopus oocytes.

Plasmid DNA (pBSTA) was linearized with Not I restriction enzyme. Linearized DNA was purified by Qiagen PCR Purification columns (Qiagen) and eluted in nuclease-free H_20 to make RNA using the mMessage mMachine T7 RNA polymerase (Ambion) transcription kit. The hHv1 constructs (made in the background of Ci-VSP 1-107/Hv1 88-STOP chimera) were expressed in *Xenopus* frog Stage V and IV oocytes for excised patch recordings. Oocytes were injected with 3-25ng of mRNA and incubated at 16ºC for 2-5 days before experiments in saline oocytes solution containing (mM): 100 NaCl, 2KCl, 1.8 $CaCl_2$, 1 $MgCl_2$, 10 HEPES, 0.1 EDTA, 2 Na-Pyruvate buffered to pH7.4 with NaOH. Electrophysiological recordings were done at 20 ± 0.5ºC. The recordings were done with an AM systems patch clamp amplifier. To generate command voltage pulses and digitize data, a National Instruments data acquisition device DAQ (IN USB-6221) was used in conjunction with custom LabVIEW-based acquisition software (*JustAcquire*; C. A. Villalba-Galea, details available upon request) running on a PC computer. Currents were acquired at 200-1000 μs/point and digitized at 10-200 μs/point. Experimental data was converted to ascii format using a custom Java-based application (*JustAnalysis*; C. A. Villalba-Galea, details available upon request) and analyzed using Clampfit9 (Molecular Devices) and Microcal Origin 6.0 (Microcal). Macropatch oocyte clamp was performed using an A-M Systems model 2400 patch clamp amplifier. Recording solutions as are described for mammalian cells, except that the pipette solution contained the extracellular recording solution (typically pH6.5) and the bath contained the intracellular recording solutions at various pH.

3. Expression in mammalian cell lines

Creation of isogenic tetracycline-inducible cell lines was achieved by transfection of pcDNA cDNA5/FRT/TO plasmids containing the indicated Hv1 constructs together with a Flp recombinase expression construct in the pOG44 plasmid (Life Technologies) into Flp-In 293 T-REx (Life Technologies) cells using Lipofectamine 2000 (Life Technologies) and selection in Hygromycin B (100 µg/ml) for >3 weeks. In some experiments, GFP-Hv1 constructs in pQBI25-fC3 (Ramsey, et al. 2006) were transiently expressed in either HEK-293 and 293T cells by Lipofectamine 2000 transfection. Flp-In 293 T-REx, HEK-293 and 293T cells were cultured in DMEM:F12 (Hyclone) supplemented with 10% certified tetracycline-free fetal bovine serum (Atlanta Biologicals) and 10 U/ml Penicillin-Streptomycin (Hyclone). Transfected cells were lifted by trypsinization and plated on glass coverslips in culture medium for whole-cell patch clamp electrophysiology 12-48 hr later. Expression of Hv1 in Flp-In 293 T-REx cells was induced by addition of 0.5-1 µg/ml tetracycline to the culture medium and assessed 24-48 hours later by EGFP epifluorescence excited by a broad-spectrum source (X-Cite 120, EXFO) directed via fiber optic cable to an upright microscope (AxioExaminer, Zeiss) equipped with an appropriate dichroic mirror and filter set (49002, Chroma). Whole-cell H^+ currents were measured at 22-24°C with a 5 kHz low-pass analog filter using a A-M Systems model 2400 amplifier. Data were acquired and analyzed as described for excised patch. Intracellular and extracellular solutions contained: 100 mM pH buffer used near its pKa (MES, pH 5.5; Bis-Tris, pH 6.5; HEPES, pH 7.5), 1 mM EGTA, 8 mM HCl and pH was adjusted using TMAOH and $HMeSO_3$ to a final osmolality of 310-320 mOsm. Data was analyzed using ORIGIN 6.0. In experiments where Zn^{2+} was used, the bath and pipette solutions contained (in mM) 100 Bis-Tris, pH 6.5; 0.1 EGTA, 5 $MgCl_2$ (310-320 mOsm) and an acidified 1 M $ZnCl_2$ solution was serially diluted to in the recording solution to achieve the desired final concentration. Free [Zn^{2+}] was calculated using WEBMAXC (http://maxchelator.stanford.edu/downloads.htm). Liquid junction potential correction and series resistance compensation were not applied. I_{STEP} represents the mean current during a 5-10 ms

interval near the end of a variable voltage step where the current had apparently reached steady-state; the amplitude of I_{TAIL} was determined by extrapolation of single exponential fits of the deactivating current at a fixed potential to the instant at which the voltage was changed. V_{THR}, the apparent threshold for activation of I_{TAIL} was estimated from visual inspection of I_{TAIL} as previously described[20,23]. Steady-state conductance (G_{STEP}) during voltage steps was calculated from $G_{STEP} = I_{STEP}/V\text{-}V_{REV}$ where V_{REV} is the zero-current potential determined from inspection of the I_{STEP}-V relation and V is the voltage at which I_{STEP} was elicited. In some experiments, we changed V_{TAIL} (after V_{STEP} to a fixed potential) to determine V_{REV} of tail currents as previously described[20,23].

Chapter III. Results

1. Electrophysiological properties of R205H His mutant Hv1 proteins

To examine VS activation in Hv1, we mutated the first S4 arginine in Hv1 was to histidine (R205H) and measured currents elicited by voltage steps over a wide range of potentials. Figure 10 shows whole-cell currents elicited by voltage steps from -130 mV to +100 mV in WT Hv1 and R205H mutant under symmetric pH conditions (pH_I6.5/pH_O6.5) after tetracycline induction of protein expression in a stably transfected Flp-In 293 T-REx cell lines (see Methods). As reported previously, WT Hv1 produces no current at negative voltages, when channels are closed, but steps to voltages more positive than E_{H^+} elicit time-dependent outward H^+ currents (I_{STEP}); R205H also mediates I_{STEP} (Fig. 10B). The main differences between I_{STEP} in WT Hv1 and R205H are that the currents activate faster in R205H and appear to monotonically rise toward steady-state, while outward currents in WT Hv1 activate more slowly exhibit a prominent sigmoid-shaped time course (Fig. 10A, B).

The mean I_{STEP} measured over the last 5 ms of the voltage pulse plotted as a function of membrane potential (I_{STEP}-V) shows that in WT Hv1, outward rectifying currents begin to increase at depolarized potentials, and only small linear leak currents are measured at negative potentials. In marked contrast to WT Hv1, R205H mediates prominent steady-state inward currents at hyperpolarized membrane potentials (Fig. 10B). The inward currents mediated by R205H are strikingly similar to resting-state currents previously reported in Shaker R362H[121–123,156]. We measure only small inward leakage currents in cells expressing WT Hv1 (Fig. 10C), and Ser or Cys substitutions at the R205 position in Hv1 are insufficient to confer a measurable resting-state current (data shown in Sec. 5). The results here for R205H differ from a previous report by Kulleperuma et al. where the authors observed no resting-state H^+ current at negative voltages[126]. We interpret the difference in results for the R205H mutant to be due to differences in expression levels because current expression in our studies are much

larger than those previously reported[126]. The I_{STEP}-V relation in R205H exhibits double rectification with an apparent plateau at intermediate voltages (~-20 mV to +10 mV) and is different from WT Hv1, where only outward rectification is observed (Fig. 10C). The large inward current seen in R205H at the most negative potentials (Fig 10A,C) decreases with each depolarizing step. The double rectification observed in R205H I_{STEP} is also seen in Shaker R362H that exhibits inward H^+ current and outward K^+ current [121–123,156]. R1 substitution with other residues (R1S>R1C>R1V>R1A) in Shaker and other voltage gated channels (VGCs) produce non-selective cation ('Omega' or 'gating pore') currents in the resting state and outward selective 'alpha currents' in the activated state[103,129,174,176,178]. The most straightforward interpretation for double rectification is that R205H mutation generates a voltage-dependent His-mediated resting state 'shuttle' conductance (G_{SH}) at negative potentials, but does not abolish the intrinsic 'aqueous' conductance (G_{AQ}) at more positive potentials.

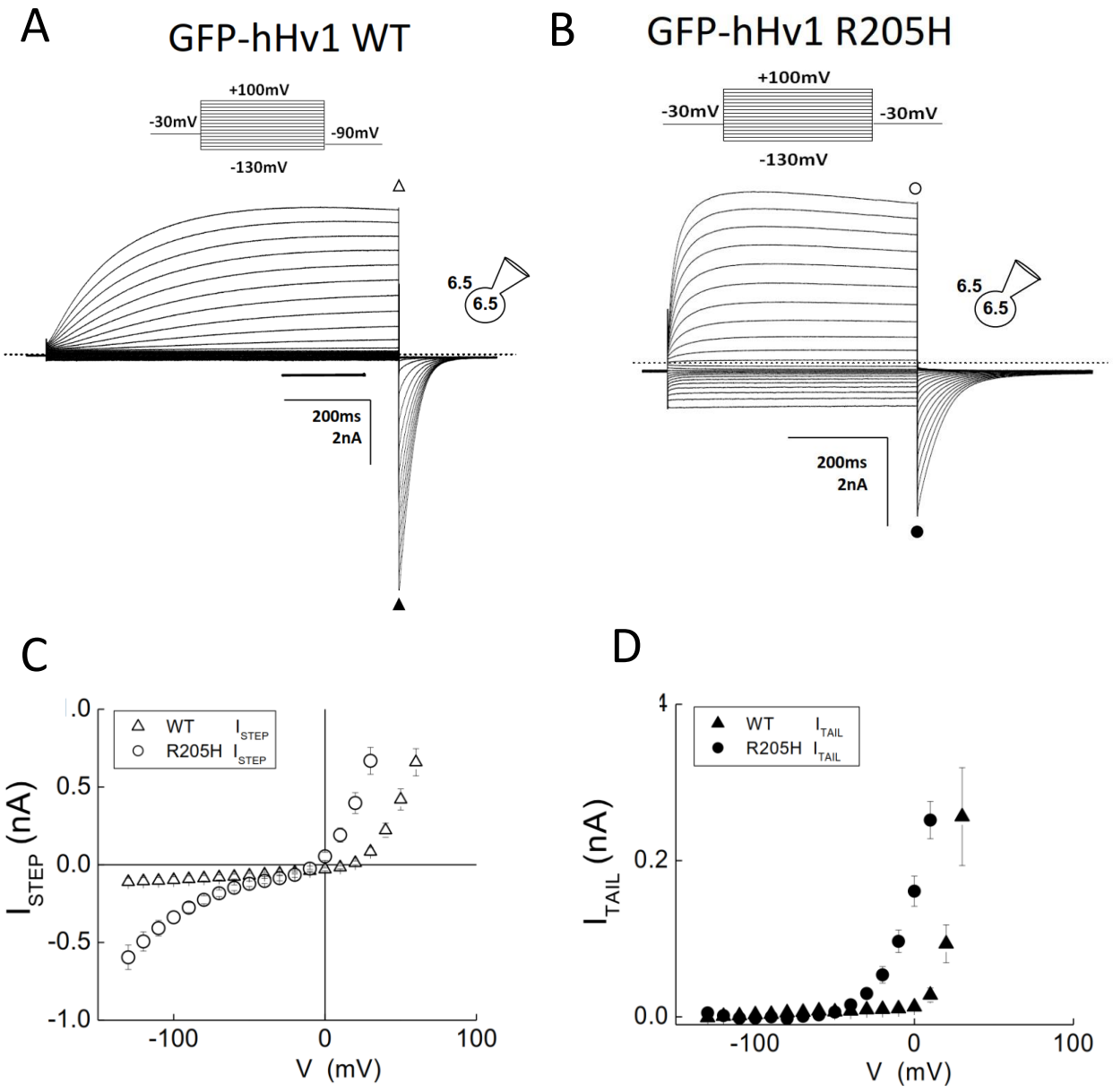

Figure 10. Hv1 R205H confers resting state current 'shuttle' current
A. Representative WT hHv1 current traces from a Flp-In 293 T-REx cell. HP= -30mV (V_{STEP}= +100 mV to -130 mV in 10 mV increments) V_{TAIL}= -90mV, (pH_O = pH_I = 6.5); dashed lines indicate zero current. **B.** Representative Hv1 R205H current traces from a Flp-In 293 T-REx cell. HP= -30mV (V_{STEP}= +100 mV to -130 mV in 10 mV increments) V_{TAIL}= -390mV, (pH_O = pH_I = 6.5); dashed lines indicate zero current. **C.** Steady state proton current (I_{STEP}) voltage dependence (pH_O = pH_I = 6.5). Means ± SEM from *n*=4 WT hHv1 (triangles), *n*=6 R205H (circles). **D.** Tail current (I_{TAIL}) absolute value of linear leak-subtracted current (pH_O = pH_I = 6.5). The full experimental voltage range is reduced to emphasize the difference in the positions of the apparent P_{OPEN}-V relation. Means ± SEM from *n*=6 WT hHv1 (triangles), *n*=6 R205H (circles).

The voltage dependent gating of G_{AQ} was determined from tail current-voltage relations (I_{TAIL}-V). Tail currents were elicited by stepping to a fixed negative potential (V_{TAIL}) after variable pulses and then fit to single exponential over the time course of current decay. Current values taken from the intercept of the fit at time zero of V_{TAIL} were plotted as a function of test potentials to yield I_{TAIL}-V relation. We believe the I_{TAIL}-V relation reports the approximate open probability (P_{OPEN}) for only the aqueous conductance (G_{AQ}). The shape of the I_{TAIL}-V relations clearly shows that in both WT Hv1 and R205H, G_{AQ} is closed at negative voltages and P_{OPEN} evidently rises as the membrane is depolarized (Fig. 10D). The most negative voltage at which channels open is defined as V_{THR}, and it reports the voltage dependence of G_{AQ} opening [10,28]. The voltage range over which G_{AQ} becomes large enough to measure, is shifted toward more negative potentials in R205H (Fig. 10D). We estimated V_{THR} by visually inspecting current records as previously described [10,28]. The mean V_{THR} value was shifted from +10.0 ± 1.5 mV (n = 10) in WT Hv1 to -25.3 ± 1.9 mV (n = 20) in R205H, indicating that the R205H mutation shifts the apparent steady-state $P_{OPEN-AQ}$-V relation negatively by ~40 mV. The outwardly rectifying shape of the I_{TAIL}-V relation in R205H illustrates that G_{AQ} is closed at negative potentials (where G_{SH} is open) and the apparent P_{OPEN} for G_{AQ} rises with increasing depolarization, as reported for WT Hv1 [10,28]. Thus, the addition of a resting-state conductance in R205H does not preclude voltage-dependent gating of G_{AQ}.

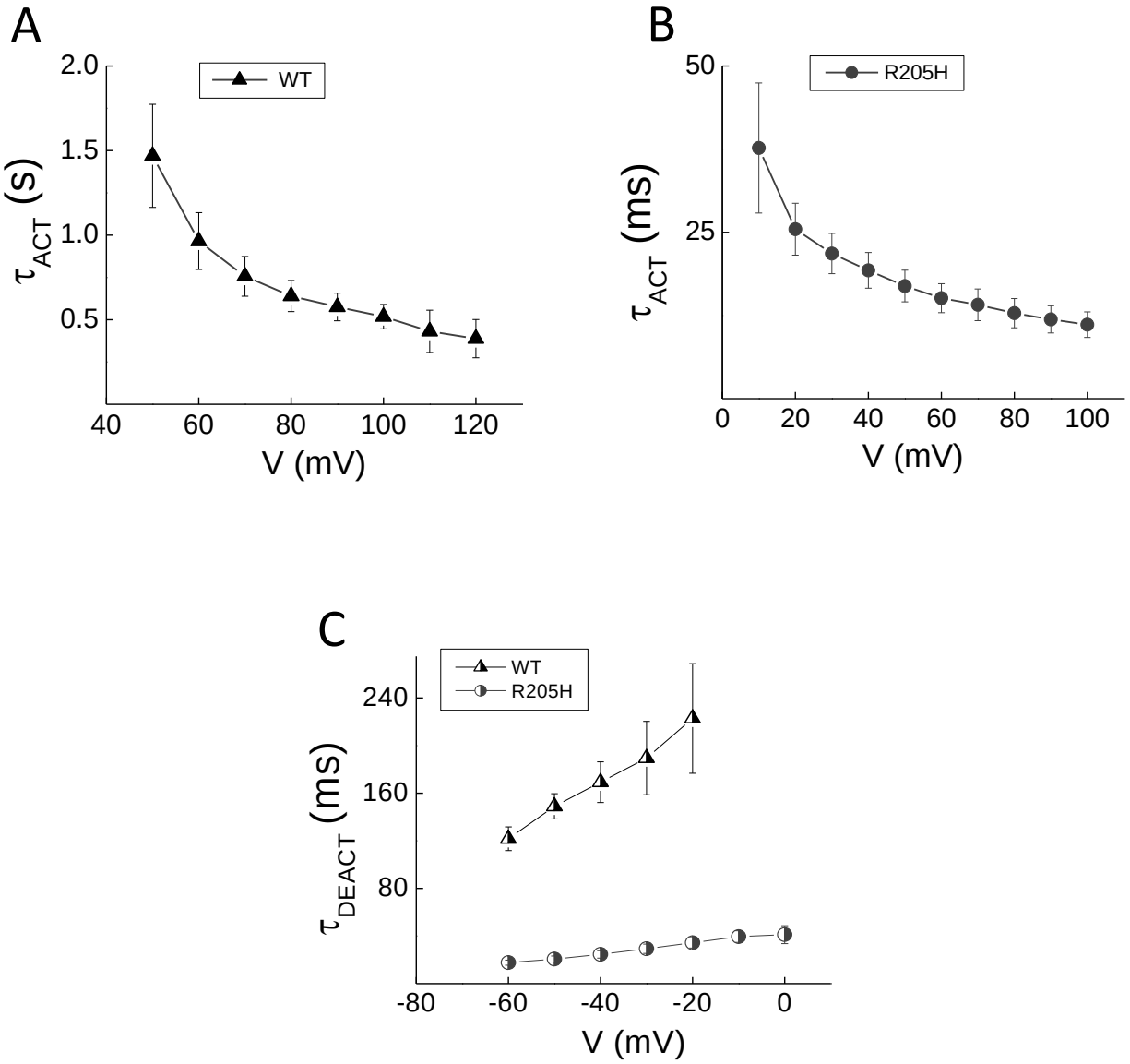

Figure 11. Hv1 R205H and WT Hv1 rate constants for current activation and deactivation
Plot of rate constants for activation and deactivation in function of membrane potential for WT Hv1 and R205H Hv1. **A.** τ_{ACT}–V for WT Hv1. **B.** τ_{ACT} –V for R205H. **C.** τ_{DEACT} –V for WT Hv1 (triangles) and R205H (circles). τ_{ACT} was measured from single exponential fits to outward currents elicited at positive potentials after the initial delay at the onset of current activation. τ_{DEACT} was measured from single exponential fits to tail currents elicited over a range of potentials after an initial fixed depolarizing step (+80mV) to open G_{AQ}. All measurements done in symmetric pH conditions (pH_O = pH_I = 6.5). Notice the decrease in both τ_{ACT} (~40-fold) and τ_{DEACT} (~10-fold) for R205 compared to WT Hv1.

The rate constants for G_{AQ} activation (τ_{ACT}) for R205H and WT Hv1 were measured from single exponential fits to outward currents elicited at positive potentials after the initial delay at the onset of current activation (Fig. 11A,B), as previously reported by the DeCoursey laboratory[24,25]. The rate constants for G_{AQ} deactivation (τ_{DEACT}) were measured from single exponential fits to tail currents elicited over a range of potentials after an initial fixed depolarizing step (+80mV) to open G_{AQ}. Both τ_{ACT} and τ_{DEACT} are strongly voltage-dependent for both constructs. In both WT Hv1 and R205H , τ_{ACT} decreases monotonically with depolarization, but the τ_{ACT} for R205H is nearly 40-fold smaller than WT Hv1 at every voltage analyzed (Fig. 11A,B). τ_{DEACT} also decreases monotonically with increasingly negative potential for both In R205H and WT, but τ_{DEACT} is is approximately 10-fold smaller at all potentials analyzed for R205H than it is for WT (Fig. 11C). The faster kinetics of activation and deactivation seen in R205H are consistent with the effect of neutralizing mutations at the R205 position in both human and mouse Hv1 channels [20,21]. The full τ_{ACT}-V relation for resting-state current activation is not plotted because the rapid activation and residual capacitive current prevented an unambiguous analysis of current kinetics; nonetheless, it is clear that activation of I_{STEP} at negative voltages in R205H is faster still than that which is measured at positive voltages (at -200 mV, estimated $\tau_{ACT} = 1.3 \pm 0.2$ ms, n = 4).

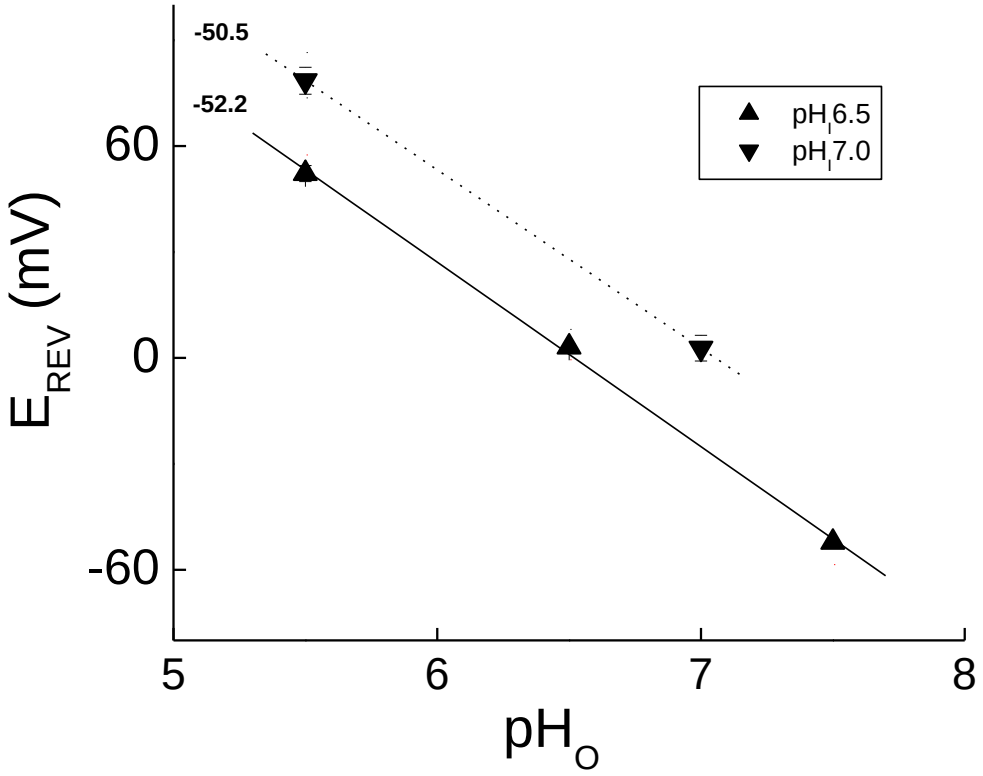

Figure 12. R205H mutant retains H^+ selective conductance Hv1 R205H is H^+ selective
I_{TAIL} was measured at various voltages after opening G_{AQ} by depolarization to a fixed potential at various pH_O and the reversal potentials (V_{REV}) were determined from mono-exponential fits to the decaying I_{TAIL} as previously described[23]. Data represent means ± SEM from n = 4-10 (pH_O6.5, n=8; pH_O5.5 n=10; pH_O7.5, n=2) cells. Lines represent linear fits to the mean V_{REV} values and demonstrate shifts of 52.2 mV/pH unit (pH_I6.5, solid black line) and 50.5 mV/pH unit (pH_I7.0, dashed gray line), both of which are close to the expected value for a H^+-selective conductance predicted by the Nernst equation (~56 mV/pH unit under our recording conditions).

Ion selectivity of G_{AQ} in R205H was determined by first stepping to a fixed depolarized potential to open G_{AQ}, and then measuring the reversal potential (E_{REV}) of I_{TAIL} at various voltages, as described previously [20,21]. E_{REV} measured at various pH gradients is plotted as a function of extracellular pH (pH_O) and the data fit to a straight line (Fig. 12). The slope of the E_{REV} vs. pH_O relation reflects the relative selectivity of the measured conductance for H^+ vs. other ions. A perfectly H^+-selective conductance (i.e., E_{REV} = Nernst potential for H^+) will exhibit a slope of -56 mV/pH unit on the plot shown in Figure 12 under our recording conditions. At pH_I6.5, we calculate a slope factor of 52.2 mV/pH unit, and at pH_I 7.0 the slope is 50.5 mV/pH unit (Fig. 12). Both slopes are similar to the Nernst prediction, indicating that the H^+ selectivity of G_{AQ} in R205H is similar to WT Hv1 [20,21].

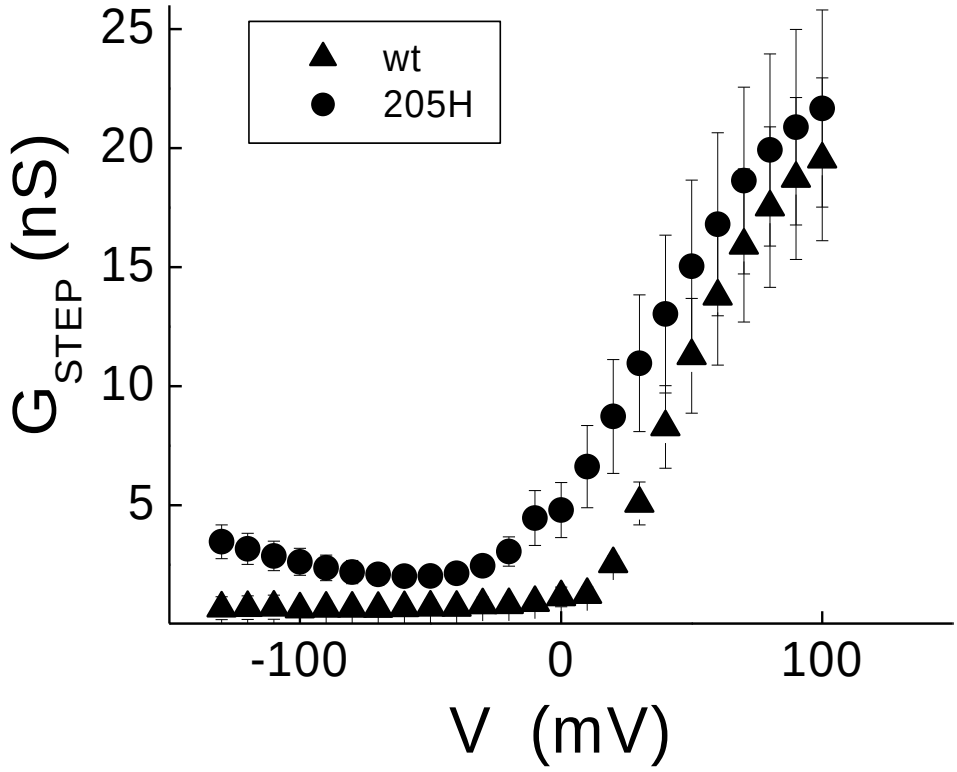

Figure 13. Conductance-votlage relations for WT Hv1 and Hv1 R205H.
Calculated conductance is plotted as a function of step voltage (G_{STEP}–V). Symbols represent means ± SEM; n=4 for Hv1 WT (triangles) and n=6 for R205H (circles). Note that the R205H G_{STEP}–V relation is U-shaped (biphasic), and the amplitude of G_{SH} at negative potentials is smaller than G_{AQ} at positive potentials. All experiments done in symmetric pH conditions ($pH_O = pH_I = 6.5$).

We next calculated membrane conductance from steady-state I_{STEP} measured at various potentials ($G_{STEP} = I_{STEP}/V\text{-}V_{REV}$, where V_{REV} is the observed current reversal potential for I_{STEP}) and plotted G_{STEP} as a function of membrane potential to reveal the conductance-voltage (G_{STEP}-V) relation. A plot of the mean G_{STEP}-V relations for WT Hv1 and R205H shows that the shapes are distinct (Fig. 13). The G_{STEP}-V for WT Hv1 is flat at negative potentials and rises at positive voltages, as previously reported[8]. The G_{STEP}-V for R205H in contrast is biphasic, with a U-shape; the arms of the U are not equally tall (Fig. 13). The U-shaped G_{STEP}-V relation in R205H suggests that two conductances with distinct voltage dependencies contribute to the total conductance and potentially explains the doubly-rectifying I_{STEP}-V for R205H. In order to conceptually discriminate G_{AQ} from the resting-state H^+ conductance in Hv1 R205H, we operationally define G_{SH} (the H^+ 'shuttle' conductance) as that which produces channel-like steady-state inward currents at negative voltages where the voltage sensor (VS) is likely to be in its resting state (Fig. 10A). We extend the definition of G_{SH} to include Arg to His substitutions in other VS domain-containing proteins that have similar biophysical features [121–123,156]. The non-zero minimum conductance at the bottom of the U-shape can be explained if voltage-dependent closure of G_{SH} is not complete at potentials where the voltage-dependent activation of G_{AQ} becomes measurable. Thus the R205H G_{STEP}-V at intermediate voltages may reflect a 'window current' contributed by G_{SH} and G_{AQ} in addition to any membrane leakage current. V_{THR} for G_{AQ} in R205H is near -40 mV (Fig 10D) and the observed minimum conductance (G_{MIN}) is larger in R205H than WT (Fig. 13). We interpret the difference in G_{MIN} between WT and R205H observed near -40 mV to result from both 'window current' and leakage current. The most parsimonious explanation for a U-shaped G_{STEP}-V is that the 'shuttle' conductance is reporting a voltage dependent transition that takes place early in the activation pathway relative to the opening of the 'aqueous' conductance.

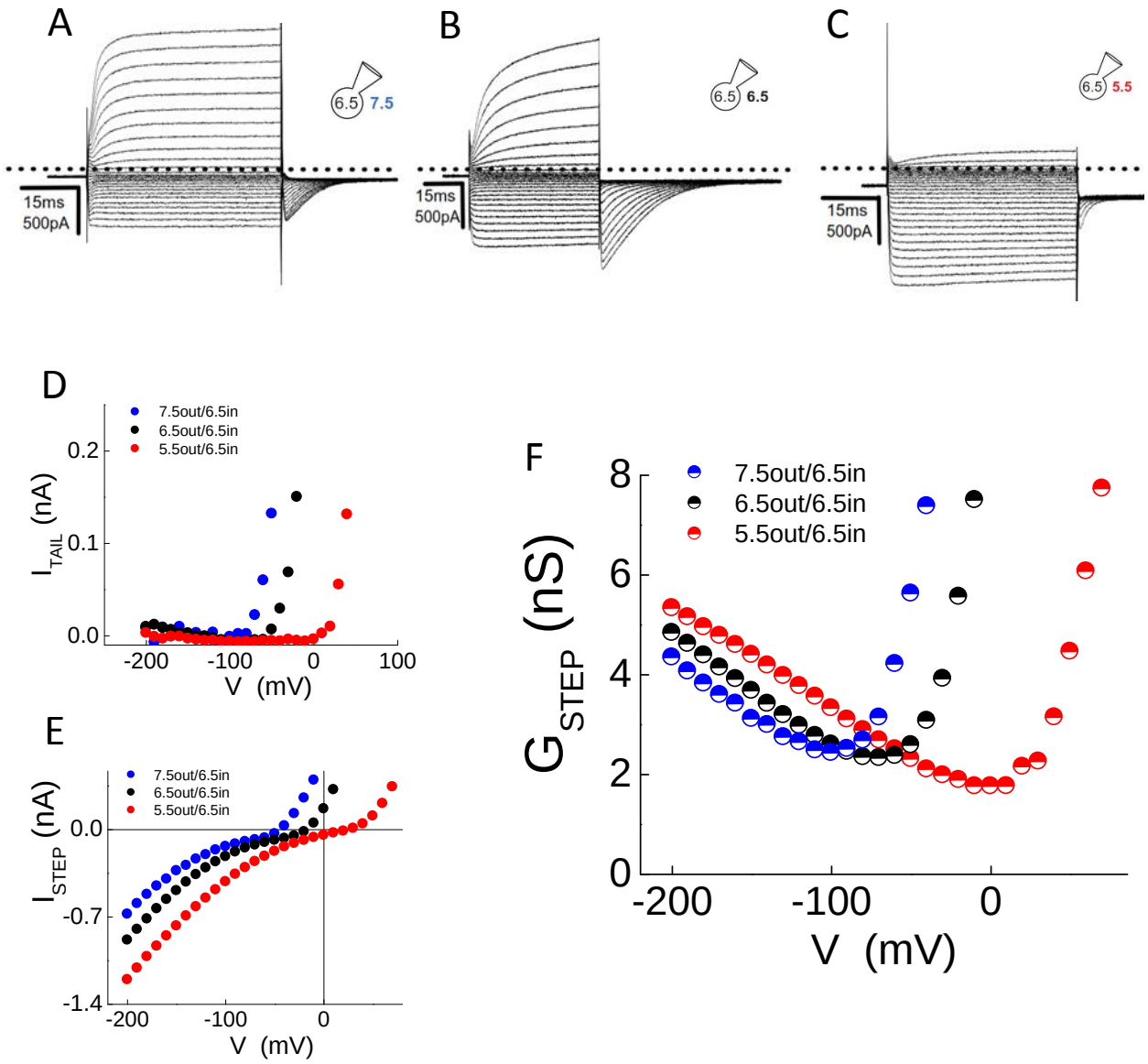

Figure 14. R205H G_{SH} and G_{AQ} voltage dependence at 3 pH_O
Representative whole-cell current records elicited from a Flp-In 293 T-REx cell expressing R205H. Currents were elicited from a holding potential of -50mV, V_{STEP} = +60mV to -200mV in 10mV increments, V_{TAIL}= -90mV. Three pH conditions were imposed by TMA/$MeSO_3^-$ bath solutions buffered to pH_O 7.5(**A**), pH_O 6.5 (**B**) or pH_O 5.5 (**C**), and pH_I=6.5 in the pipette. **D.** Linear-leak subtracted I_{TAIL}-V relation for traces in A-C. **E.** I_{STEP}-V relation for traces in A-C. **F**. Conductance (G_{STEP}) was calculated from I_{STEP} (shown in panel E) is plotted as a function of membrane potential for G_{STEP}-V relations. Notice the U-Shaped G_{STEP}-V relations at all three pH_O and that minimum conductance decreases with decreasing pH_O. The rise in G_{STEP}-V relations seen at positive voltages (right arm of U-Shapes) relates G_{AQ} activation that shifts rightward with decreasing pH_O.

Given that we could measure an early step in voltage sensor activation (G_{SH}) separately from opening of the 'aqueous' conductance, we wondered whether the two conductances would exhibit similar sensitivity to changes in the pH gradient. As I mentioned earlier, it is well established that under these recording conditions G_{AQ} will shift about 40 mV/pH unit[20,21]. Next we sought to determine whether or not changes in the pH gradient would differentially affect the early voltage dependent conformational change reported by the R205H "shuttle" conductance. In an initial attempt to separate the voltage-dependent gating of G_{AQ} and G_{SH}, we imposed changes in pH_O that are known to shift the position of the G_{AQ}-V relation [20,21]. The effects of changes in ΔpH on G_{AQ} and G_{SH} in R205H can be seen in current traces elicited at three pH_O gradients (Fig. 14A-C). The current traces shown in Figure 14 were elicited by voltage steps from +60mV to -200mV in 10mV increments with pH_I6.5 in the pipette and either pH_O7.5, pH_O6.5, or pH_O5.5 in the bath. At all three pH_O, time-dependent outward current exhibited a steep monotonic rise at depolarized potentials.

The I_{STEP}-V relations for all pH_O (Fig. 14E) show a non-linear inward 'shuttle' current at negative voltages that turns off prior to opening of the aqueous pathway, as evidenced by a distinct plateau prior to the opening of G_{AQ}. The plateau shifts with each change in pH_O. The I_{TAIL}-V relation indicates that G_{AQ} activation shifts accordingly with changes in pH_O (Figure 14E). A linear fit to the mean V_{THR} at three pH_O was done to estimate the pH-dependent shift in G_{AQ} opening. The slope factor (-45.0 ± 4 mV/pH unit, N=17) shows that the apparent $P_{OPEN-AQ}$-V relation for R205H shifts by ~40 per unit pH, as reported for WT Hv1[20,21]. Net extracellular acidification (from pH_O6.5 to pH_O5.5) produces an inwardly-directed H^+ gradient (Fig. 14C,F) and there is notable 2-fold decrease of the amplitude of outward aqueous currents and a ~2-fold increase in the amplitude of inward 'shuttle' current, as expected for a H^+ selective conductance.

The G_{STEP}-V relation for R205H at three pH_O, has a distinct U-shape at each pH_O. The amplitude of G_{SH} increases with lower pH_O (Fig. 13 G), but strikingly, G_{MIN} decreases with lower pH_O. As stated earlier, the G_{STEP}-V at intermediate potentials in R205H likely reflects the contribution of both of G_{SH} and G_{AQ} in addition to membrane leak current. The sharp increase in G_{STEP} at positive potentials reflects the opening of G_{AQ} (Fig. 14F). The voltage at which G_{AQ} begins to open evidently shifts rightward with lower pH_O (Fig. 14F), but is it is difficult to determine whether G_{AQ} shifts relative to G_{SH} because the amplitude of G_{SH} increases with lower pH_O and G_{MIN} decreases with lower pH_O. The data suggest that G_{SH} and G_{AQ} each contribute to total membrane conductance at all pH_O tested. The apparent overlap of G_{SH}-V and G_{AQ}-V relations in R205H at all pH_O examined here unfortunately prevents a straightforward analysis of the voltage dependence of either conductance in isolation. In the following section we describe experimental strategies designed to isolate G_{SH} from G_{AQ} and to quantify the voltage dependence of G_{SH} gating.

2. Electrophysiological properties of double mutant containing N214R-R205H

In order to dissect G_{SH} from G_{AQ}, we introduced a second mutation (N214R) into the background of Hv1 R205H. Both thiol labeling of N214C and N214R substitution are both reported to dramatically reduce or abolish outward H^+ current in Hv1[94,135–137]. The mechanism for N214R block of outward G_{AQ} current in human Hv1 presumably involves an S4 transition that moves the cationic guanidinium side chain of 214R into a position that prevents outward movement of protons through the G_{AQ} pathway[94,135–137]. Evidently, the block of I_{STEP} is relieved at negative potentials where I_{TAIL} is measured [94,135–137]. We hypothesize that N214R, when incorporated into the background of R205H, will not block 'shuttle' currents at negative voltages when the VS domain is in the resting-state conformation and that the R205H-N214R double mutant could potentially serve to experimentally isolate G_{SH} from G_{AQ}. In cells expressing R205H-N214R we measure inward steady-state voltage-dependent currents that are similar to those in R205H alone (Fig. 15A). In contrast to R205H, the R205H-N214R double mutant does not appear to generate any outward current mediated by G_{AQ} at positive potentials (Fig. 15B). The residual small current at positive potentials in R205H-N214R has a linear I_{STEP}-V relation and is presumed to reflect the contribution of a nonspecific background membrane leakage current (Fig. 15B). Our results for R205H-N214R are consistent with the previously reported effect of the N214R mutation to block G_{AQ} [94,135–137].

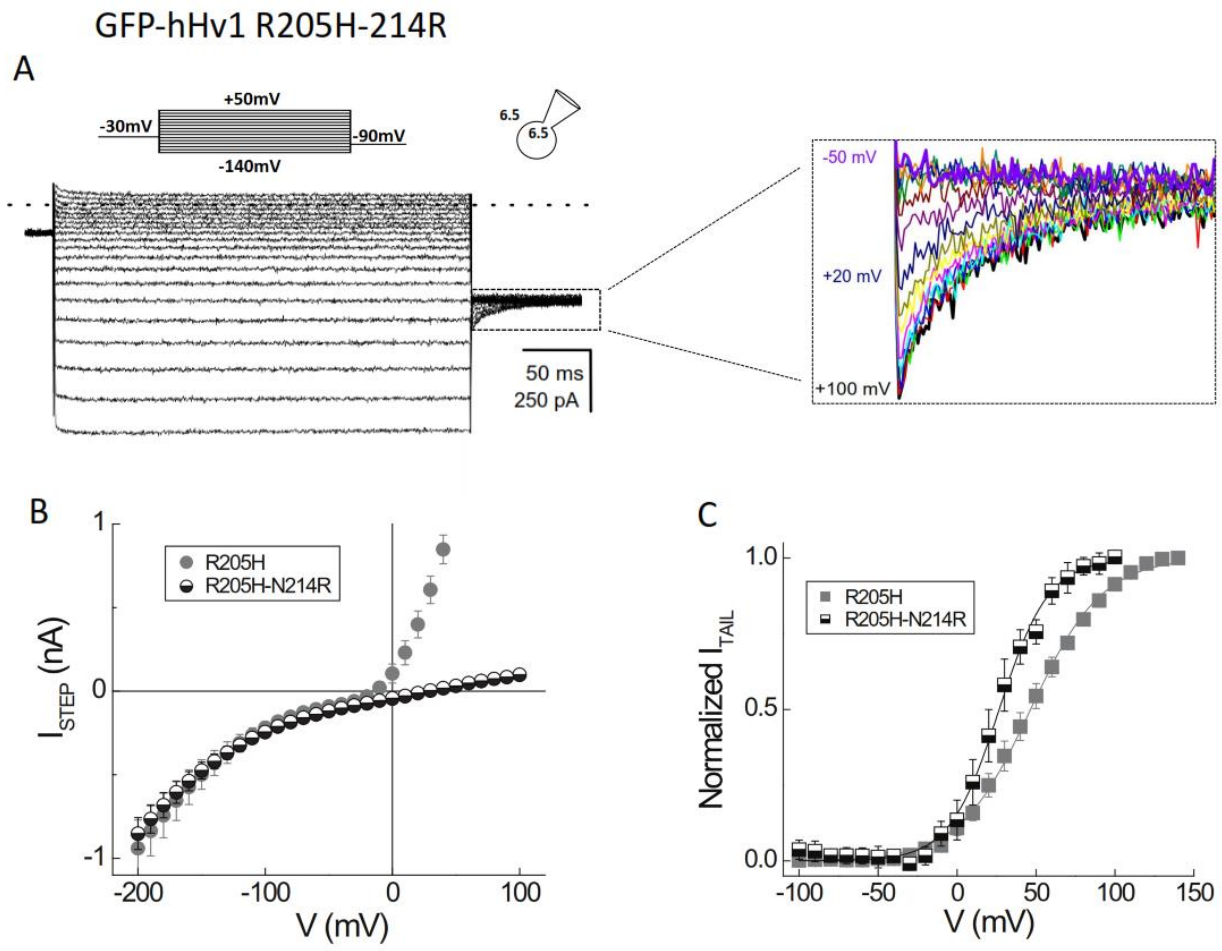

Figure 15. 214R-205H blocks outward aqueous H^+ current, but the P_{OPEN} of G_{AQ} in R205H-N214R can be measured from tail currents.

A. Representative whole-cell current traces in a cell expressing N214R-R205H. Current measured from HP= -30mV (V_{STEP}= -150 mV to +40 mV in 10 mV increments) V_{TAIL}= -90mV, (pH_O = pH_I = 6.5); dashed lines indicate zero current. **B.** I_{STEP} measured at the end of the voltage step is plotted as a function of the step potential for R205H-N214R (half-filled circles). R205H (filled gray squares) is shown for comparison. Data represent means ± SEM from *n* = 6 (R205H) or *n* = 4 (214R-R205H) cells. **C.** Normalized I_{TAIL} for 214R-R205H (half-filled squares) and 205H (filled gray squares) is plotted in function of the step potential (*side panel*, magnification of tail currents, V_{STEP} indicated corresponds to color of current trace). Data represent means ± SEM from n = 4 (R205H) or *n* = 8 (R205H-N214R) cells.

Just as in N214R alone [94,135–137], R205H-N214R generates a measurable I_{TAIL} at negative voltages (Fig. 15A, inset). The instantaneous I_{TAIL}-V relation in R205H-N214R indicates that increasingly positive potentials increase apparent $P_{OPEN-AQ}$ in double-mutant channels similarly to WT Hv1 (Fig. 15B-C). N214R thus appears to eliminate the contribution of the outward H^+ current that is normally carried by G_{AQ} from the total membrane conductance, while the inward current mediated by G_{SH} is unchanged in R205H-N214R (Fig. 15B). In support of this interpretation, we find that the I_{TAIL}-V relations for R205H and R205H-N214R are similar (Fig. 15C). The steady-state voltage dependence of G_{AQ} gating, as estimated by V_{THR}, is also similar in R205H and R205H-N214R: V_{THR} for activation of R205H-N214R (-20.7 ± 2.2 mV, n = 14) is not significantly different from R205H alone (-25.0 ± 1.9 mV, n = 20), indicating that the N214R mutation does not measurably alter the $P_{OPEN-AQ}$-V relation (Table 1, pg. 84). In contrast to V_{THR}, the apparent midpoint of the I_{TAIL}-V relation in R205H is more positive than R205H-N214R (Fig. 15C); one possible explanation for the apparent discrepancy in the sensitivity of V_{THR} vs. $V_{0.5}$ values to the addition of N214R is that the large outward H^+ current mediated by G_{AQ} in R205H (which is absent in R205H-N214R) could affect the position and/or slope of the I_{TAIL}-V curve. I_{TAIL} is most accurately measured near V_{THR}, where I_{STEP} is small. Smaller outward I_{STEP} amplitudes are less likely to cause ΔpH to deviate from the value nominally imposed by pH_I and pH_O [8,20,21]. Because R205H-N214R mediates no detectable I_{STEP}, deviations in ΔpH that can influence the shape and position of the I_{TAIL}-V relations are less likely to occur, and the data from R205H-N214R are thus interpreted to represent a more accurate estimate of the apparent $P_{OPEN-AQ}$-V relation than the data from R205H alone.

The flat G_{STEP}-V relation in R205H-N214R is at positive potentials (Fig. 16A) suggests that G_{SH} approaches a minimum value that can be estimated in the absence of G_{AQ}. R205H-N214R thus isolates G_{SH} by blocking the contribution of G_{AQ} to the aggregate G_{STEP}. A comparison of the calculated G_{STEP}-V relations for R205H and R205H-N214R demonstrates that while the G_{STEP}-V relation for R205H is biphasic, the G_{STEP}-V relation for R205H-N214R is apparently monophasic. Note that the saturating minimum G_{STEP} for R205H-N214R is smaller than the local minimum measured in R205H alone (Fig. 16A). The residual conductance measured at large positive voltages in R205H-N214R is likely to reflect the contribution of G_{LEAK}; G_{LEAK} is defined as any non-specific membrane current that contributes to G_{STEP}.

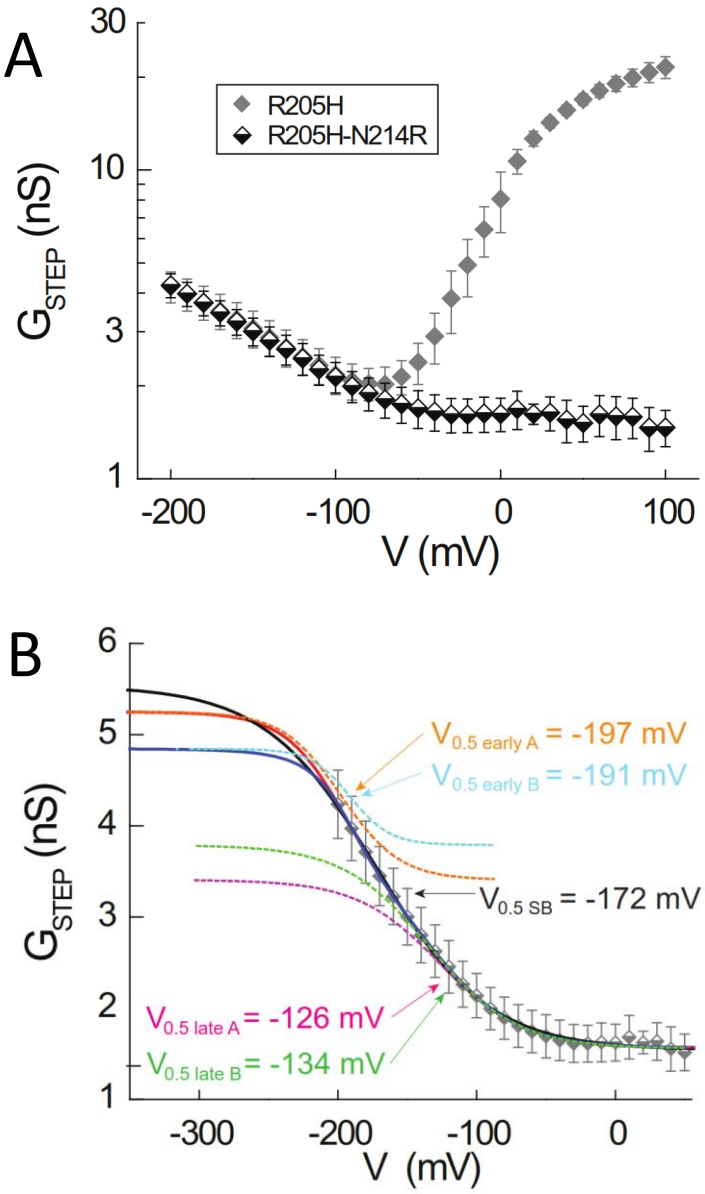

Figure 16. 214R-205H mutant isolates G_{SH}.
A. Mean conductance calculated from I_{STEP} is plotted in function of the step voltage. No leak subtraction is applied. Note the log scale for G_{STEP} and distinctive 'U' shape of the G_{STEP}-V relation. Data represent means ± SEM from n = 3 (R205H) or n = 3 (R205H-N214R) **B.** The mean G_{STEP}-V for R205H-N214R (data from **D**) relation is fit to either a single Boltzmann (black line: $G_{MIN\ SB}$ = 1.5 nS, $G_{MAX\ SB}$ = 5.5 nS, dx_{SB} = 40.4, $V_{0.5\ SB}$ = -172.1 mV) or the sum of 'early' and 'late' Boltzmann functions (red and blue lines). Double-Boltzmann fits in which the fractional contribution of each Boltzmann component was set at 50% of the total response (DB-A, sold red line; f_{early} = f_{late} = 0.5) or allowed to vary during the curve fitting (DB-B, solid blue line) are shown. Dashed lines represent only the early or late components of double-Boltzmann fits in isolation (dashed orange line, DB-A early: $G_{MIN\ early\ DB\text{-}A}$ = 3.9 nS, $G_{MAX\ early\ DB\text{-}A}$ = 5.2 nS, $dx_{early\ DB\text{-}A}$ = 21.1, $V_{0.5\ early\ DB\text{-}A}$ = -197.5 mV; dashed magenta line, DB-A late: $G_{MIN\ late\ DB\text{-}A}$ = 1.6 nS, $G_{MAX\ late\ DB\text{-}A}$ = 3.9 nS, $dx_{late\ DB\text{-}A}$ = 30.0, $V_{0.5\ late\ DB\text{-}A}$ = -126.2 mV; dashed cyan line, DB-B early: $G_{MIN\ early\ DB\text{-}B}$ = 3.3 nS, $G_{MAX\ early\ DB\text{-}B}$ = 4.8 nS, $dx_{early\ DB\text{-}B}$ = 14.3, $V_{0.5\ early\ DB\text{-}B}$ = -191.3 mV; dashed green line, DB-B late: $G_{MIN\ late\ DB\text{-}B}$ = 1.6 nS, $G_{MAX\ late\ DB\text{-}B}$ = 3.3 nS, $dx_{late\ DB\text{-}B}$ = 31.1, $V_{0.5\ late\ DB\text{-}B}$ = -134.1 mV).

In order to quantify voltage dependence of G_{SH} gating, we first fit the G_{STEP}-V relation to a Boltzmann function. As described previously (Section 5.0; Fig. 5), the G_{STEP}-V in Shaker R362H is not well-fit to a Boltzmann function, but the data can be fit to the sum of two Boltzmann distributions[121–123,156]. The double-Boltzmann fits suggest that the two distinct gating steps might operate over distinct ranges of potential, resulting in a complex G_{STEP}-V relation[121–123,156]. The G_{STEP}-V for R205H-N214R does not saturate over the measured range of voltages down to -200mV (Fig. 16B). Although a single Boltzmann fits the G_{STEP}-V reasonably well at more positive potentials (~ -50 mV to 0 mV), the data at negative potentials do not appear to reach a saturating maximum (Fig. 16B), raising uncertainty about the interpretation of fits of the data to a saturable function. A single Boltzmann fit to G_{STEP}-V yields an estimated midpoint ($V_{0.5}$ = -197 mV) that strongly depends on the extrapolated value of G_{MAX} (Fig. 16F). We also fit the G_{STEP}-V relation for R205H-N124R to the sum of two Boltzmann distributions, as previously described for Shaker R362H[121–123,156]. Figure 16B shows the results of two separate fitting sessions in which either G_{MAX} or the fractional contributions of the 'early' and 'late' transitions was differentially constrained. The double-Boltzmann fits do not produce obviously better fits to the data than the single-Boltzmann fit (Fig. 16B). We conclude that in the absence of a measurable saturation in G_{STEP} at negative voltages, the interpretation of $V_{0.5}$ values derived from fits to Boltzmann-type functions is uncertain, and efforts to quantify the voltage dependence of G_{SH} gating using only curve fitting approaches are necessarily limited.

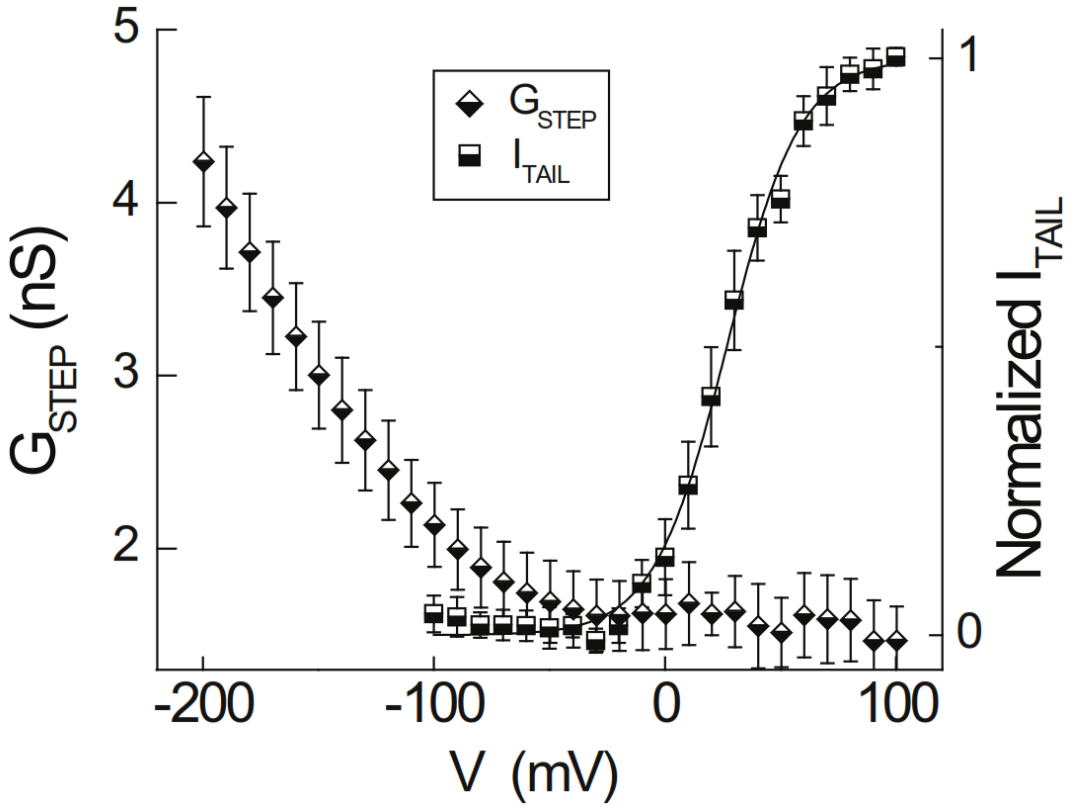

Figure 17. Comparison of G_{SH} and G_{AQ} in R205H-N214R.
An overlapping plot of G_{STEP}-V (G_{SH}) and normalized I_{TAIL}-V (G_{AQ}) relations to emphasize the large difference in voltage dependencies of G_{SH} and G_{AQ} gating. Note the different axes are for G_{STEP}-V (left) and normalized I_{TAIL}-V (right). Symbols represent mean G_{STEP} (half-filled diamonds) ± SEM (n = 3) and mean normalized I_{TAIL} (half-filled squares) ± SEM (n = 8). The solid line represents a Boltzmann fit to mean I_{TAIL} ($V_{0.5}$ = +26.7 mV).

Despite our inability to unambiguously quantify steady-state G_{SH} gating parameters using standard Boltzmann curve fitting, visual comparison of the R205H and R205H-N214R G_{STEP}-V relations leads to an important insight into the Hv1 gating mechanism. The range of voltages over which G_{SH} and G_{AQ} are gated are clearly distinct (Fig. 17). The G_{STEP}-V and I_{TAIL}-V relations appear to overlap slightly near ~-50 mV (Fig. 17), close to the voltage at which G_{MIN} is observed in R205H alone (Fig. 13, Fig 14F. A simple interpretation of the data is that G_{SH} and G_{AQ} gating have widely disparate voltage dependencies. One possible explanation for the data is that the separation of G_{SH} and G_{AQ} gating along the voltage axis is that VS activation (as reported by voltage-dependent closure of the resting-state conduction pathway) and opening of the intrinsic aqueous H^+ pore are distinct thermodynamic transitions in the Hv1 activation pathway. Next we employ a novel analytical approach to empirically estimate steady-state G_{SH} gating parameters.

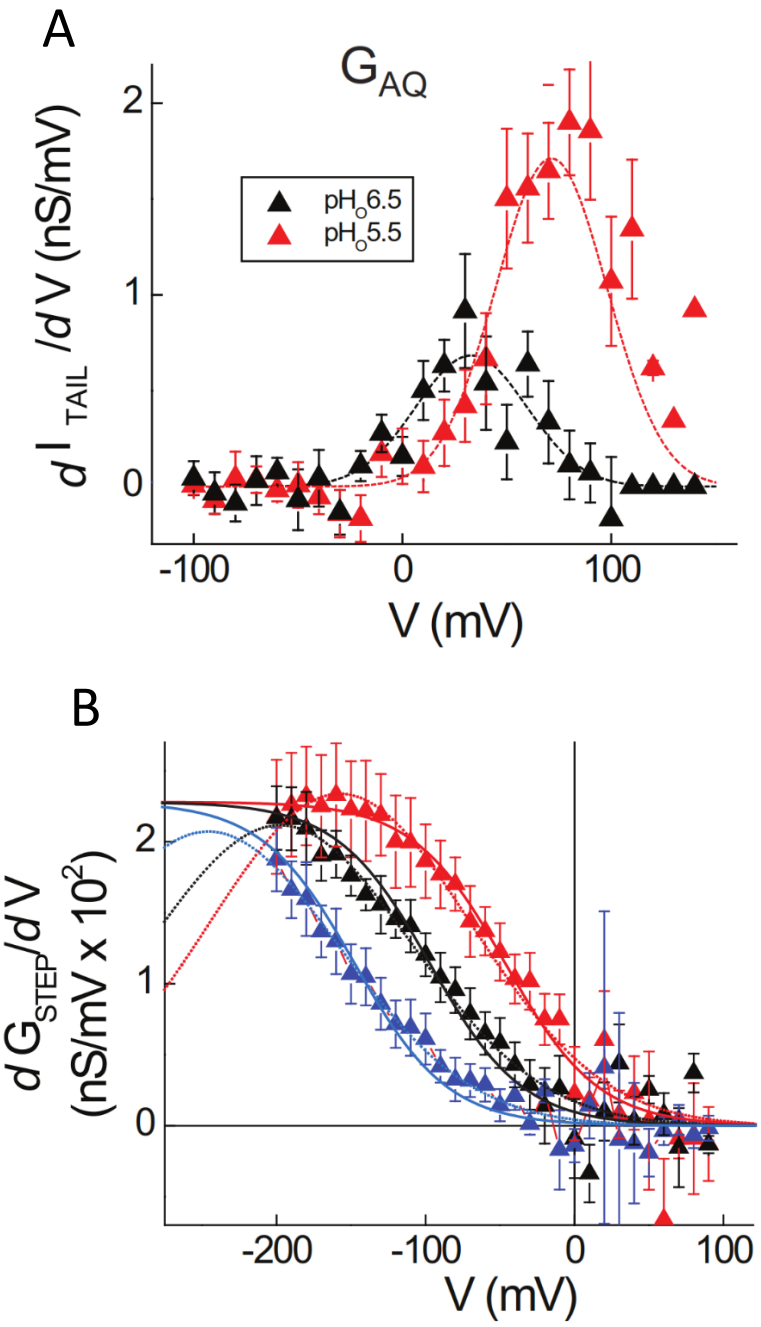

Figure 18. First derivative analysis of G_{SH}-V relations for R205H-N214R at 3 different pH_O.
A. The first derivatives of linear leak-subtracted R205H-N214R I_{TAIL}-V relations used to calculate the normalized I_{TAIL}-V data shown in Fig. 3H are fit to the Gaussian functions (pH_O6.5: A = 45.7, w = 53.3, V_{PEAK} = +33.0 mV; pH_O5.5: A = 114.3, w = 53.3, V_{PEAK} = +71.3 mV) shown by dotted lines. **B.** Mean dG_{STEP}/dV values for R205H-N214R are shown in function of the step potential. Symbol colors are as in D. Symbols represent means ± SEM from n = 8 (pH_O5.5), n = 12 (pH_O6.5) or n = 10 (pH_O7.5) cells. Fits of the mean dG_{STEP}/dV-V relations at three pH_O to a Gaussian function are shown by dotted lines (red, pH_O5.5: A = 5.2, w = 176.4, V_{PEAK} = -157.4 mV; black, pH_O6.5: A = 4.7, w = 176.4, V_{PEAK} = -197.6 mV; blue, pH_O7.5: A = 4.6, w = 176.4, V_{PEAK} = -245.7 mV) and fits to the falling phase of the mean dG_{STEP}/dV-V relations to a Boltzmann function are shown by solid lines (red, pH_O5.5: $(dG_{STEP}/dV)_{MAX}$ = 0.023, dx = 31.1, $V_{0.5\text{-}PEAK}$ = -46.3 mV; black, pH_O6.5: $(dG_{STEP}/dV)_{MAX}$ = 0.023, dx = 31.1, $V_{0.5\text{-}PEAK}$ = -97.0 mV; blue, pH_O7.5: $(dG_{STEP}/dV)_{MAX}$ = 0.023, dx = 31.1, $V_{0.5\text{-}PEAK}$ = -147.4 mV).

To more accurately describe steady-state G_{SH} gating parameters in R205H-N214R, we considered empirical analyses that, in contrast to Boltzmann fitting, are a model-independent and do not require assumptions about the value of G_{MAX} or the number of gating transitions that contribute to the measured changes in G_{STEP}. First we calculated the first derivative of G_{STEP} because the first derivative of a sigmoidally shaped and voltage dependent X-V relation plotted in function of V (dX/dV vs. V) exhibits a bell shape. For a simple Boltzmann type X vs. V distribution, the peak of the dX/dV-V relation (V_{PEAK}) is located at $V_{0.5}$. As a test of this method, we analyzed I_{TAIL} in experiments like those shown in Figures 16C and 17 for R205H-N214R at two different pH_O. As shown previously, I_{TAIL}-V data for R205H-N214R are well-fit by a Boltzmann function, suggesting that the dI_{TAIL}/dV-V can be expected to manifest a bell–shaped distribution as illustrated in Figure 18A. We estimated the voltage at which dI_{TAIL}/dV-V reaches V_{PEAK} by fitting the data to a Gaussian function. The values for V_{PEAK} derived from Gaussian fits to dI_{TAIL}/dV-V and $V_{0.5}$ derived from single Boltzmann fits to I_{TAIL}-V compare favorably (pH_O6.5: V_{PEAK} = +33.0 mV, $V_{0.5}$ = +26.3 mV: pH_O5.5: V_{PEAK} = +71.3 mV; $V_{0.5}$ = +67.0 mV). The data confirm that first derivative analysis can be suitable for identifying the approximate midpoint of a sigmoid I_{TAIL}-V relation even when maximal I_{TAIL} may not be within the range of voltages that are amenable to experimental measurement. Next we apply this analytical method to G_{SH} gating in R205H-N214R.

In order to estimate the effect of changes in pH_O on the apparent voltage dependence of G_{SH} gating, we calculated the first derivative of leak-subtracted R205H-N214R G_{STEP}-V relations measured at three different pH_O. As seen previously (Figs. 16 and 17), we find that G_{SH} does not obviously saturate at negative voltages in any pH_O tested, but the dG_{STEP}/dV-V relation does appear to reach a clear peak, at least at pH_O5.5 (Fig. 18). The mean of V_{PEAK} values determined by Gaussian fitting of dG_{STEP}/dV-V data from separate experiments, exhibits a strong dependence on pH_O (V_{PEAK} pH_O7.5 = -245 ± 8.7 mV, n = 11 cells; V_{PEAK} pH_O6.5 = -197.6 ± 6.6 mV, n = 14 cells; V_{PEAK} pH_O5.5 = -157.4 ± 10.3 mV, n = 8 cells). Gaussian fits to the mean dG_{STEP}/dV-V data reveal a similar trend: the apparent V_{PEAK} shifts in function of

pH_O (Fig. 18B). We interpret the shift in R205H-N214R dG_{STEP}/dV-V relations as a strong indication of pH_O dependent gating in the isolated G_{SH}. The gating transition reported by G_{SH} is evidently sensitive to changes in both membrane potential and pH_O. The shifts in V_{PEAK} that result from changes in pH_O are approximately ~40mV/pH unit, and have a striking consistency with the pH_O dependent shifts (40mV/pH unit) observed for G_{AQ}.

We used an additional strategy for estimating the pH_O-dependent shift in G_{SH} gating. The dG_{STEP}/dV relation has two phases that form the bell shape and they determine the position of the peak. We fit the falling phase (i.e., at voltages that are positive to the peak potential) to a sigmoid function. This method yields $V_{0.5\text{-}PEAK}$, the voltage at which 50% of the V_{PEAK} is reached (Fig. 18B). We fit the mean dG_{STEP}/dV data to single Boltzmann functions to determine $V_{0.5\text{-}PEAK}$. This approach assays the slope of the falling phase and the shift in the position of the falling phase. Visual inspection of Gaussian fits to dI_{TAIL}/dV-V indicate a similar pH_O dependent shift in falling phase along the voltage axis (Fig. 18A). The Boltzmann functions, shown by solid lines in Figure 18B, yield $V_{0.5\text{-}PEAK}$ values that are pH_O dependent and slope values that compare well (pH_O5.5: $V_{0.5\text{-}PEAK}$ = -46.3 mV, dx = 31.1; pH_O6.5: $V_{0.5\text{-}PEAK}$ = -97.0 mV, dx = 31.1; blue, pH_O7.5: $V_{0.5\text{-}PEAK}$ = -147.4 mV, dx = 31.1). Thus Boltzmann fits to the falling phase of dG_{STEP}/dV are in good agreement with agreement with pH_O dependent V_{PEAK}. The data demonstrate a pH_O sensitivity to G_{SH} gating.

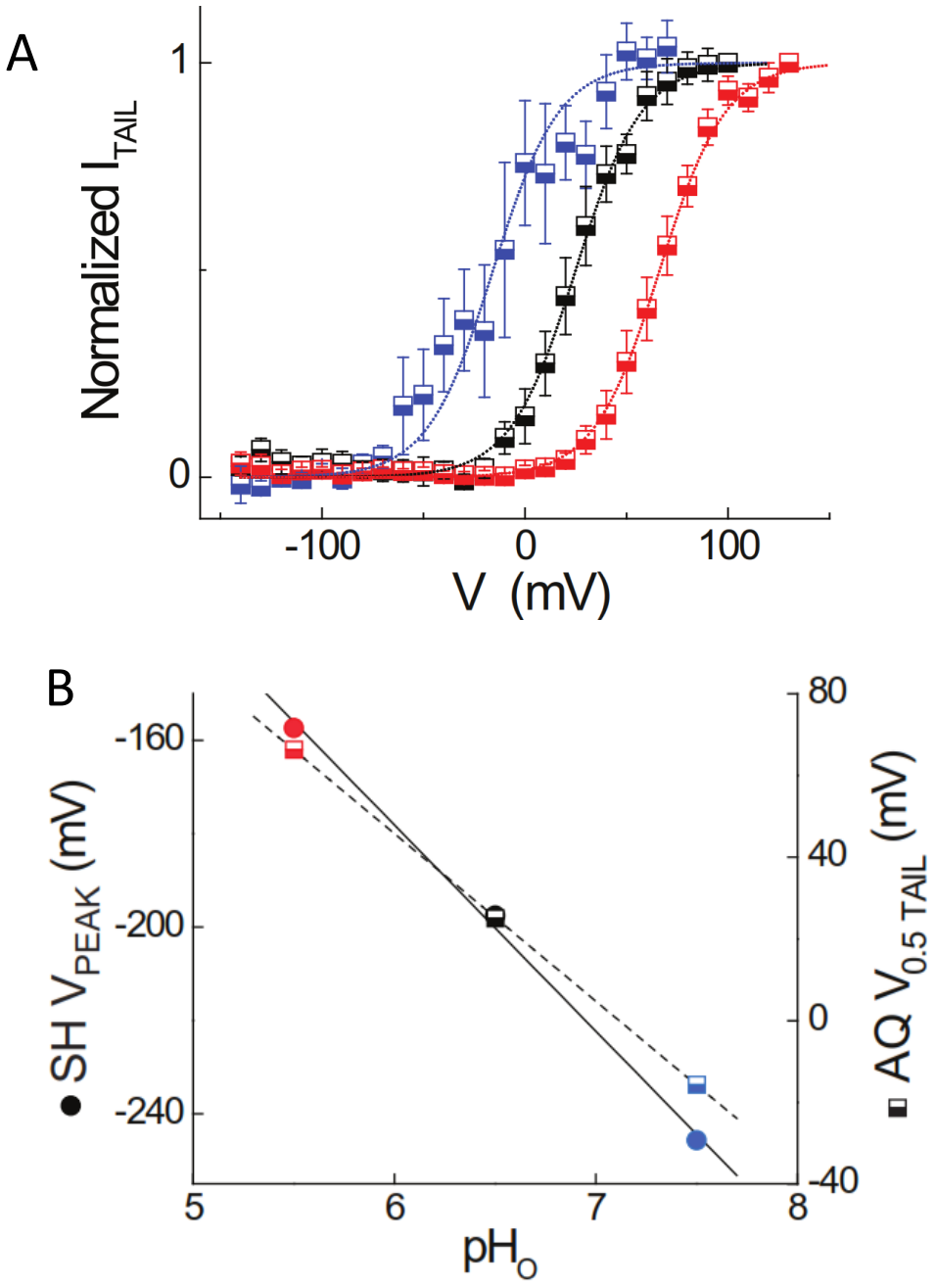

Figure 19. Both G_{SH} and G_{AQ} have pH_O dependent gating in R205H-N214R.
A. I_{TAIL}-V relations for R205H-N214R measured at the indicated pH_O are normalized to their respective maximum amplitudes and plotted in function of the step potential. Symbols represent means ± SEM from *n* =9 (red, pH_O5.5), *n* = 10 (black, pH_O6.5) or *n* = 4 (blue, pH_O7.5) cells. Fits of the mean I_{TAIL}-V relations to a Boltzmann function are shown by solid lines (red, pH_O5.5: dx = 16.1, $V_{0.5}$ = +67.0 mV; black, pH_O6.5: dx = 16.3, $V_{0.5}$ = +26.3 mV; blue, pH_O7.5: dx = 16.2, $V_{0.5}$ = -15.7 mV). **B.** Fitted V_{PEAK} (filled circles, data from **18B**) and $V_{0.5}$ (half-filled squares) determined from Boltzmann fits to the mean data in **A** are shown in function of pH_O. Lines represent linear fits to the data with slope values of 50.6 mV/pH unit (V_{PEAK}, solid line) and 41.0 mV/pH unit ($V_{0.5}$, dashed line). Symbol color indicates bath solution pH (blue, pH_O7.5; black, pH_O6.5; red, pH_O5.5). Note that the axes for V_{PEAK} and $V_{0.5\ TAIL}$ are scaled differently.

The results of dG_{STEP}/dV analysis and Boltzmann fits to the falling phase, both indicate pH_O dependent gating for G_{SH}, so we next compare G_{SH} with the gating of G_{AQ} in R205H-N214R. We determine the effect of changes in pH_O on G_{AQ} gating from I_{TAIL} that was measured at three different pH_O and normalized to the apparent maximum (Fig. 19A). Single Boltzmann fits to the I_{TAIL}-V relations indicate that the voltage dependence of apparent $P_{OPEN-AQ}$ shifts ~40mV per log unit change in pH gradient (Fig. 19A, Table 1). V_{THR} values determined for the experiments shown in Figure 19A also exhibit a ~40mV/pH unit shift (Table 1). Therefore pH-dependent modulation of G_{AQ} gating is unchanged in R205H-N214R. The pH_O-dependence of G_{SH} (as determined from dG_{STEP}/dV) and G_{AQ} (determined from single Boltzmann fits to I_{TAIL}-V) gating in R205H-N214R is summarized in Figure 19B. Linear fits to the data yield slope values near -40mV/pH unit (Fig. 19B), and are therefore similar to that which is measured for V_{THR} in WT Hv1 and other Hv1 point mutations[20]. The pH dependence of G_{SH} gating therefore compares favorably with that of the intrinsic G_{AQ} in Hv1. In conclusion, the data argue that pH_O-dependent gating in Hv1 occurs early in the activation pathway.

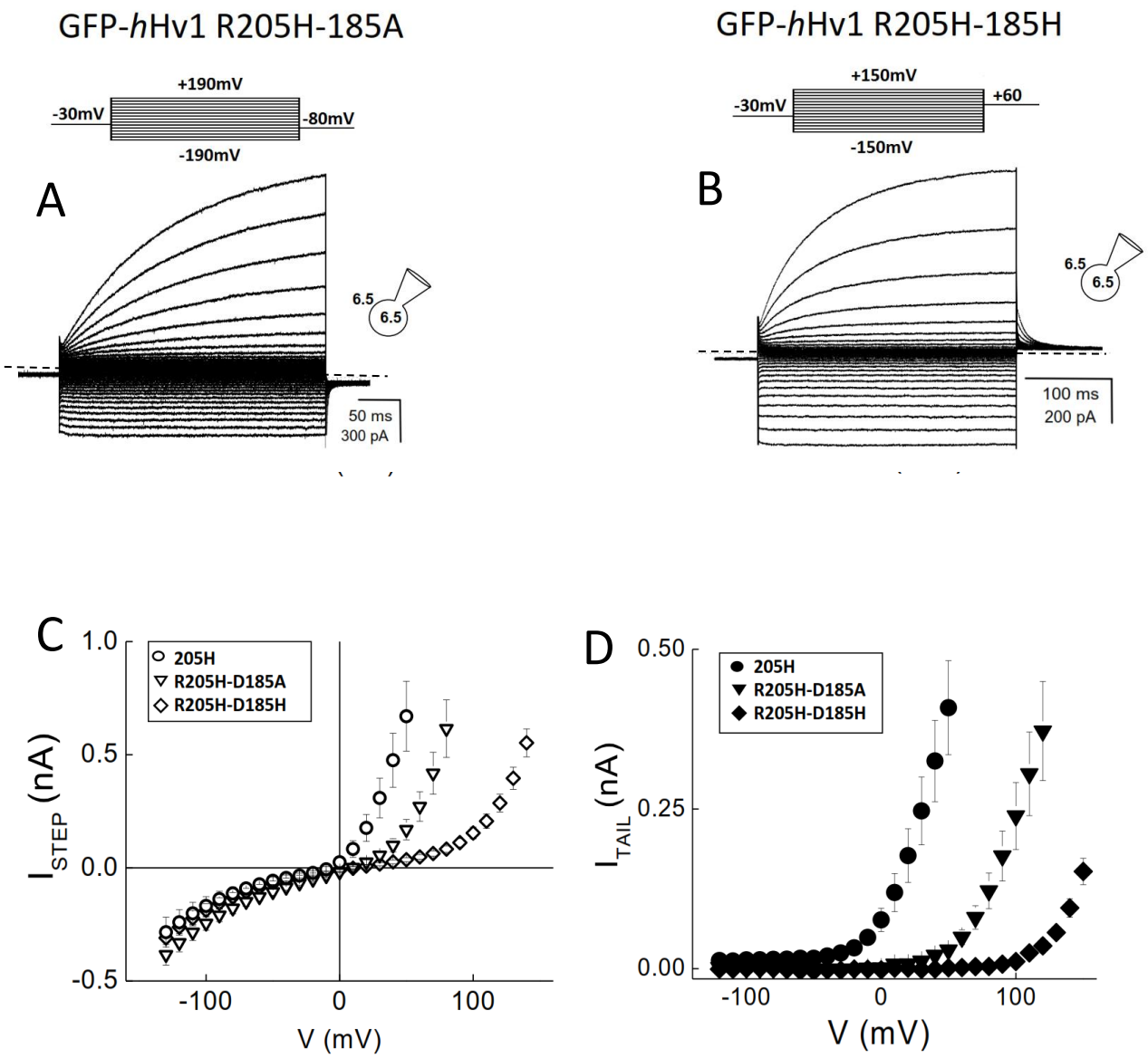

Figure 20. Substitutions at D185 uncouple early VS activation ('shuttle' currents), from the opening of the ('aqueous' pathway) H^+ conductance

A. Representative recording from a cell expressing R205H-D185A. Currents elicited from a holding potential of -30 mV, V_{STEP} = -190 mV through +190 mV in increments of 10 mV, V_{TAIL}=-80mV. **B.** Representative recording from a cell expressing R205H-D185H. Currents elicited from a holding potential of -30 mV, V_{STEP} = -150 mV through +150 mV in increments of 10 mV, V_{TAIL} = +60mV. The dashed line indicates zero current. **C.** I_{STEP}-V relations. Mean ± SEM current from n=9 R205H (open circles, data similar to Fig.10C), n=9 R205H-D185A (open triangles) and n=10 R205H-D185H (open diamonds). **D.** I_{TAIL}-V relations. Mean ± SEM current from n=9 R205H (closed circles, data similar to Fig.10D), n=9 R205H-D185A (closed triangles) and n=10 R205H-D185H (closed diamonds).

3. Electrophysiological properties of double mutants containing R205H- D185H

We sought to further test the idea of pH_O dependent G_{SH} gating in the background of an alternative second site mutation that would allow direct measurement of outward G_{AQ} mediated current, but also maintain isolation of G_{SH} at negative voltages. A previous reports indicates that neutralizing substitutions of a conserved acidic residue in S3 (D185) caused large rightward shifts in V_{THR} in Hv1 > +70mV [20]. We show here that the addition of D185A or D185H in the background of R205H also causes a rightward shift in the voltage dependence of G_{AQ} gating (Fig. 20A,B,D). V_{THR} for D185A and D185H is shifted +60mV and +100mV, respectively, compared to R205H alone (R205H-D185A: V_{THR} = 40.0 ± 1.9 mV, n = 13; R205H-D185H: V_{THR} = 80.0 ± 3.8 mV, n = 7). Plots of mean I_{TAIL} illustrate the large rightward shifts in V_{THR} (Fig. 20D). Plot of I_{STEP}-V, for and R205H, R205H-D185A and R205H-D185H double mutants (Fig. 20C) also mediate large resting-state currents at negative voltages that are similar to R205H-N214R (Fig. 20B).

In R205H-D185H, the voltage dependencies of G_{SH} and G_{AQ} are separated over a wider voltage range than in R205H alone or R205H-N214R. The G_{STEP}-V plotted for R205H-D185H alongside R205H shows a clear plateau in the double mutant that reaches a minimal conductance at voltages where G_{AQ} is rising in R205H alone (Fig. 21). Various mutants in our studies (R205H-D185A, R205H-D185H and R205H-N214R) differ is in the position of the G_{AQ}-V rather than G_{SH}-V. Second-site mutations of D185 in the background of R205H therefore appear to selectively affect a transition that is associated with opening of G_{AQ}. The R205H-D185A (not shown) and R205H-D185H double mutations separate the G_{SH}-V and G_{AQ}-V relations, producing a distinct plateau in the aggregate G_{STEP}-V where the G_{MIN} can be more clearly defined than it is in R205H alone (Fig. 21).

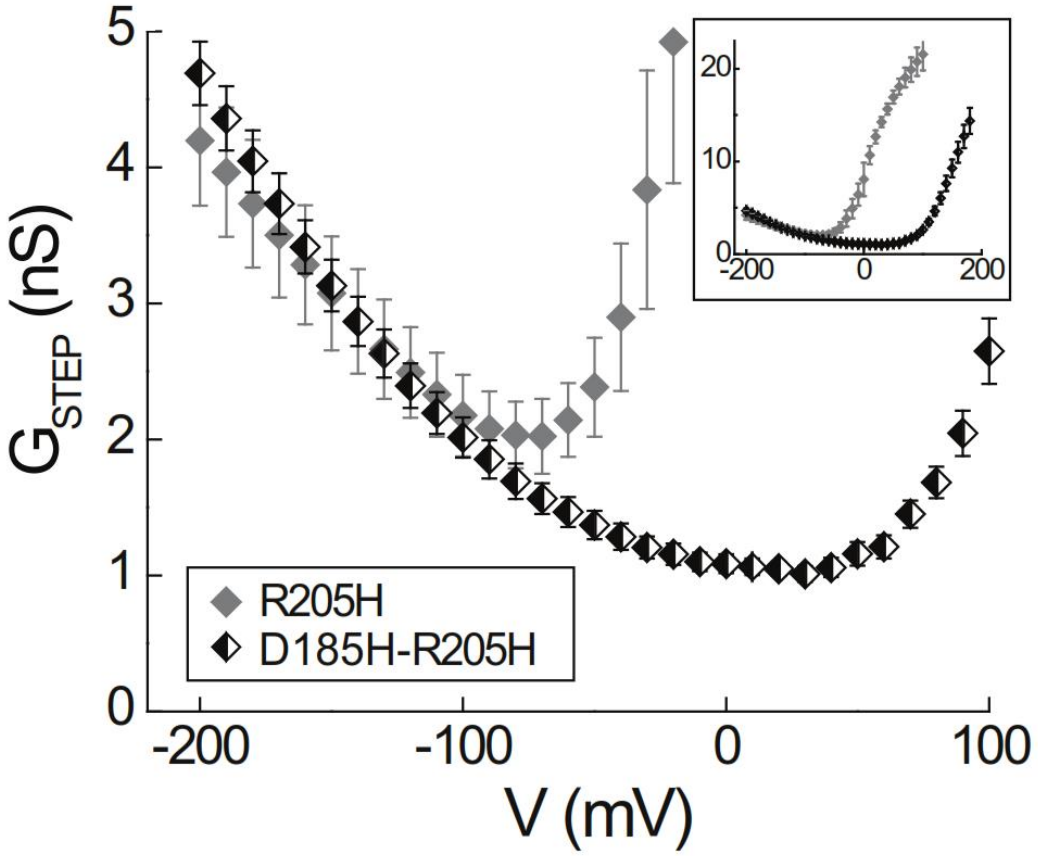

Figure 21. R205H-D185H separates G_{SH} from G_{AQ}
Mean G_{STEP}-V relation for D185H-R205H (half-filled diamonds) is shown in function of the step potential up to +100 mV. *Inset* shows the D185H-R205H G_{STEP}-V relation up to +200 mV. R205H data from Fig. 2 (gray symbols) are shown for comparison to D185H-R205H.

We next asked whether changes in the pH gradient differentially affect the apparent voltage dependence of the initial VS activation reported by G_{SH} and opening of G_{AQ}. Here we focus on R205H-D185H because the magnitude of the rightward shift in G_{AQ}-V is larger than in R205H-D185A. We test the effect of pH_O on G_{SH} in R205H-D185H and observed a distinct plateau at intermediate voltages in all three pH_O, thus G_{SH} isolation is consistent with R205H-N214R. In addition, the aqueous conductance G_{AQ} is observed in G_{STEP}-V relations at extreme positive potentials and exhibits a sigmoid shape (Fig 21, inset), particularly at pH_O7.5 (not shown). We use first derivative analysis on R205H-D185H to evaluate pH_O effects. . A plot of the dG_{STEP}/dV-V relation for R205H-D185H has a striking biphasic shape (Fig. 22) that is different from R205H-N214R. In D185H-R205H, contributions of both G_{SH} and G_{AQ} to the dG_{STEP}/dV-V relation result in two apparent bell-shaped distributions with amplitudes of opposite sign that are separated on the voltage axis (Fig. 22). The differences in amplitude, shape and orientation of the two bell-shaped groups of the dG_{STEP}/dV-V relation, unambiguously distinguish G_{SH} at negative voltages and G_{AQ} at positive voltages. The V_{PEAK} for G_{SH} determined from Gaussian fits to dG_{STEP}/dV-Vd (pH_O5.5: V_{PEAK} = -138.0 mV; pH_O6.5: V_{PEAK} = -208.5 mV; pH_O7.5: V_{PEAK} = -241.1 mV), indicate a pH_O dependent shift in gating. Linear fits of V_{PEAK} values for individual experiments (each at three pH_O in one cell) were averaged and the mean slope value is close to ~40 mV/pH unit (Table 1, pg. 84). Thus first derivative analysis for R205H-D185H demonstrates a pH_O dependent shift in G_{SH} gating that is in good agreement with our analysis for R205H-N214R.

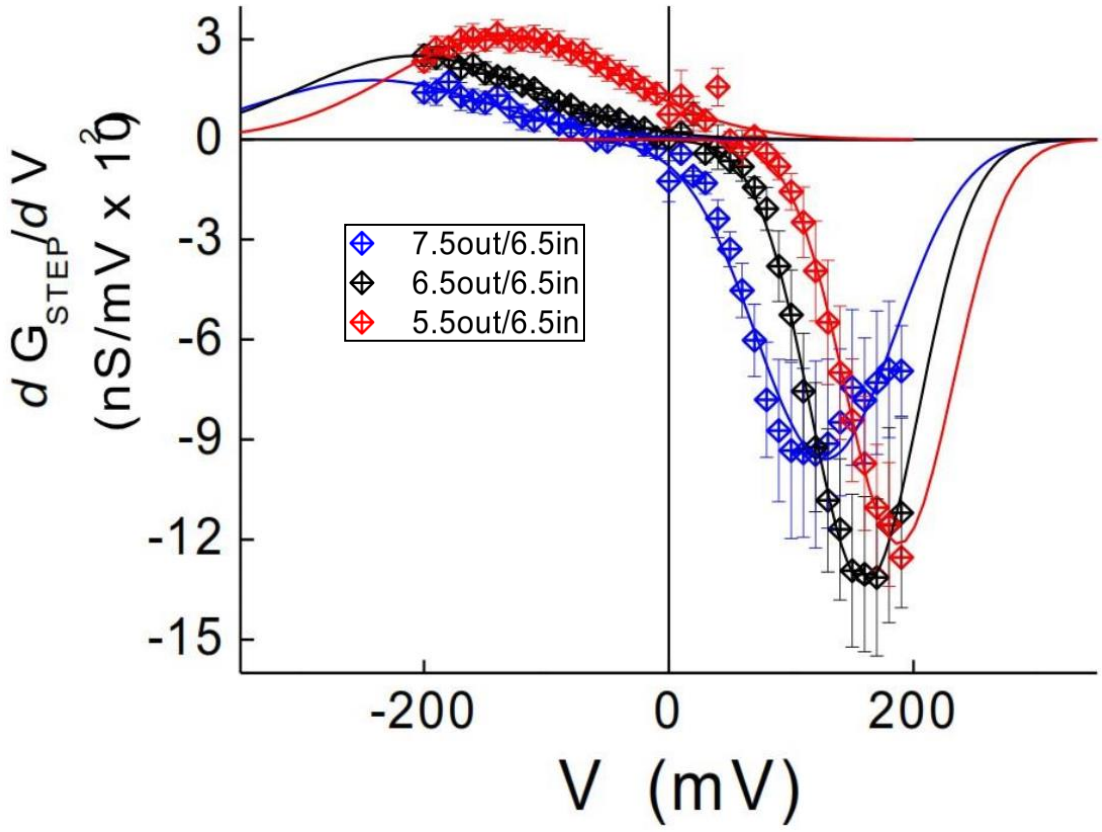

Figure 22. First derivative analysis of R205H-D185H shows pH_O dependent gating in both G_{SH} and G_{AQ} at 3pH_O

Mean dG_{STEP}/dV values for D185H-R205H are shown in function of the step potential. Symbol colors are as in A. Symbols represent means ± SEM from n = 6 (pH_O5.5), n = 6 (pH_O6.5) or n = 4 (pH_O7.5) cells. Fits of the mean dG_{STEP}/dV-V relations at three pH_O to a Gaussian function are shown by lines at negative voltages for ('shuttle') G_{SH} dG_{STEP}/dV-Vd (red, pH_O5.5: A = 7.1, w = 198.8, V_{PEAK} = -138.0 mV; black, pH_O6.5: A = 6.0, w = -138.0, V_{PEAK} = -208.5 mV; blue, pH_O7.5: A = 4.2, w = 187.3, V_{PEAK} = -241.1 mV) or at more positive voltage range for ('aqueous') G_{AQ} dG_{STEP}/dV-Vd (red, pH_O5.5: A = -11.7, w = 87.2, V_{PEAK} = 190.4 mV; black, pH_O6.5: A = -14.7, w = 88.7, V_{PEAK} = 160.6 mV; blue, pH_O7.5: A = -13.8, w = 128.0, V_{PEAK} = 127.9.7 mV).

The pH-dependent gating of G_{AQ} is unchanged in R205H-D185H, which is in agreement with previous reports for D185A pH sensitive gating[20]. To determine the effect of pH_O on G_{AQ} gating in R205H-D185H we measure V_{THR} values. Mean V_{THR} values are plotted against pH_O and the linear regression slope of V_{THR} vs. pH_O relations indicates that the shift in V_{THR} is close to -40mV/pH unit. As an additional comparison we perform Gaussian fits to the mean dG_{STEP}/dV-Vd relation at positive voltages where the bell shaped distributions correspond to G_{AQ} (Fig. 22). The dG_{STEP}/dV-V has larger amplitude peaks and steeper slopes at positive potentials and that reflects larger and steeper increases of conductance values for G_{AQ} over that range. Gaussian fits yield V_{PEAK} values (pH_O7.5, V_{PEAK} = 127.9.7; pH_O6.5, V_{PEAK} = 160.6 mV; pH_O5.5V_{PEAK} = 190.4 mV) that indicate a ~40mV/pH shift and is in agreement with shift for V_{THR}. In summary, two separate analytical methods (dG_{STEP}/dV-V and V_{THR}) independently support a conclusion that the pH_O-dependence of G_{SH} gating is quantitatively similar to that of G_{AQ} in Hv1 D185H-R205H.

Table 1. Mean of determinations in *n* individual experiments.

construct	G_{AQ} V_{THR} (mV)[a]	SEM	*n*	G_{AQ} $V_{THR}/\Delta pH$ (mV/pH unit)	SEM	*n*	G_{SH} $V_{0.5}$ (mV)[b]	SEM	*n*	G_{SH} V_{PEAK} (mV)[c]	SEM	*n*	G_{SH} $V_{PEAK}/\Delta pH$ (mV/pH unit)	SEM	*n*
WT	+7[d]	2	6	-38 [d]	2	6	ND	--	--	ND	--	--	ND	--	--
N214R	+17 [d]	3	4	-40 [d]	2	4	ND	--	--	ND	--	--	ND	--	--
R205A	+6 [d]	3	4	-48 [d]	3	4	ND	--	--	ND	--	--	ND	--	--
R205H	-25.0	1.9	20	-45.0	4.0	17	ND	--	--	ND	--	--	ND	ND	--
R205H-N214R	-20.7	2.2	14	-51.6	4.0	6	-102.8	1.9	4	-180.8	6.6	14	-41.18	3.3	8
D185H-R205H	+80.0	3.8	7	-41.0	2.5	5	-101.1	6.7	7	-176.3	4.4	6	-36.3	5.9	6
D185A-R205H	+40.0	1.9	13	-38.6	4.6	7	-100.2	6.5	5	ND	--	--	ND	--	--

[a] From visual inspection of I_{TAIL} (pH_O6.5/pH_I6.5).
[b] Late component from double Boltzmann fits to G_{STEP} (pH_O6.5/pH_I6.5).
[c] From Gaussian fits to dG_{STEP}/dV (pH_O6.5/pH_I6.5).
[d] Data from Ramsey, et al. (2010).

4. Other mutations in the background of R205H

To generate resting state currents in Hv1 monomer subunits, we introduce R205H into the background of Hv1 with a stop codon inserted after Lys221 (Hv1ΔC). As previously reported, C-terminal truncation is sufficient to monomerize Hv1[131,137–139]. We expect that R205H-ΔC monomers will produce resting state 'shuttle' current just as in the dimer. In representative traces from whole cell patch experiments in HEK293 cells (Fig. 23A,B) there is a time dependent rise in current with increasing depolarizations. We limit our analysis to voltage dependent gating in R205H-ΔC. The I_{STEP}-V relation for current in symmetric pH conditions (pH_O6.5/pH_O6.5) exhibits double rectification with a shallow plateau at intermediate voltages (Fig. 23A,B). Like R205H alone, lowering pH_O (pH_O5.5) increases the amplitude of inward resting-state current (Fig. 23C). Voltage-dependent opening of G_{AQ}, as estimated from V_{THR}, also shifts ~40mV/pH unit in R205H-ΔC (Fig. 23B,C). The most straightforward interpretation of the data is that R205H-ΔC alters neither voltage-dependent G_{SH} gating at negative potentials nor G_{AQ} gating at more positive potentials, and that the pH-sensitivity of G_{SH} and G_{AQ} gating is unperturbed in Hv1 monomer subunits.

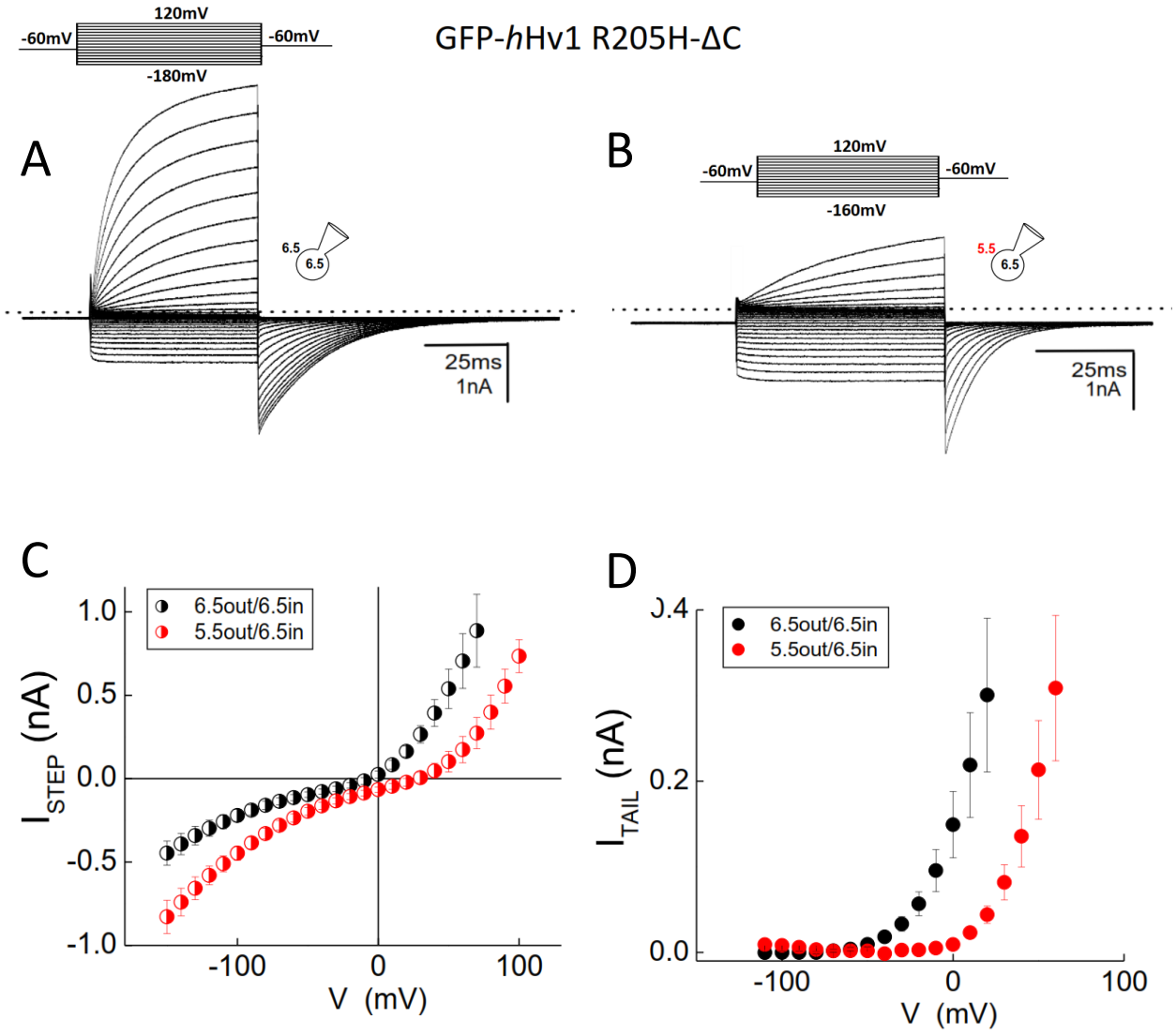

Figure 23. R205H-ΔC H^+ shuttle currents show that VS activation is measurable in Hv1 monomers. A-B) Representative whole-cell current records in a cell expressing R205H-ΔC. Current was elicited from a holding potential HP= -60 mV, V_{STEP}=+120mV to -180mV, V_{TAIL}=-60mV. Solutions were TMA/$MeSO_3^-$ with (A) pH_O6.5 and (B) pH_I5.5 bath solutions with in the pipette. Mean values for I_{STEP} (C; open symbols) or the absolute value of linear leak-subtracted I_{TAIL} (D; filled symbols) is plotted as a function of the voltage step (pH_O = 6.5, black circles; or pH_O = 5.5, red circles). In D, the full experimental range of voltages is reduced to shown to emphasize the difference in the positions of the apparent P_{OPEN}-V relations. Symbols in C and D represent means ± SEM from n = 5 (I_{STEP}, pH_O = 6.5_O), n = 4 (I_{STEP}, pH_O = 5.5_O), n = 3 (I_{TAIL}, pH_O = 6.5_O), or n = 3 (I_{TAIL}, pH_O = 5.5_O). Apparent V_{THR} at two gradients were measured by visual inspection of current records, mean ± SEM of recording with pH_I6.5 (V_{THR} pH_O6.5 = -26.7mV ± 6.1; V_{THR} pH_O5.5 = +23.3± 5.6).

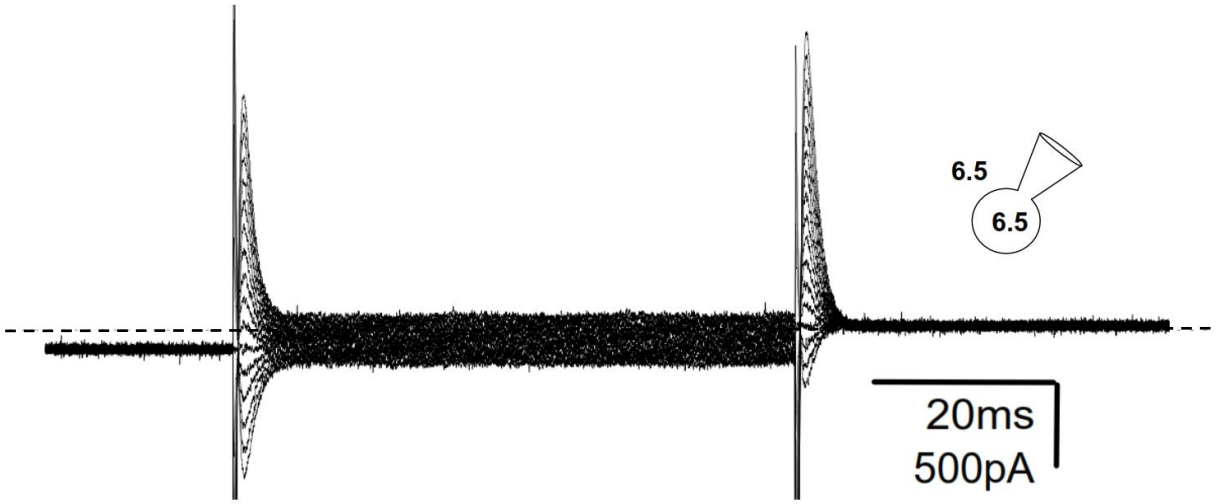

Figure 24. No voltage-dependent 'shuttle' or 'aqueous' currents from R205H-D112V expression
Representative recording whole-cell current record in a cell expressing D112V-R205H. Currents elicited from a holding potential of -30mV, V_{STEP} = +80mV to -80mV in increments of 10mV, V_{TAIL}=0mV. (pHO = pHI = 6.5).

Mutations of a conserved aspartate residue in S1 (D112) were shown to perturb the normally exquisite H^+ selectivity of Hv1[166,167]. D112 mutations also either shift voltage-dependent opening of G_{AQ}[166,167] or abrogate G_{AQ} entirely (D112V) [166,167]. It remains unclear whether the effects of D112V result from a perturbation of the H^+ conducting G_{AQ} pathway or disruption of a gating transition that is required to open G_{AQ}. We are unable to measure either activated- or resting-state currents in cells expressing D112V-R205H. One possible explanation for the lack of H^+ current is a defect in plasma membrane targeting of mutant channels. However, this explanation seems unlikely because the visible distribution of epifluorescence from the N-terminal EGFP in our fusion protein constructs is consistent with plasma membrane residence (not shown). Although we cannot at this time definitively rule out the possibility that second-site mutation of D112V abolished membrane expression, a simpler explanation for the data is that this mutation either abrogates G_{SH} and/or G_{AQ} gating in Hv1 or disrupts an aqueous crevice in Hv1 that is necessary for H^+ transfer via both the 'shuttle' and 'aqueous' pathways.

5. Electrophysiological properties of S1, S3 and S3 Hv1 His mutations

We performed histidine scanning mutagenesis on select residues of S1-S4 in Hv1 that we predict line the aqueous crevice or lie within the narrow trans-membrane 'hydrophobic gap' in the closed state. We use a homology model of Hv1 (open-state) based on Kv1.2-2.1 chimera[94] to select target residues. The expectation is that histidine mutagenesis of selected residues will create resting-state H^+ 'shuttle' currents at hyperpolarized membrane potentials, just as His substitutions at positions in S1 and S2 of the Shaker K^+ VS domain were found to yield resting-state H^+ 'shuttle' currents [106,121–123,156]. This 'closed-state' assay tests the hypotheses that specific residues along S1-S4 lie at the constriction point of Hv1 in the resting state. The residues that are predicted to be at the center most positions (within an extracellular to intracellular span) and that have R-groups facing the aqueous crevice in the homology model structure, were assigned a high probability of producing current at hyperpolarized potentials; (S1-V108,V109), (S2-I146,L147), (S3-V177, V178), (S4-I202,R205H). We also test adjacent candidate residues in **S1** (L111, L114) and **S4** (R205S, R205C, R211). Constructs were expressed either in HEK293 cells for mammalian whole cell patch or in *Xenopus* oocytes for excised patch voltage clamp experiments. The mutants are tested by voltage steps ranging from +100 to -140mV to measure both 'aqueous' H^+ currents and His mediated H^+ 'shuttle' currents. No His mutant was sufficient to elicit convincing resting-state 'shuttle' currents; however, representative current traces illustrate profound effects in a few candidates and suggest that some mutants have an important functional role in the G_{AQ} pathway.

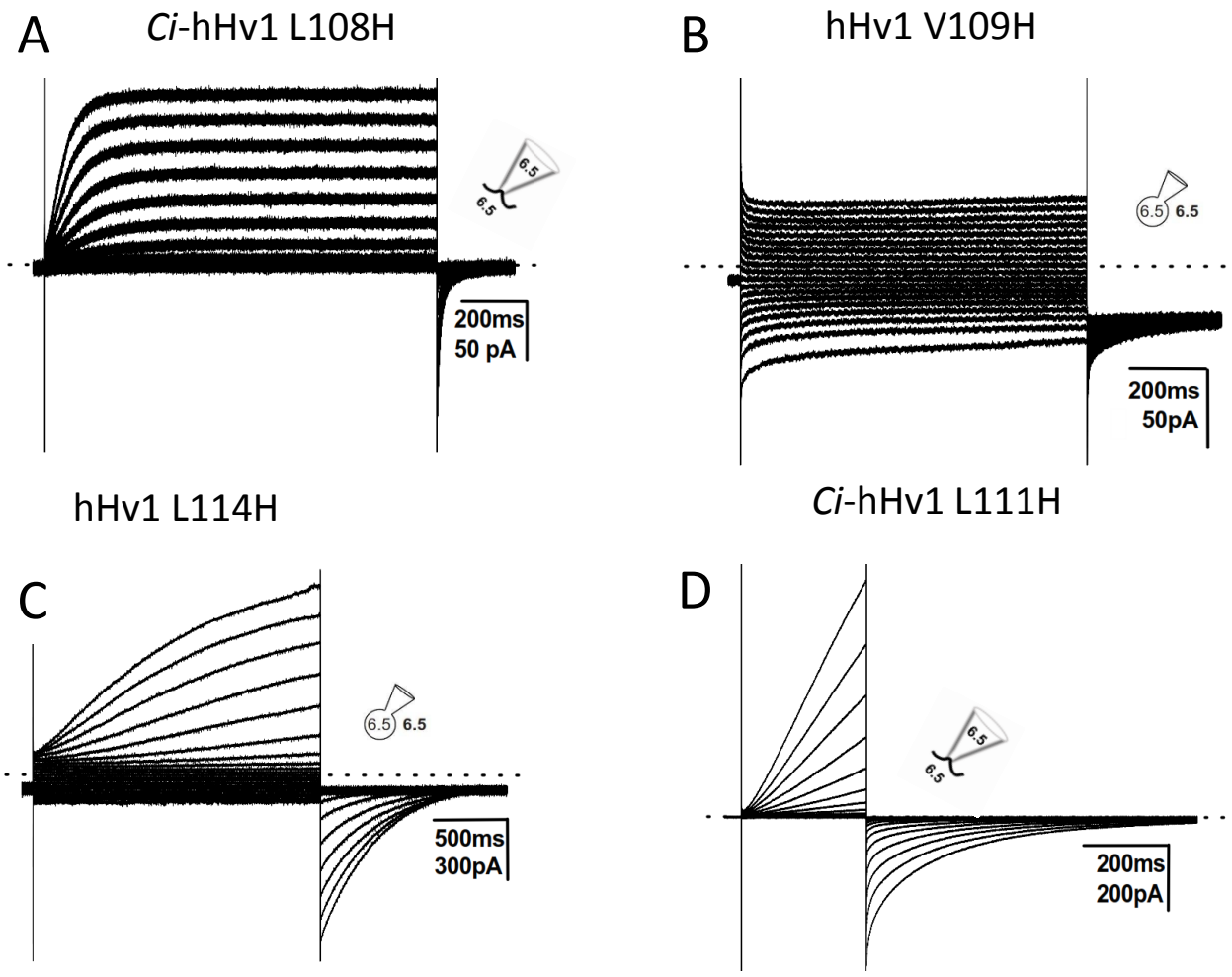

Figure 25. Hv1 S1 Histidine scanning L108H, V109H, L111H, and L114: no 'shuttle current' but profound effects from L108H and V109H.

A. Representative recording from an excised patch of *Xenopus* oocyte expressing L108H Hv1 (Ci-VSP N-terminal chimera). Currents elicited from a holding potential of -60 mV, V_{STEP} = -70 mV through +80 mV in increments of 10 mV, V_{TAIL}=-80mV. Note the effects of mutation on current activation compared to other His mutants of S1. **B.** Representative recording from a cell expressing V109H. Currents elicited from a holding potential of -80 mV, V_{STEP} = -80 mV through +100 mV in increments of 10 mV, V_{TAIL} = -60mV. **C.** Representative recording from a cell expressing V114H. Currents elicited from a holding potential of -60 mV, V_{STEP} = -100 mV through +100 mV in increments of 10 mV, V_{TAIL} = -60mV. **D.** Representative recording from an excised patch of *Xenopus* oocyte expressing L111H Hv1 (Ci-VSP N-terminal chimera). Currents elicited from a holding potential of -60 mV, V_{STEP} = -100 mV through +130 mV in increments of 10 mV, V_{TAIL}=-80mV. All recordings done in symmetric pH conditions (pH_O = pH_I = 6.5). The dashed lines indicates zero current level.

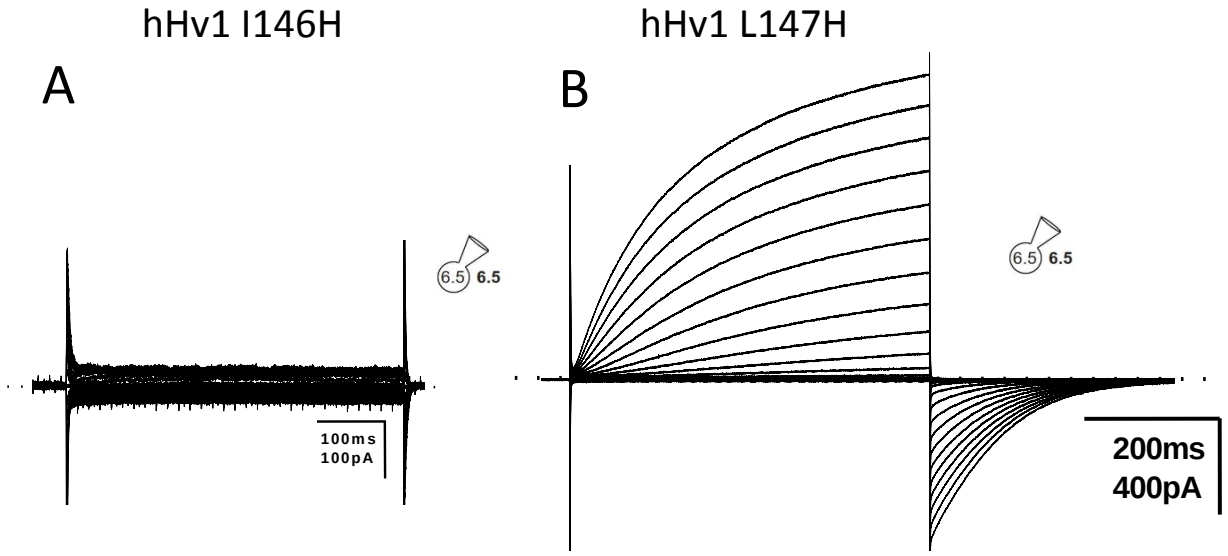

Figure 26. Hv1 S2 Histidine scanning I146H, L147H: no 'shuttle current' but profound effects from I146.

A. Representative recording from an excised patch of a cell expressing I146H. Currents elicited from a holding potential of 0 mV, V_{STEP} = -100 mV through +100 mV in increments of 10 mV, V_{TAIL}=-30mV. Note the effects of mutation on current activation compared to the other His mutant of S2.
B. Representative recording from a cell expressing L147H. Currents elicited from a holding potential of -80 mV, V_{STEP} = -100 mV through +150 mV in increments of 10 mV, V_{TAIL} = -60mV. Both recordings done in symmetric pH conditions. (pH_O = pH_I = 6.5). The dashed lines indicates zero current level.

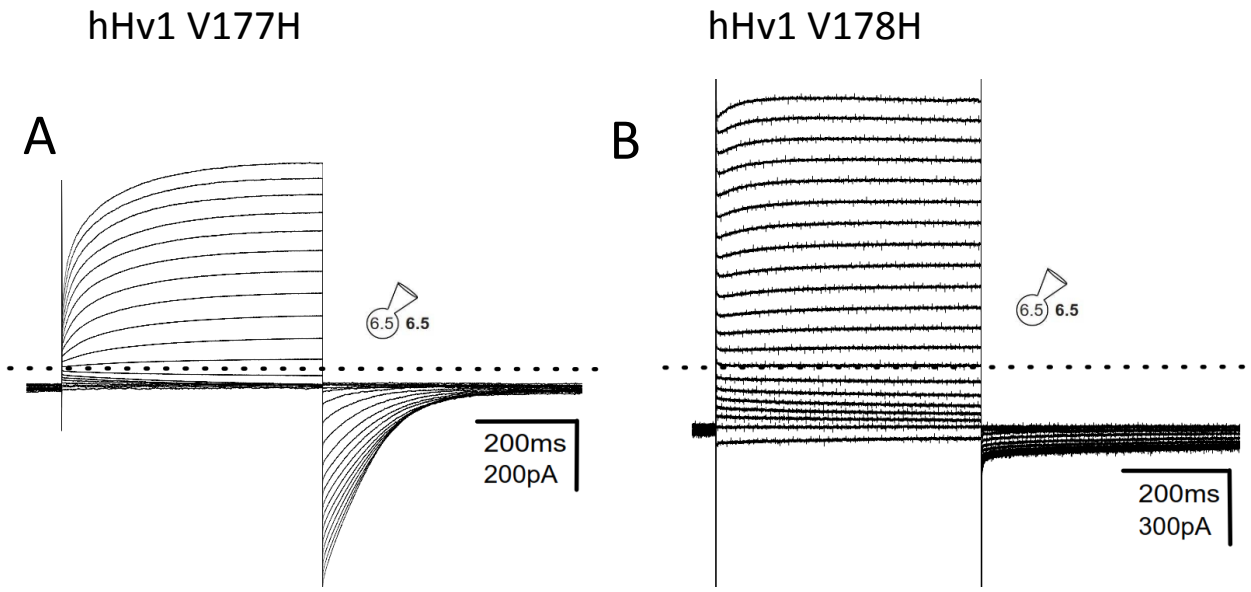

Figure 27. Hv1 S3 Histidine scanning V177H, V178H: no 'shuttle current' but G_{AQ} shifted to negative potentials.
A. Representative recording from an excised patch of a cell expressing V177H. Currents elicited from a holding potential of -60 mV, V_{STEP} = -100 mV through +130 mV in increments of 10 mV, V_{TAIL}= -80mV. **B.** Representative recording from a cell expressing V178H. Currents elicited from a holding potential of -90 mV, V_{STEP} = -100 mV through +100 mV in increments of 10 mV, V_{TAIL} = -90mV. Both recordings done in symmetric pH conditions. (pH_O = pH_I = 6.5). The dashed lines indicates zero current level. Note, both mutations shift current activation to very negative potentials; V177, V_{THR} = ~-90mV and V178, V_{THR} = ~-90mV.

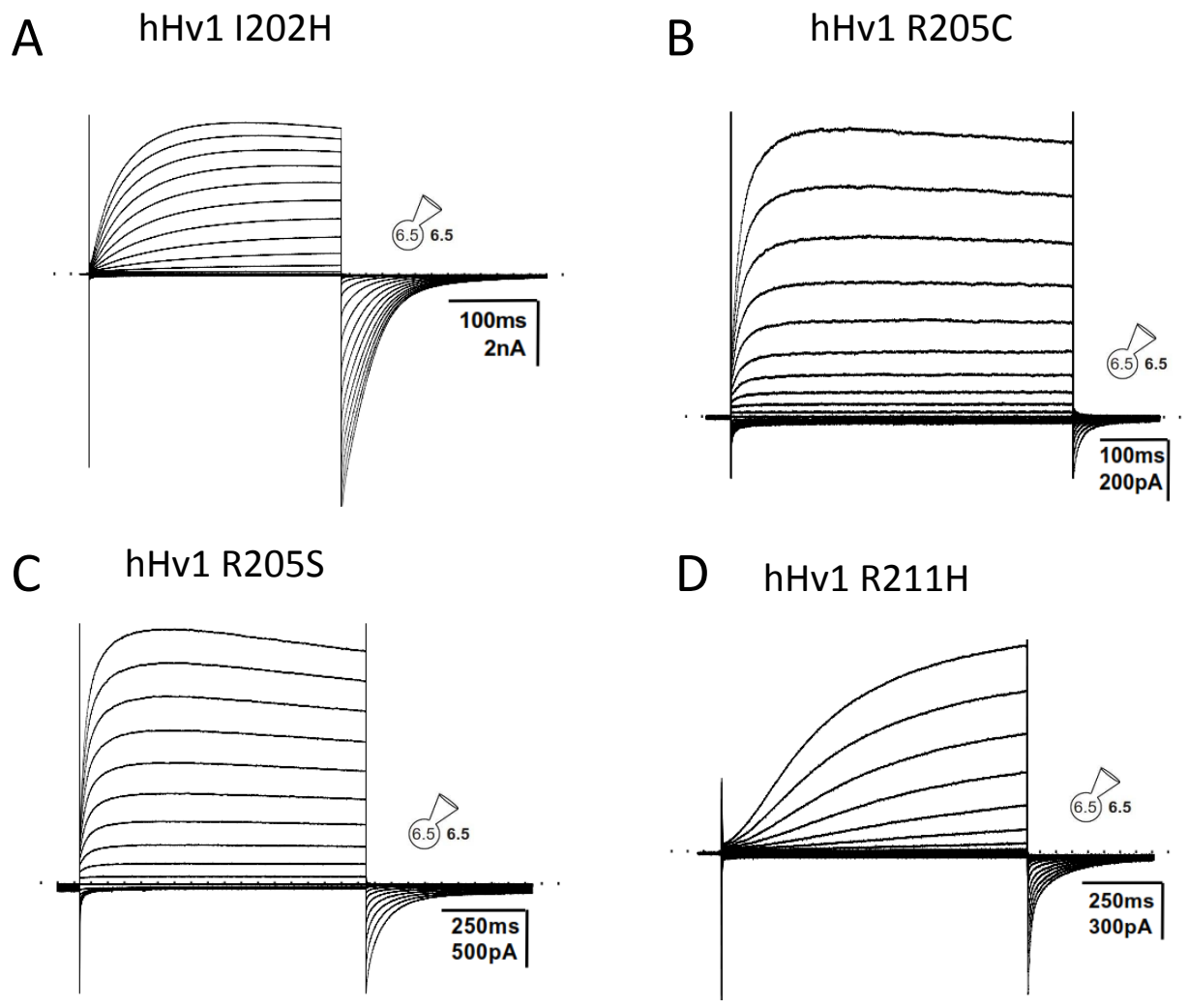

Figure 28. Hv1 S4 Histidine scanning I202H, R205S, R205C, and R211H: no 'shuttle current' in non-Histidine R205>C>S mutants

A. Representative recording from an excised patch of a cell expressing V2027H. Currents elicited from a holding potential of -30 mV, V_{STEP} = -100 mV through +100 mV in increments of 10 mV, V_{TAIL}= -70mV. **B.** Representative recording from a cell expressing R205C. Currents elicited from a holding potential of 0 mV, V_{STEP} = -100 mV through +100 mV in increments of 10 mV, V_{TAIL} = 0mV. **C**. Representative recording from an excised patch of a cell expressing V177H. Currents elicited from a holding potential of -60 mV, V_{STEP} = -100 mV through +130 mV in increments of 10 mV, V_{TAIL}= -80mV. **D.** Representative recording from a cell expressing R211H. Currents elicited from a holding potential of 0 mV, V_{STEP} = -90 mV through +100 mV in increments of 10 mV, V_{TAIL} = 0mV. All recordings done in symmetric pH conditions. (pH_O = pH_I = 6.5). The dashed lines indicates zero current level. Notice the increased rate of current activation in R205 mutants compared with R211H mutant.

In S1 mutations L108H and L109H had dramatic effects on channel activation (Fig. 25A,B). L108H increased the rate of current activation, whereas L109H appeared to have very disrupting effects on 'aqueous' pathway opening. The L109H mutant was particularly difficult to record as the mutation often had fatal effects on cells. The L111H and L114H mutants (Fig. 25C,D) did not produce resting-state currents or produce effects as those seen for L109H. We interpret the data to mean that L108H, L111H and L114H are not in the hydrophobic gap. Cells expressing L109H had round morphology and would not adhere to coverslips thus preventing further electrophysiological study. The presence or absence of resting-state currents in L109H could not be determined, thus the result is inconclusive.

In S2 mutations, there was an apparent effect from I146H substitution that was not seen in L147H (Fig. 26A,B). The I146H mutation caused dramatic decrease in expressed current, and this can be possibly be explained by low surface expression, trafficking defect or misfolding of the Hv1 protein. However, the channels were expressed with an N-terminal EGFP tag that demonstrated high intensity of light emission in the vicinity of the membrane under fluorescent microscopy. Thus we interpret the data to mean that the I146H substitution either has a blocking effect the 'aqueous' pathway or disrupts gating.

In S3, V177H and V178H mutants (Fig. 27A,B) shift current activation to more negative potentials (V177H:V_{THR} = -83mV, n=2; V178H: V_{THR} = -90mV, n=1). Because V177 and V178 are conserved hydrophobic residues, the effects seen for His substitution are particularly striking. One possible interpretation is that V177H and V178H mutations stabilize the activated state, thus the mutations affect gating rather than the 'aqueous' pathway; however we did not determine if selectivity was altered in this mutant. Another possible interpretation is that a histidine at V177 and V178 makes change in the hydrophobic gap structure. The currents would then represent contributions from both 'shuttle' current and 'aqueous' current. Both mutants caused damaging effects on cells and were difficult to record.

We expect that because I202 in Hv1 appears to be homologous to R362 in Shaker (Fig. 1), mutation to His will confer a H^+ shuttle current[106,121–123,156]. The absence of resting-state current in I202H (Fig. 28A) was interpreted to mean that this position is not in the hydrophobic gap in the resting state.

We test the whether alternate substitutions (R205S and R205C) of the first Arg in Hv1 S4 demonstrate resting state 'shuttle' or non-specific 'Omega' currents based on findings that similar substitutions in Shaker produce resting-state 'Omega' currents [106,121–123,156]. The R205S and R205C mutants (Fig. 28B,C) produced no resting-state H^+ currents, but current traces indicate that the rates of outward current activation were faster than WT Hv1, and this is consistent with faster current activation in R205H (Fig 10, Fig. 11). The R211H mutation (Fig. 28D) was expected to generate voltage dependent, alternating access H^+ transport as demonstrated for R365H and R371H mutants in Shaker K^+ channel[106,121–123,156]. However, the Shaker mutations were done in the background of a non-conducting mutant [106,121–123,156] and the 'aqueous' outward current in R211H is not disabled. The outward 'aqueous' H^+ currents would obscure H^+ 'shuttle' pump currents produced by R211H H^+ transport at positive potentials. The S4 substitutions did not produce resting state current and we interpret this to mean that His mediated currents endowed by R205H are specific to titration of the imidazole side chain. The R205S and R205C are not able to generate resting-state H^+ 'shuttle' currents.

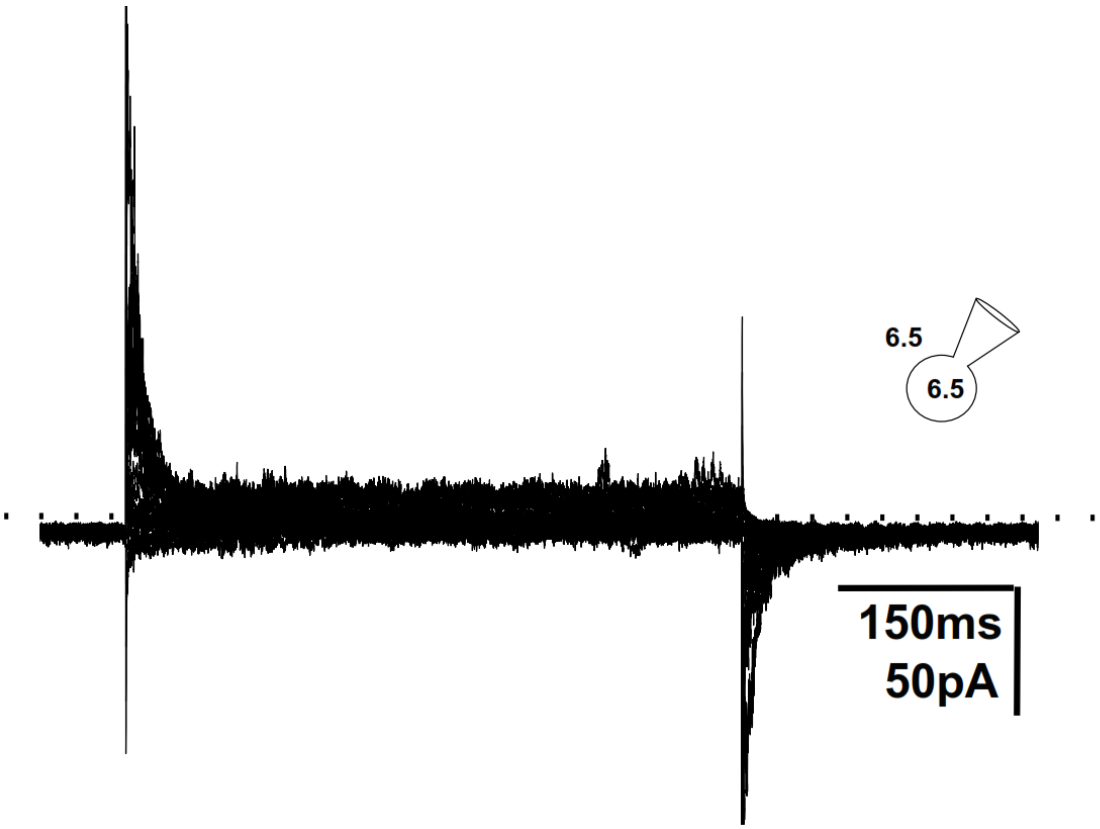

Figure 29. The 'shuttle' and aqueous' not present in R208H in c15orf27 expression. Representative recording whole-cell current record in a cell expressing c15orf27 R208H mutant. Currents elicited from a holding potential of -30 mV, V_{STEP} = + 100 mV to -100 mV in increments of 10 mV ($pH_O = pH_I = 6.5$).

6. c15of27 S4 Arg to His mutations

c15orf27 is a putative uncharacterized protein that shows strong sequence homology to the voltage sensing domains of voltage-gated cation channels and voltage-sensing phosphatases (CiVSP, TPTE and TPTE2) (Fig. 1). c15orf27 is most closely related to Hv1 the voltage-gated proton channels (Fig. 1). Unlike Hv1, c15orf27 contains a 353 amino acid C-terminal domain with unknown function and limited homology to known and predicted proteins. We make His substitutions of Arg residues (R208H, R211H, and R214H) on the predicted VS domain in human c15of27 cDNA. We expect that these Arg residues lie along a predicted VS domain S4 helix, and will produce resting state H^+ currents similar as those measured for R205H in Hv1 (Fig 10) and R362H, R365H, and R371H in Shaker K^+ channels [106,121–123,156]. The representative trace in Figure 28 of c15orf27 R208H expression in tet-induced Flp-In 293 T-REx cells in whole cell mode, demonstrates that His substitution did not produce resting state current and there were no outward time dependent channel-like currents exhibited. Our interpretation of results for R208H (Fig. 28), and similar results for R211H and R214H (not shown), are therefore limited. An alternate strategy of C-terminal deletion by inserting stop codons at various locations between the voltage sensor (S4) and CT-domain, also produced varied or uninterpretable results (not shown). We conclude that proton 'shuttle' currents could not be measured from R208H substitutions in the full length or C-terminally truncated c15orf27 putative VS domains.

Chapter IV. Discussion

1. R205H resting state currents constrain Hv1 possible resting-state structures

Substitutions R205C and R205S did not produce resting-state 'shuttle' or 'Omega' currents, but R205H generated robust, voltage dependent 'shuttle' currents at negative potentials, when the VS is in the resting state [106,121–123,156]. VS resting state conformation most likely places the introduced His at R205H into a position where it is simultaneously accessible to protons on both sides of the membrane to generate a channel-like resting-state H^+ current [106,121–123,156]. The results here for R205H differ from a previous report by Kulleperuma et al. (2013) where the authors observed no resting-state H^+ current at negative voltages[126]. We interpret the difference in results for the R205H mutant to be due to differences in expression levels because current expression in our studies are much larger than those previously reported[126]. In the resting state, the membrane dielectric is focused by the VS protein and is greatest near the location of the H^+-conducting His residue in S4 [121–123,156]**.** A likely explanation for our data, based on conclusions drawn from studies of Shaker R362H gating[121–123,156], is that in the G_{SH} open state (resting state of the Hv1 VS), 205H is located in a focused electrical field. Changes in the transmembrane electrical field drive a conformational change resulting in VS activation, causing the His introduced at position R205 to adopt a conformation that is not permissive for proton shuttling. Amino acid sequence similarity, functional homology, molecular modeling and simulation studies of Hv1 to the VS domains of other VGCs suggest that there is similar architecture [124,94,126]. The VS sequence alignment presented here (Fig. 1) indicates that R205, the first S4 Arg in Hv1 (R1) corresponds to the second Arg (R2) in the Shaker K^+ channel. However our data compellingly indicate that in Hv1 R205 is the functional analogue of R356 in Shaker, suggesting that amino acid sequence alignments are of limited utility for inferring protein function. Given that Hv1 has only three S4 arginines while four or more conserved arginine residues are found in Shaker and other VGCs, we suggest that different VS domains are likely to exhibit

some structural differences. The functional similarity between R205H in Hv1 and R362H in Shaker however suggests that the mechanism of VS activation are likely to be substantially similar.

Water invades the VS protein structure from both sides of the membrane but is restricted from crossing due to a centrally located hydrophobic barrier [80–82,119,120]. Estimates for the length or distance of this 'hydrophobic gap' vary depending on the approach used to estimate the constraints [80–82,119,120]. Cysteine scanning studies of S4 in the VS of Na^+ channels report that internal and external facing residues were separated by a hydrophobic barrier of 10Å, and estimate a gap thickness of 4Å[119,120,200]. Fluorescence (FRET) and lanthanide-based (LRET) studies for VS in K^+ channels estimate a gap size of near 3Å[35,111]. The size of the hydrophobic gap has also been estimated by mutations that create a conducting pore across the partition that bridges both aqueous compartments (i.e. 'Omega' pathway, His mediated H^+ pathway) [103,129,174,176,178]. Simulations of a Kv1.2 (R1Q) non-selective 'Omega' pathway estimate a pore size of 1.4 Å [178]. Histidine substitution of R1 (R362H) in the Shaker K^+ channel VS domain confers a H^+ transport pathway across the partition, presumably by H^+ binding and unbinding the His imidazole side chain[106,121–123,156]. If transfer of H^+ from H_2O to H_3O^+ occurs by a Grotthuss-type mechanism, then protons hop across a hydrogen bond length of ~2.4-2.8Å[9,22,143,144]. Therefore His mediated H^+ transfer (G_{SH}) across the barrier is a useful tool for estimating microscopic geometric constraints of the 'hydrophobic gap'. In contrast to other voltage gated channels, the Hv1 VS domain contains an aqueous H^+ conducting pathway (G_{AQ}) and the 'hydrophobic gap' closes G_{AQ} in the resting state[94]. The R205H meditated resting-state conductance (G_{SH}) indicates that the 'hydrophobic gap' in Hv1 is a focused and narrow barrier that separates intracellular and extracellular facing water crevices.

The recent report by Chamberlin et al. (2013) proposes that two 'hydrophobic plugs' form in the center of the Hv1 VS domain resting-state structure that exclude water molecules[118]. The study, based on homology modeling and simulations of an Hv1 resting state structure, predicts that the two stacked constriction points involve residues that protrude into the central aqueous crevice. The most external plug consist of hydrophobic residues of S1 and S4 and the second plug, located beneath the first plug (i.e., on

the intracellular side), is proposed to consist of salt bridge interactions between S4 arginines and acidic glutamate residues on S2[118]. Our results for R205H are consistent with the conclusions of previous studies in His mutant Shaker channels [106,121–123,156] in which a histidine inserted at the R205 position of Hv1 is simultaneously accessible to H^+ of intracellular- and extracellular-facing aqueous compartments. Presumably an externally located hydrophobic plug would dehydrate the aqueous crevice and would prohibit H^+ transfer from extracellular water (H_3O^+) to the introduced His and then on to intracellular water. We cannot rule out the possibility that ionizable groups residue side chains or the protein backbone that are near 205H might contribute to the formation of the H^+ 'shuttle' pathway that mediates G_{SH}. A simpler interpretation however is that proton transfer is directly mediated by the imidazole side chain of the introduced His, and that the effective thickness of the 'hydrophobic gap' is determined by the distance of hydrogen bonds between imidazole nitrogen(s) and intra- or extra-cellular waters (~2.4-2.8Å), resulting in a 'proton transfer center' of ~5 Å in length. The hypothesis that the resting state of Hv1 contains two hydrophobic gaps[118] therefore appears to be inconsistent with the existence of the robust G_{SH} in Hv1 R205H reported here. Additional experimental and theoretical studies are needed to address the structural basis of G_{SH} in R205H.

It remains unclear whether the effect of D112V to abolish both G_{SH} and G_{AQ} result from a perturbation of the H^+ conduction pathway(s) or from a disruption of a gating mechanisms. The distribution of EGFP fluorescence in cells expressing D112V-R205H is consistent with plasma membrane residence, suggesting that altered subcellular trafficking does not explain the loss of function in this mutant. Thus, the simplest interpretation our data is that D112 substitution with a hydrophobic valine residue abrogates G_{SH} and G_{AQ} gating in Hv1 because D112V disrupts an aqueous crevice in Hv1 that is necessary for H^+ transfer via both the 'shuttle' and 'aqueous' pathways. The disruption could result from change in hydrophilicity alone but also possibly from structural effects due mutation (i.e., disruption of hydrogen bond network or protein misfolding). The lack of G_{SH} could suggest that R205H on S4 is near the D112V position on S1 in the resting-state structure.

Both MTSET labeling of N214C and N214R mutations are sufficient to attenuate outward H^+ current mediated by G_{AQ} in Hv1[94,135–137]. The block of outward current by N214R is likely to result from movement of the cationic guanidinium side chain of N214R to a position on the intracellular side of the hydrophobic gap or 'proton transfer center' that prevents outward movement of protons[94,135–137]. The rapid release of the block occurs at negative potentials [94,135–137] (i.e., I_{TAIL} mediated by G_{AQ} is unaffected by the presence of N214R), suggesting that N214R blocks G_{AQ} from an intracellular site that lies in the electric field. Because H^+ permeating in G_{AQ} must move through a proton transfer center that spans the effective thickness of the electric field, 214R is likely to be close to D112 in the activated state. Voltage-dependent block of G_{AQ} does not affect G_{SH} in the resting state, as evidenced by the similarity of G_{SH}-V relations in R205H and R205H-N214R. The simplest interpretation of this finding is that 214R is not near 205H in the resting state. If we assume that S4 is a rigid α-helix, then the distance between 205H and 214R position (10.5Å) is roughly equal to the distance over which S4 is translated during Hv1 activation. Given that S4 movement is not likely to be purely vertical, S4 displacement in the Z-axis is likely to be less than 10.5Å. Our experimental data are thus in good agreement with previous estimates of S4 movement during VS activation in other channel proteins[119,120,200].

The glutamate at position 185 in Hv1 is not conserved in the VS domain sequences of other channels (Fig. 1)[94]. Although D185 substitutions shift V_{THR} for G_{AQ} activation positively, D185H is not sufficient to confer a resting-state current like R205H. We conclude that D185H is not located in the 'hydrophobic gap' in either the Hv1 resting or activated states[94]. Furthermore, our results indicate D185 substitutions do not block G_{SH} in experiments with R205H-D185H or R205H-D185A double mutants. Previous homology modeling and simulation studies suggest that D185 interacts with R2[126] or R3[94] on S4 of Hv1 VS domain. Our results for R205H-D185H possibly support D185 interactions with R2 or R3. The D185H mutation could disrupt D185 interactions with R2 and R3 that occur during late transitions of VS activation. These late transitions would occur after the movement of R1 (reported by G_{SH}) and near a

final transition to the open-state. D185H mutation would disrupt late transitions and thus cause the right shift in channel activation.

2. R205H resting state currents inform H^+ transfer mechanism

The R205H substitution confers a novel H^+ 'shuttle' transfer pathway in Hv1 that is distinct from the intrinsic 'water wire' H^+ pathway. The G_{STEP}-V relation in R205H has a biphasic U-shape that represents two distinct H^+ conductances. The arms of the U-shape are not equally tall because the conductance amplitudes are not the same at equal and opposite voltages. G_{SH} occurs at negative voltages along the G_{STEP}-V, and is nearly 10-fold lower than G_{AQ} at positive voltages. G_{SH} is attributed to H^+ binding and unbinding of a His imidazole side chain that is positioned at a narrow transmembrane gap within the VS structure [106,121–123,156]. G_{AQ} is thought to occur by H^+ binding and transport across a hydrogen bonded chain (HBC) of water within the VS structure (i.e. aqueous 'water wire'). Both pathways are in a focused electric field and both conduct H^+ down an electrochemical gradient[94], however, the 10-fold larger G_{AQ} amplitudes suggest that it is far more efficient for H^+ transport than G_{SH}. This finding has important implications for the mechanism of H^+ transport in WT Hv1. There are two distinct hypotheses for the H^+ conductance in WT Hv1. Cherny and DeCoursey (1995) hypothesized a mechanism for H^+ transfer in Hv1 in which protonation sites in the protein, become accessible or inaccessible, based on voltage dependent conformational changes[8]. Ramsey et al. (2010) hypothesized that H^+ transport occurs along an HBC 'water wire' within the protein aqueous crevice [94]. In R205H, G_{SH} demonstrates that the explicit titration of a side chain produces a much smaller amplitude H^+ conductance than that of the aqueous 'water wire' H^+. Thus R205H compares two distinct H^+ transport mechanisms within the same protein structure, and the results are in favor of an aqueous 'water wire' H^+ transport mechanism in WT Hv1.

G_{SH} reveals the presence of intracellular and extracellular aqueous crevices in Hv1, and like Shaker R362H, H^+ transfer is mediated by 'shuttling' through waters that are resident in the VS crevices. The

aqueous compartments are evidently separated by R205 in the resting state. H^+ conductance is blocked in the WT Hv1 resting state, but R205H mutation removes the block and allows for H^+ shuttling between aqueous crevices. H^+ conductance in R205H is observed in the activated and resting states.

We took advantage of N214R voltage dependent block of G_{AQ} transfer pathway to isolate G_{SH} from G_{AQ}. We measure time dependent decay of G_{AQ} closure at negative potentials (I_{TAIL}), and we interpret this as a voltage dependent release of the N214R block. G_{SH} is also measured at negative potentials, thus His mediated H^+ conductance is not blocked by N214R in the resting state. The simplest interpretation is that N214R adopts a blocking position when S4 undergoes a voltage dependent outward translation during VS activation. Outward movement of S4 pulls the N214R into a position that disrupts the aqueous 'water wire' pathway from the intracellular side. A negative voltage step is sufficient to cause rapid release the block because S4 moves into the resting state. The block is released prior to the closure of G_{AQ} and this is evidenced by time dependent decay of G_{AQ} tail current. Our results are in agreement with previous studies of N214R [94,135–137] and also cysteine accessibility studies of N214 that demonstrated MTSET labeling of a cysteine at this position is sufficient to abrogate outward H^+ conductance [94,135–137].

C-terminal truncation is believed to be sufficient to monomerize Hv1 channels and monomer subunits retain the ability for G_{AQ} function [131,133–135,139]. In the R205H-ΔC mutant, G_{SH} and G_{AQ} mediated currents are observed and this demonstrates that monomer subunits have resting- and activated state structures that are the same or very similar to dimers in Hv1. The presence of G_{SH} in monomer subunits indicates that the dimer structural configuration is not required for the resting state structure in Hv1. The C-terminal coiled coil motif tethers two Hv1 conducting subunits together. When it was removed at the K221 position on S4, in the background of R205H substitution, the monomer produced large resting-state currents at negative potentials. The simplest interpretation is that R205H monomer subunits are capable of resting-state H^+ transfer and dimer configuration is not required for G_{SH}.

3. R205H resting state currents inform H^+ gating mechanism

The lack of a direct method to assay early steps in the Hv1 activation pathway has represented a major obstacle to understanding the mechanisms of VS activation and pH sensitive gating in Hv1. In S1-S6 TM channels early transitions represent VS activation and charge movement (Q-V) that is coupled to the opening of the S5-S6 pore domain[5,156]. Early and late transitions can be experimentally separated, thus VS activation and opening are two thermodynamically distinct processes that occur in the activation pathway[5,93,96,129,169–171]. By comparing the Q-V, that relates voltage sensor movement, with the P_{OPEN}-V, that relates the concerted opening of ion pores, it can be seen that most of the charge moves at voltages negative to where the channel pores begin to open[5,93,96,129,169–171]. Thus voltage sensing precedes channel opening but importantly, VS activation is coupled to pore opening[189]. The results presented for Hv1 are consistent with channel activation in S1-S6 type voltage gated channels. We find that initial VS activation and opening of the 'aqueous' conductance in Hv1 are experimentally separable. Furthermore, VS activation and opening of the 'aqueous' conducting pathway are two distinct processes that occur over very different ranges of voltage. The charged arginine residues in S4, required for sensitivity to changes in membrane voltage, are conserved on the Hv1 voltage sensor. R205H substitution creates resting-state 'shuttle' current that is analogous to the R362H Shaker K^+ channel mutant[106,121–123,156] and the R223H Ci-VSP mutant[100]. In voltage-gated channels, resting-state currents are not transient gating currents, but rather they represent a proxy for the movement of protein associated charge during VS activation. VS activation in Hv1 is thus reported by voltage-dependent His mediated H^+ 'shuttle' conductance (G_{SH}) in the R205H mutant. G_{SH} is gated open at negative potentials when VS is in the resting state, but it exhibits strong voltage dependent rectification at positive voltages and is gated closed prior to opening of the aqueous H^+ conducting pathway (G_{AQ}). Thus, gating of G_{SH} represents an early voltage-dependent step. The work here converges on the idea that Hv1 possesses authentic voltage sensor function, like other known S4 type VS domain proteins. Similarly, in other voltage-gated channels, early voltage-dependent transitions in Hv1 are coupled to the opening of the conduction pathway.

Substitutions at R205A have been shown to speed channel activation in Hv1[94], and the same is true for R205H. The G_{AQ} activation rate in R205H is much faster than that seen in wild type. The τ_{ACT} is decreased nearly 40-fold at every voltage analyzed (Fig. 11A,B). G_{AQ} deactivation rate is also faster in R205H. The τ_{DEACT} is decreased approximately 10-fold at all potentials analyzed (Fig. 11C). Decreased rate constants observed in R205H indicate that it has much faster gating kinetics than WT Hv1. One explanation for these results is that salt bridge interactions of R205 with residues along S1-S3 are disrupted or altered. Histidine is thought to preserve the charge at R1 position, but its charge is based on ionization state [106,121–123,156]. Nonetheless, many studies converge on the idea that charged arginines on S4 form ion pairs with negatively charged amino acid residues on neighboring S1, S2 and S3 helices[82,94,99.76]. Upon depolarization and VS activation the positively charged arginines on S4 make a series of ion pairs with negative charges[82,94,99.76]. Thus R205H might lower energy barrier for VS activation. A recent homology modeling and simulation study of a Ci-Hv1 resting state structure, predicts an interaction between the first arginine on S4 with a glutamate residue on S2[118]. The profound changes in gating kinetics for R205H suggest it might be a good candidate to study side chain interactions during VS gating.

The τ_{ACT} for resting state current in R205H mutants was difficult to measure because fast rate of G_{SH} activation occurs at earliest time period of voltage steps that open G_{SH}. Capacitance settling over the same time period contributed to time-dependent current measured and τ_{ACT} values were often scattered. However, τ_{ACT} values at extreme negative voltages could be measured and demonstrate that G_{SH} activation rate much smaller than G_{AQ}. Thus G_{SH} has a much faster rate of activation than G_{AQ}. Ideally, measured activation rates for both G_{AQ} and G_{SH} could be used to derive rate constants for closed to open ($R \leftrightarrow O$) state transitions at equilibrium. With refined experimental technique this may be achievable, but is beyond the scope of this study.

In order to dissect G_{SH} from G_{AQ}, we introduced a second mutation (N214R) into the background of Hv1 R205H. The addition of an arginine residue at the N214 position does not alter G_{AQ} gating. Altering the number of charges on S4 has been shown to alter voltage-dependent gating in other VGCs [82,98,113–115] and it was important consider in our studies of Hv1. V_{THR} measurements were used to define G_{AQ} opening because it is measured at the most negative voltages where the aqueous pathway begins to open. We observe no significant shift in V_{THR} between R205H and R205H-N214R and interpret this to mean that the addition of an arginine to S4 at the N214 position did not alter gating of G_{AQ}.

Gating of the aqueous H^+ conducting pathway (G_{AQ}) in Hv1 proton channels is coordinately controlled by changes in both the transmembrane voltage and pH gradients (V_m and ΔpH, respectively) [23,49,190]. Changes in ΔpH alter the apparent voltage dependence of G_{AQ} open probability ($P_{OPEN-AQ}$), indicating that gating is a cooperative process. Modulation of $P_{OPEN-AQ}$ by changes in ΔpH constitutes a form of 'electrochemical transduction' (ET) in the Hv1 gating mechanism. ET in G_{AQ} gating in Hv1 is characterized by a ~40 mV shift in the voltage dependence of $P_{OPEN-AQ}$ for each unit change in the pH gradient [23,49,190]. Cherny and DeCoursey (1995) hypothesized a mechanism for ET in Hv1 in which protonation sites in the protein, become accessible or inaccessible, based on voltage-dependent conformational changes. Their model predicts the pH_O coupling to opening of G_{AQ} is maintained in every Hv1 point mutant in which it has been examined[24,40], including those that alter the selectivity for ion conduction[24,40]. However, the effect of ΔpH changes on VS activation in Hv1 has not been measured independently of G_{AQ} gating.

This results from 205H-N214R demonstrates that electrochemical coupling in Hv1 represents a composite response that is attributable to at least two experimentally separable gating transitions. The novel and centrally important finding of this study is that changes in pH_O modulate VS activation in Hv1. Thus, the ΔpH-sensitive gating transition occurs early in the Hv1 activation pathway, and G_{AQ} gating inherits its apparent ΔpH dependence from and earlier transition. The results force a new scheme that differs from Cherny and DeCoursey's 1995 model[24,40]. Our findings raise fundamental questions about the

mechanism of ΔpH sensing in VS domains and suggests that the pH sensitivity observed in Hv1 may be conserved among related VS domain-containing proteins.

In Shaker and other VGC's, it is believed that charge translocation (Q-V) is nearly independent of pH_O and rightward shifts observed in Shaker Q-V (~7mV/pH unit) with lower pH_O are considered to result from surface charge screening by H^+[106,121–123,156]. The effects of changes in pH on VS activation in Hv1 have not been measured in isolation from the intrinsic 'aqueous' ionic H^+ conductance and the lack of a direct method to assay early steps in the Hv1 activation pathway represented a major obstacle to understanding the mechanisms of VS activation and pH sensitive gating in Hv1. We demonstrate here that changes in pH_O modulate early voltage-dependent transitions that are then inherited by later open state transitions. Introducing the second site N214R mutation in the background of voltage sensing reporter R205H (G_{SH}), abrogates the intrinsic aqueous conductance (G_{AQ}) and we test the effect of changes in transmembrane pH gradient on VS activation (G_{SH}) in isolation. A unique feature of the R205H-N214R mutant, is that I_{TAIL} (Fig. 6B) can still be measured, thus the effect of ΔpH on P_{OPEN} of the aqueous conducting pathway can be determined for comparison to G_{SH}. Results here demonstrate for the first time, that changes in the pH gradient have equal effects on both VS activation (G_{SH}-V) and activation of aqueous H^+ conductance (G_{AQ}). Consistent with our results demonstrating that VS activation (G_{SH}) is an early step in the activation pathway of Hv1, pH sensitive transitions must also occur very early in the activation pathway; either preceding VS activation or concomitantly.

The results here demonstrate that Hv1 possesses a form of electromechanical coupling (EC) that is similar to that which is seen in other VGCs. In Drosophila K^+ Shaker with the 'ILT' mutant, identified in the Aldrich laboratory, the P_{OPEN}-V is shifted relative to Q-V and this effect is referred to as, change in VS-pore coupling[189]. Many studies have converged on a basic mechanism in which voltage sensors move independently in response to voltage change, but a final concerted transition among all 4 VS domains is required to open the ion conducting pathway[5,97,98,113,157,169,189,201–203]. The expectation is that EC coupling would be absent from voltage gated H^+ channels, that lack the type of pore domain found in other ion

channels. In Shaker for example, the degree to which Q-V (or G_{SH}-V) and or G_{K^+}-V (or P_{OPEN}-V) relations are separated on the voltage axis reflect the extent to which VS activation and concerted opening of the ion permeation pathway are coupled. We now know that in Hv1, the Q-V (or G_{SH}-V) and or G_{AQ}-V (or P_{OPEN}-V) relations are separated on the voltage axis, and reflect the extent to which VS activation and opening of the aqueous H^+ conducting pathway are coupled within the shared VS domain. We test the idea that mutations reported to shift Hv1 channel activation to more positive potentials, act on channel opening but not voltage sensing. The mutation D185A, as reported by Ramsey et al 2010, shifts V_{THR} in Hv1 > +70mV on the voltage axis. We make a D185H substitution at this position in the background of R205H and measure resting state H^+ 'shuttle' currents and intrinsic aqueous H^+ currents in this mutant. Analysis demonstrates that R205H-185H mutants show resting state currents at negative potentials that both rectify before opening of the intrinsic aqueous pathway. Voltage sensor activation in Hv1 is reported here using R205H substitution along with a second site mutation D185H to demonstrate that coupling between VS activation and channel opening in Hv1 can be perturbed and produce robust shifts in G_{AQ}-V that have relatively little effect on G_{SH}-V. There is a marked shift in the activation of intrinsic aqueous H^+ channel current for 205H-D185H relative to G_{SH} indicating that VS activation and pore opening in Hv1 are electromechanically coupled.

Unlike other voltage gated channels, Hv1 lacks a pore domain and VS domain physically interacts with an adjacent Hv1 VS via a C-terminal coiled-coil motif and the extracellular S1-S2 linker to form a dimer [131,133–135,139]. Several groups have demonstrated that C-terminal truncation is sufficient to 'monomerize' Hv1 channels, and the prevailing dogma is that monomeric Hv1 channels remain functional but lack inter-subunit interactions that underlie cooperative gating. Truncation of the coiled-coil by deletion of both the N- and C-termini (Hv1ΔNΔC) reduces the propensity for dimer formation but does not alter the apparent valence of gating charge moved by each VS domain, suggesting that a single VS is sufficient for voltage-dependent gating in Hv1 [131,133–135,139]. The ΔpH sensitivity of G_{AQ} gating is apparently unperturbed in an Hv1 C-terminal truncation mutant produced by introducing a stop codon

after Lys221 (Hv1ΔC), suggesting that modulation of voltage-dependent gating, like H^+-selective permeation, is intrinsic to each individual Hv1 VS domain [131,137–139].

4. Hv1 S1, S3 and S3 His mutations

We did histidine scanning mutagenesis of residues predicted to line the aqueous crevice or lie within the narrow trans-membrane gap in the closed state, Hv1 pore domain. A crystal structure of Hv1 has not yet been determined so we test structural constraints of the protein using electrophysiology. To find target residues we use a homology model generated in study by Ramsey et al. of Hv1 (open-state) based on Kv1.2-2.1 chimera[76 94]. Histidine mutagenesis of selected residues is used to create "closed-state" H^+ shuttle currents at hyperpolarized membrane potentials. This "closed-state" assay informs us to which residues create a closed state H^+ shuttle current and tests the hypotheses that specific residues along S1-S4 lie at the constriction point of Hv1 in the resting state. Considering that the upper limit of H^+ transfer distance is near (2.8Å), our data suggests residues most of the residues chosen in S1-S4 have extremely limited access to H_2O in resting state conformation or do not lie in the narrow transmembrane gap in a focused electric field. None of the mutants tested display channel-like resting state currents or bell shaped I-V current plots, suggesting that histidine at these positions do not confer 'shuttle' or state dependent proton transfer. We interpret the results to mean that the candidate residues we tested are not in the 'hydrophobic gap' in the resting state. Two notable results in the I146H and V109H mutants suggest that these residues are located in the aqueous pathway and are sufficient to disrupt open-state G_{AQ}.

5. c15orf27, S4 Arg to His mutations

The goal of this research was to characterize the voltage sensing mechanism of a novel protein c15orf27. This putative uncharacterized protein shows strong sequence homology to the voltage sensing domains of voltage-gated cation channels and voltage-sensing phosphatases (CiVSP, TPTE and TPTE2). c15of27 is most closely related to Hv1. Unlike Hv1, c15of27 contains a 353 amino acid C-terminal domain with unknown function and limited homology to known and predicted proteins. Expression of the human c15of27 fused to EGFP tag shows high expression in HEK293 cells but voltage clamp experiments result in no detectable voltage gated ionic currents in varying temperature and pH gradients. Because c15of27 does not show unambiguous ionic currents or gating currents, we predict that the voltage sensing function is strongly coupled to its C-terminal domain. There is no published data for voltage gating in c15orf27 protein; however, a study conducted in the DeCoursey lab possibly explains the lack of current expression in c15orf27[167]. Substitutions based on sequence positions that differ between hHv1 and c15orf27 were predicted to be structurally tolerated in Hv1 and could be used to assay for residues responsible for proton conduction. An interesting and notable finding from study was that a D112V substitution in Hv1, which was based on V111 in c15orf27, abolished G_{AQ} mediated current and this is consistent with R205-D112V and R208H c15orf27 results in our research.

6. Analysis of G_{SH} to define voltage dependence

We employed multiple analytical approaches to derive G_{SH} gating parameters. One approach to estimate the voltage dependence of G_{SH} gating is to fit the G_{STEP}-V relation to a Boltzmann function. Boltzmann fitting requires two assumptions: 1. there are two and only two states, closed (C) and open (O); 2. gating is measured at equilibrium. If $G = N \cdot \gamma \cdot P_{OPEN,}$ where N is the number of channels, γ is the unitary conductance and P_{OPEN} is the open probability[35,92,96,169,186]. Assuming that both N and γ are fixed under the experimental conditions used to measure G_{STEP}, then the G-V relation will mirror the P_{OPEN}-V relation. G_{AQ} gating conforms to both of the underlying assumptions[156,186,187]. G_{SH} gating appears to be more complicated than G_{AQ} gating because the G_{STEP}-V relation does not saturate over the range of voltages that are readily amenable to whole-cell voltage clamp recording (+200 to -200 mV).

A non-saturating G_{STEP}-V relation for G_{SH}, such as that which we measure for Hv1 R205H or that seen in the Starace et al. (2004) report[122] for Shaker R362H, indicates that either: a) more than two transitions contribute to the measured change in G_{STEP}; b) N is not constant; or c) γ is not constant ;however, a-c are not mutually exclusive. We expect that N is constant in our R205H experiments and this is evidenced from measurements of the macroscopic G_{AQ}. We were unable to determine whether γ is constant from variance analysis (data not shown). Variance analysis for G_{SH} in Shaker R362H[122] suggests that it is channel-like, so it seems reasonable to assume that G_{SH} is constant in Hv1 R205H as well. Thus, the G_{STEP}-V may represent a composite response of several gating steps, the voltage dependencies of which can be estimated by fitting G_{STEP}-V to the sum of >1 Boltzmann functions (see Equations) [121–123,156]. We predicted that the shape of G_{SH}-V reflects the contributions of at least two distinct voltage-dependent gating steps, and could therefore be fit to the sum of two Boltzmann distributions in order to estimate gating parameters for each gating component[35,92,96,169,186]. This method and the interpretation of Starace et al. (2004) is not strongly convincing because G_{STEP} at the most negative potentials does not appear to follow a sigmoid Boltzmann distribution and thus prediction of midpoints and $G_{STEP\text{-}MAX}$ are subject to arbitrary values of fit parameters.

The V_{PEAK} analysis using Gaussian fits to dG_{STEP}/dV-V relations, was an additional method for interpreting data because, 1st derivative calculations demonstrate how the slope of a voltage-dependent process changes in function of membrane potential. The first derivative of a conductance that obeys Boltzmann-type gating exhibits a clear peak at the midpoint ($V_{0.5}$) of the Boltzmann distribution, suggesting that the location of such a peak can be used to determine the approximate midpoint of the P_{OPEN}–V relation even when G_{STEP} near the maximal P_{OPEN} is not experimentally measurable. V_{PEAK} determined from Gaussian fits to dG_{STEP}/dV-V exhibit a ~40mV shift in function of pH_O. Likewise, the falling phase of the dG_{STEP}/dV relation (i.e., at voltages that are positive to the peak potential), can be fit to a sigmoid function to estimate the voltage at which 50% of the peak amplitude is reached. $V_{0.5\text{-}PEAK}$ analysis using Boltzmann fits to the falling phase of dG_{STEP}/dV-V, estimate a slope and $V_{0.5\text{-}PEAK}$ that also exhibit a ~40mV shift in function of pH_O.

7. Simplest model to explain our data for voltage and pH dependent gating transitions in Hv1

The results presented here for R205H mutants directly demonstrate for the first time that voltage sensing and H^+ channel opening are separable processes in Hv1. Hv1 channel gating cannot therefore be described by a simple closed (C) to open (O) transition. The simplest model that can explain our data has 3 states: a resting (R) conformation in which the H^+ shuttle current in R205H flows, an intermediate activated (A) conformation, and an open (O) conformation in which the intrinsic aqueous H^+ current flows (Fig 30) The transitions between these states have different voltage and ΔpH sensitivities. The lack of a direct method to assay early steps in the Hv1 activation pathway has represented a major obstacle to understanding the mechanisms of VS activation and pH sensitive gating in Hv1. The data are consistent with a model in which VS activation represents an early voltage-dependent step and channel opening is a late event in the activation pathway and both are equally modulated by changes in ΔpH. The constant for early, pre-open transitions (α' and β') are pH and voltage dependent, whereas the constant for open state transition (α and β) is thought to also be pH dependent only. We interpret our findings to mean that a pH sensitive step must occur early in the activation of Hv1, and later state transitions to the open state have inherited pH sensitivity from the early step.

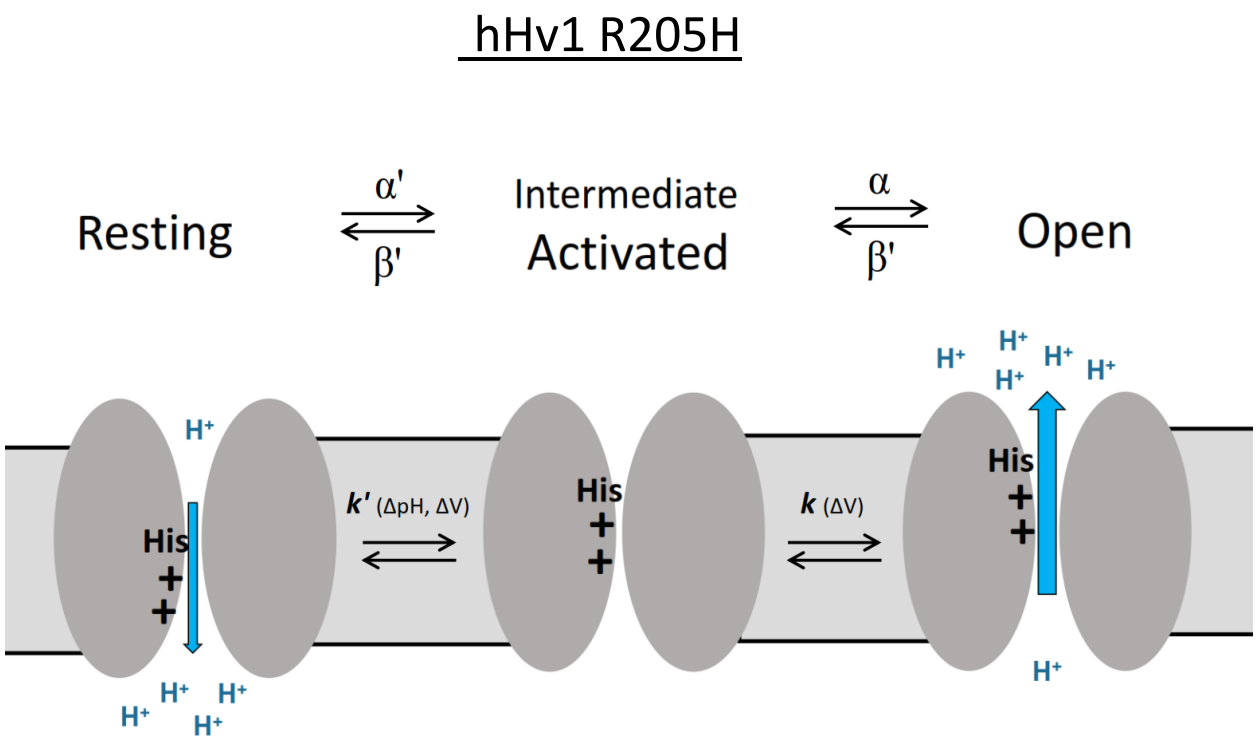

Figure 30. Cartoon of Hv1 gating mechanism
Model depicts two separate H^+ transport pathways in R205H and voltage sensor movement of the His at R1 (**His**) and the R2, R3 Arg charges (**+**). (*Left*) Histidine mediated H^+ 'shuttle' pathway is open in the Resting-state. (*Center*) The 'shuttle' H^+ pathway is closed and the 'aqueous' H^+ pathway is not open in the Activated-state. (*Right*) The 'aqueous' H^+ pathway is open in the Open-state. The transition from Resting to Activated (R ↔ A) is both pH_O- and voltage-dependent, described by rate constant *(k)*. The transition from Activated to Open states (A↔ O) is only voltage-dependent and is described by rate constant *(k')*.

8. Conclusions

Voltage sensing in Hv1 occurs prior to the opening of the intrinsic H^+ aqueous permeation pathway during Hv1 activation. R205H exhibits double-rectifying I_{STEP}-V and U-shaped G_{STEP}-V relations over a wide range of potentials. The resting-state H^+ 'shuttle' conductance (G_{SH}) flows at negative (<-50 mV) membrane potentials where the intrinsic aqueous H^+ conductance (G_{AQ}) remains closed. G_{SH} in Hv1 R205H is reminiscent of Shaker R362H, where the position of the G_{SH}-V relation was previously shown to be well-correlated with the Q-V relation determined from gating current measurements[106,121–123,156]. The G_{SH}-V relation for I_{SH} in Hv1 R205H is therefore likely to represent a 'pseudo Q-V' curve that reports voltage-sensing transitions in the voltage-gated H^+ channel Hv1. Voltage sensing and H^+ channel opening are distinct and separable processes in Hv1. The G_{SH}-V and G_{AQ}-V relations in Hv1 R205H are separated on the voltage axis by a distinct minimum conductance plateau. The width of this plateau is exacerbated by mutations (i.e., D185A) that cause marked rightward shifts in the G_{AQ}-V relation without substantially affecting the G_{SH}-V relation. The midpoints of the G_{SH}-V and G_{AQ}-V relations in Hv1 are thus separated by ~100 mV (R205H) or more (R205H-D185H). Separation of the Q-V and G_{AQ}-V relations in Hv1 is reminiscent of 6-TM voltage-gated cation channels, indicating that Hv1 channels exhibits electromechanical coupling despite lacking a pore domain. The effects of truncating the C-terminal coiled-coil dimerization motif on Hv1 GSH relative to GAQ are evidently minimal. Current measured from cells expressing R205H-ΔC, suggest that VS activation, as reported by G_{SH}, precedes opening of the aqueous H^+ conductance, just as in the dimer, and that cooperative inter-subunit interactions in dimeric channel proteins are not required for early voltage and pH dependent activation steps.

Hv1 voltage sensor activation (G_{SH}) and opening of the aqueous H^+ conducting pathway (G_{AQ}) are equally sensitive to changes in ΔpH. Whereas the G_{AQ}-V relation shifts ~40mV when ΔpH is changed by 1 unit, G_{SH}-V changes equally (~40 mV/pH unit). Voltage sensor activation is therefore equally sensitive to changes in ΔpH as is H^+ channel opening. Here we conclude that the Hv1 gating pathway must contain at least two transitions with distinct dependencies on changes in membrane potential and ΔpH. The data shown here, demonstrates for the first time that voltage sensor activation and opening of the aqueous H^+ selective conducting pathway, are separable processes in Hv1. Furthermore, the ΔpH-dependent steps in Hv1 gating occur early in the activation pathway. Hv1 channel gating cannot therefore be described by a simple closed (C) to open (O) transition. The simplest model that can explain our data has 3 states: a resting (R) conformation in which the H^+ shuttle current in R205H flows, an intermediate activated (A) conformation, and an open (O) conformation in which the intrinsic aqueous H^+ current flows.

REFERENCES

1. Meech R. A contribution to the history of the proton channel. *Wiley Interdiscip Rev Membr Transp Signal*. 2012;1(5):533–557.

2. Doroshenko PA, Kostiuk PG, Tsyndrenko AI. *Neiřofiziologiia = Neurophysiol*. Separation of potassium and calcium channels in the nerve cell soma membrane. 1978;10(6):645–53.

3. Thomas RC, Meech RW. Hydrogen ion currents and intracellular pH in depolarized voltage-clamped snail neurones. *Nature*. 1982;299(5886):826–828.

4. Barish ME, Baud C. A voltage-gated hydrogen ion current in the oocyte membrane of the axolotl, Ambystoma. *J Physiol*. 1984;352:243–262.

5. Bezanilla F, Perozo E, Stefani E. Gating of Shaker K+ channels: II. The components of gating currents and a model of channel activation. *Biophys J*. 1994;66(4):1011–1021.

6. Hodgkin AL, Huxley AF. A quantitative description of membrane current and its application to conduction and excitation in nerve. *J Physiol*. 1952;117(4):500–44.

7. Henderson LM, Chappell JB, Jones OT. The superoxide-generating NADPH oxidase of human neutrophils is electrogenic and associated with an H^+ channel. *Biochem J*. 1987;246(2):325–9.

8. DeCoursey TE. Hydrogen ion currents in rat alveolar epithelial cells. *Biophys J*. 1991;60(5):1243–1253.

9. DeCoursey TE. Voltage-gated proton channels. *Compr Physiol*. 2012;2(2):1355–85.

10. DeCoursey TE. Voltage-gated proton channels and other proton transfer pathways. *Physiol Rev*. 2003;83(2):475–579.

11. DeCoursey TE, Cherny V V. Potential, pH, and arachidonate gate hydrogen ion currents in human neutrophils. *Biophys J*. 1993;65(4):1590–8.

12. Gordienko D V, Tare M, Parveen S, Fenech CJ, Robinson C, Bolton TB. Voltage-activated proton current in eosinophils from human blood. *J Physiol*. 1996;496 Pt 2:299–316.

13. Musset B, Morgan D, Cherny V V, et al. A pH-stabilizing role of voltage-gated proton channels in IgE-mediated activation of human basophils. *Proc Natl Acad Sci U S A*. 2008;105(31):11020–5.

14. Kapus A, Romanek R, Qu AY, Rotstein OD, Grinstein S. A pH-sensitive and voltage-dependent proton conductance in the plasma membrane of macrophages. *J Gen Physiol*. 1993;102(4):729–60.

15. Eder C, DeCoursey TE. Voltage-gated proton channels in microglia. *Prog Neurobiol*. 2001;64(3):277–305.

16. Schilling T, Gratopp A, DeCoursey TE, Eder C. Voltage-activated proton currents in human lymphocytes. *J Physiol*. 2002;545(Pt 1):93–105.

17. Bernheim L, Krause RM, Baroffio A, Hamann M, Kaelin A, Bader CR. A voltage-dependent proton current in cultured human skeletal muscle myotubes. *J Physiol*. 1993;470:313–33.

18. Nordström T, Rotstein OD, Romanek R, et al. Regulation of cytoplasmic pH in osteoclasts. Contribution of proton pumps and a proton-selective conductance. *J Biol Chem*. 1995;270(5):2203–12.

19. Gu X, Sackin H. Effect of pH on potassium and proton conductance in renal proximal tubule. *Am J Physiol*. 1995;269(3 Pt 2):F289–308.

20. Ramsey IS, Moran MM, Chong JA, Clapham DE. A voltage-gated proton-selective channel lacking the pore domain. *Nature*. 2006;440(7088):1213–1216.

21. Sasaki M, Takagi M, Okamura Y. A voltage sensor-domain protein is a voltage-gated proton channel. *Science*. 2006;312(5773):589–92.

22. Musset B, DeCoursey T. Biophysical properties of the voltage gated proton channel H(V)1. *Wiley Interdiscip Rev Membr Transp Signal*. 2012;1(5):605–620.

23. Musset B, Cherny V V, Morgan D, et al. Detailed comparison of expressed and native voltage-gated proton channel currents. *J Physiol*. 2008;586(10):2477–86.

24. Cherny V V, Markin VS, DeCoursey TE. The voltage-activated hydrogen ion conductance in rat alveolar epithelial cells is determined by the pH gradient. *J Gen Physiol*. 1995;105(6):861–96.

25. DeCoursey TE, Cherny V V. Effects of buffer concentration on voltage-gated H+ currents: does diffusion limit the conductance? *Biophys J*. 1996;71(1):182–93.

26. DeCoursey TE, Cherny V V. Voltage-activated proton currents in membrane patches of rat alveolar epithelial cells. *J Physiol*. 1995;489 (pt 2):299–307.

27. Musset B, DeCoursey T. Biophysical properties of the voltage gated proton channel H(V)1. *Wiley Interdiscip Rev Membr Transp Signal*. 2012;1(5):605–620.

28. Musset B, Cherny V V, Morgan D, DeCoursey TE. The intimate and mysterious relationship between proton channels and NADPH oxidase. *FEBS Lett*. 2009;583(1):7–12.

29. DeCoursey TE. Voltage-gated proton channels. *Cell Mol Life Sci*. 2008;65(16):2554–73.

30. Cherny V V, Murphy R, Sokolov V, Levis RA, DeCoursey TE. Properties of single voltage-gated proton channels in human eosinophils estimated by noise analysis and by direct measurement. *J Gen Physiol*. 2003;121(6):615–28.

31. DeCoursey TE, Cherny V V. Potential, pH, and arachidonate gate hydrogen ion currents in human neutrophils. *Biophys J*. 1993;65(4):1590–8.

32. Cherny V V, DeCoursey TE. pH-dependent inhibition of voltage-gated H(+) currents in rat alveolar epithelial cells by Zn(2+) and other divalent cations. *J Gen Physiol*. 1999;114(6):819–38.

33. Demaurex N, Grinstein S, Jaconi M. Proton currents in human granulocytes: regulation by membrane potential and intracellular pH. *J*. 1993;466:329–344.

34. Mahaut-Smith MP. Separation of hydrogen ion currents in intact molluscan neurones. *J Exp Biol*. 1989;145:439–54.

35. Hille B. *Ionic Channels of Excitable Membranes*. Sinauer Associates, Incorporated; 2001:814.

36. Luecke H, Schobert B, Richter HT, Cartailler JP. Structural changes in bacteriorhodopsin during ion transport at 2 angstrom resolution. *Science (80-)*. 1999;286(5438):255–261.

37. Buch-Pedersen MJ, Pedersen BP, Veierskov B, Nissen P, Palmgren MG. Protons and how they are transported by proton pumps. *Pflugers Arch*. 2009;457(3):573–9.

38. Hu F, Schmidt-Rohr K, Hong M. NMR Detection of pH-Dependent Histidine–Water Proton Exchange Reveals the Conduction Mechanism of a Transmembrane Proton Channel. *J Am*. 2011;134(8):3703–3713.

39. Leiding T, Wang J, Martinsson J, DeGrado WF, Arsköld SP. Proton and cation transport activity of the M2 proton channel from influenza A virus. *Proc Natl Acad Sci U S A*. 2010;107(35):15409–14.

40. DeCoursey TE, Cherny V V. Voltage-activated hydrogen ion currents. *J Membr Biol*. 1994;141(3):203–23.

41. COLE KS, MOORE JW. Potassium ion current in the squid giant axon: dynamic characteristic. *Biophys J*. 1960;1:1–14.

42. Henderson LM, Chappell JB, Jones OT. Superoxide generation by the electrogenic NADPH oxidase of human neutrophils is limited by the movement of a compensating charge. *Biochem J*. 1988;255(1):285–90.

43. Henderson LM, Chappell JB, Jones OT. Internal pH changes associated with the activity of NADPH oxidase of human neutrophils. Further evidence for the presence of an H+ conducting channel. *Biochem J*. 1988;251(2):563–7.

44. DeCoursey TE. Voltage-gated proton channels find their dream job managing the respiratory burst in phagocytes. *Physiology (Bethesda)*. 2010;25(1):27–40.

45. Ramsey IS, Ruchti E, Kaczmarek JS, Clapham DE. Hv1 proton channels are required for high-level NADPH oxidase-dependent superoxide production during the phagocyte respiratory burst. *Proc Natl Acad Sci U S A*. 2009;106(18):7642–7647.

46. Cherny V V, Henderson LM, Xu W, Thomas LL, DeCoursey TE. Activation of NADPH oxidase-related proton and electron currents in human eosinophils by arachidonic acid. *J Physiol*. 2001;535(Pt 3):783–94.

47. DeCoursey TE, Cherny V V. Pharmacology of voltage-gated proton channels. *Curr Pharm Des*. 2007;13(23):2400–20.

48. DeCoursey TE, Cherny V V. Pharmacology of voltage-gated proton channels. *Curr Pharm Des*. 2007;13(23):2400–20.

49. DeCoursey TE. Voltage-gated proton channels: molecular biology, physiology, and pathophysiology of the H(V) family. *Physiol Rev*. 2013;93(2):599–652.

50. Rada BK, Geiszt M, Káldi K, Timár C, Ligeti E. Dual role of phagocytic NADPH oxidase in bacterial killing. *Blood*. 2004;104(9):2947–53.

51. Clark RA, Leidal KG, Pearson DW, Nauseef WM. NADPH oxidase of human neutrophils. Subcellular localization and characterization of an arachidonate-activatable superoxide-generating system. *J Biol Chem*. 1987;262(9):4065–74.

52. Bánfi B, Schrenzel J, Nüsse O, et al. A novel H(+) conductance in eosinophils: unique characteristics and absence in chronic granulomatous disease. *J Exp Med*. 1999;190(2):183–94.

53. DeCoursey TE, Morgan D, Cherny V V. The voltage dependence of NADPH oxidase reveals why phagocytes need proton channels. *Nature*. 2003;422(6931):531–4.

54. Cherny V V, Henderson LM, Xu W, Thomas LL, DeCoursey TE. Activation of NADPH oxidase-related proton and electron currents in human eosinophils by arachidonic acid. *J Physiol*. 2001;535(Pt 3):783–94.

55. Murphy R, DeCoursey TE. Charge compensation during the phagocyte respiratory burst. *Biochim Biophys Acta*. 2006;1757(8):996–1011.

56. Femling JK, Cherny V V, Morgan D, et al. The antibacterial activity of human neutrophils and eosinophils requires proton channels but not BK channels. *J Gen Physiol*. 2006;127(6):659–72.

57. DeCoursey TE, Cherny V V, DeCoursey AG, Xu W, Thomas LL. Interactions between NADPH oxidase-related proton and electron currents in human eosinophils. *J Physiol*. 2001;535(Pt 3):767–81.

58. Wu L-J, Wu G, Akhavan Sharif MR, et al. The voltage-gated proton channel Hv1 enhances brain damage from ischemic stroke. *Nat Neurosci*. 2012;15(4):565–73.

59. Zhu X, Mose E, Zimmermann N. Proton channel HVCN1 is required for effector functions of mouse eosinophils. *BMC Immunol*. 2013;14:1–24.

60. Capasso M, Bhamrah MK, Henley T, et al. HVCN1 modulates BCR signal strength via regulation of BCR-dependent generation of reactive oxygen species. *Nat Immunol*. 2010;11(3):265–272.

61. Reth M, Dick TP. Voltage control for B cell activation. *Nat Immunol*. 2010;11(3):191–192.

62. Fischer H. Mechanisms and function of DUOX in epithelia of the lung. *Antioxid Redox Signal*. 2009;11(10):2453–2465.

63. Schwarzer C, Machen TE, Illek B, Fischer H. NADPH oxidase-dependent acid production in airway epithelial cells. *J Biol Chem*. 2004;279(35):36454–61.

64. Fischer H. Function of proton channels in lung epithelia. *Wiley Interdiscip Rev Membr*. 2012;1(3):247–258.

65. Iovannisci D, Illek B, Fischer H. Function of the HVCN1 proton channel in airway epithelia and a naturally occurring mutation, M91T. *J Gen Physiol*. 2010;136(1):35–46.

66. Iovannisci D, Illek B, Fischer H. Function of the HVCN1 proton channel in airway epithelia and a naturally occurring mutation, M91T. *J Gen Physiol*. 2010;136(1):35–46.

67. Lishko P V., Botchkina IL, Fedorenko A, Kirichok Y. Acid Extrusion from Human Spermatozoa Is Mediated by Flagellar Voltage-Gated Proton Channel. *Cell*. 2010;140(3):327–337.

68. Lishko P V, Kirichok Y. The role of Hv1 and CatSper channels in sperm activation. *J Physiol*. 2010;588(Pt 23):4667–72.

69. Saaranen M, Suistomaa U, Kantola M, Saarikoski S, Vanha-Perttula T. Lead, magnesium, selenium and zinc in human seminal fluid: comparison with semen parameters and fertility. *Hum Reprod*. 1987;2(6):475–9.

70. Taylor AR, Brownlee C, Wheeler GL. Proton channels in algae: reasons to be excited. *Trends Plant Sci*. 2012;17(11):675–684.

71. Taylor AR, Chrachri A, Wheeler G, Goddard H. A voltage-gated H+ channel underlying pH homeostasis in calcifying coccolithophores. *PLoS Biol*. 2011;9(6):1–14.

72. Smith SME, Morgan D, Musset B. Voltage-gated proton channel in a dinoflagellate. *Proc*. 2011;108(44):18162–18167.

73. Yarov-Yarovoy V, DeCaen PG, Westenbroek RE, et al. Structural basis for gating charge movement in the voltage sensor of a sodium channel. *Proc Natl Acad Sci U S A*. 2012;109(2):E93–102.

74. Zhang X, Ren W, DeCaen P, et al. Crystal structure of an orthologue of the NaChBac voltage-gated sodium channel. *Nature*. 2012;486(7401):130–4.

75. Long SB, Campbell EB, MacKinnon R. Crystal structure of a mammalian voltage-dependent Shaker family K+ channel. *Science*. 2005;309(5736):897–903.

76. Long SB, Tao X, Campbell EB, MacKinnon R. Atomic structure of a voltage-dependent K+ channel in a lipid membrane-like environment. *Nature*. 2007;450(7168):376–382.

77. Long SB, Campbell EB, MacKinnon R. Voltage sensor of Kv1. 2: structural basis of electromechanical coupling. *Science*. 2005;309(5736):903–908.

78. Villalba-Galea CA. New insights in the activity of voltage sensitive phosphatases. *Cell Signal*. 2012;24(8):1541–1547.

79. Yu FH, Catterall WA. The VGL-chanome: a protein superfamily specialized for electrical signaling and ionic homeostasis. *Sci STKE*. 2004(253):1-17.

80. Bezanilla F. Voltage-Gated Ion Channels. *IEEE Trans Nanobioscience*. 2005;4(1):34–48.

81. Chanda B, Bezanilla F. A Common Pathway for Charge Transport through Voltage-Sensing Domains. *Neuron*. 2008;57(3):345–351.

82. Catterall WA. Ion channel voltage sensors: structure, function, and pathophysiology. *Neuron*. 2010;67(6):915–28.

83. Jiang Y, Lee A, Chen J, et al. X-ray structure of a voltage-dependent K+ channel. *Nature*. 2003;423(6935):33–41.

84. Villalba-Galea CA, Miceli F, Taglialatela M, Bezanilla F. Coupling between the voltage-sensing and phosphatase domains of Ci-VSP. *J Gen Physiol*. 2009;134(1):5–14.

85. Murata Y, Iwasaki H, Sasaki M, Inaba K, Okamura Y. Phosphoinositide phosphatase activity coupled to an intrinsic voltage sensor. *Nature*. 2005;435(7046):1239–43.

86. Sutton KA, Jungnickel MK, Jovine L, Florman HM. Evolution of the voltage sensor domain of the voltage-sensitive phosphoinositide phosphatase VSP/TPTE suggests a role as a proton channel in eutherian mammals. *Mol Biol Evol*. 2012;29(9):2147–55.

87. Iwasaki H, Murata Y, Kim Y, et al. A voltage-sensing phosphatase, Ci-VSP, which shares sequence identity with PTEN, dephosphorylates phosphatidylinositol 4,5-bisphosphate. *Proc Natl Acad Sci U S A*. 2008;105(23):7970–5.

88. Sakata S, Hossain MI, Okamura Y. Coupling of the phosphatase activity of Ci-VSP to its voltage sensor activity over the entire range of voltage sensitivity. *J Physiol*. 2011;589(Pt 11):2687–705.

89. Catterall WA. Molecular properties of voltage-sensitive sodium channels. *Annu Rev Biochem*. 1986;55:953–85.

90. Guy HR, Seetharamulu P. Molecular model of the action potential sodium channel. *Proc Natl Acad Sci U S A*. 1986;83(2):508–12.

91. Bezanilla F. How membrane proteins sense voltage. *Nat Rev Mol Cell Biol*. 2008;9(4):323–32.

92. Seoh SA, Sigg D, Papazian DM, Bezanilla F. Voltage-sensing residues in the S2 and S4 segments of the Shaker K+ channel. *Neuron*. 1996;16(6):1159–67.

93. Seoh SA, Sigg D, Papazian DM, Bezanilla F. Voltage-sensing residues in the S2 and S4 segments of the Shaker K+ channel. *Neuron*. 1996;16(6):1159–67.

94. Ramsey IS, Mokrab Y, Carvacho I, Sands ZA. An aqueous H+ permeation pathway in the voltage-gated proton channel Hv1. *Nat Struct*. 2010;17(7):869–875.

95. Seoh SA, Sigg D, Papazian DM, Bezanilla F. Voltage-sensing residues in the S2 and S4 segments of the Shaker K+ channel. *Neuron*. 1996;16(6):1159–67.

96. Aggarwal SK, MacKinnon R. Contribution of the S4 Segment to Gating Charge in the Shaker K+ Channel. *Neuron*. 1996;16(6):1169–1177.

97. Zagotta W, Hoshi T, Dittman J, Aldrich R. Shaker potassium channel gating. II: Transitions in the activation pathway. *J Gen Physiol*. 1994;103(2):279–319.

98. Liman ER, Hess P, Weaver F, Koren G. Voltage-sensing residues in the S4 region of a mammalian K+ channel. *Nature*. 1991;353(6346):752–6.

99. Pay J, Payandeh J, eh, Scheuer T, Zheng N, Catterall WA. The crystal structure of a voltage-gated sodium channel. *Nature*. 2011;475(7356):353–358.

100. Carlos A Villalba-Galea, Ludivine Frezza, Walter Sandtner FB. Sensing charges of the Ciona intestinalis voltage-sensing phosphatase. *J Gen*. 2013;142(5):543–55.

101. Ma Z, Lou XJ, Horrigan FT. Role of charged residues in the S1-S4 voltage sensor of BK channels. *J Gen Physiol*. 2006;127(3):309–28.

102. Paldi T. Deprotonation of Arginines in S4 is Involved in NaChBac Gating. *J Membr Biol*. 2012;245(11):761–771.

103. Tombola F, Pathak MM, Isacoff EY. Voltage-sensing arginines in a potassium channel permeate and occlude cation-selective pores. *Neuron*. 2005;45(3):379–388.

104. Blanchet J, Pilote S, Chahine M. Acidic residues on the voltage-sensor domain determine the activation of the NaChBac sodium channel. *Biophys J*. 2007;92(10):3513–23.

105. Shi YP, Cheng YM, Van Slyke AC, Claydon TW. External protons destabilize the activated voltage sensor in hERG channels. *Eur Biophys J*. 2013.

106. Campos F V, Chanda B, Roux B. Two atomic constraints unambiguously position the S4 segment relative to S1 and S2 segments in the closed state of Shaker K channel. *Proc*. 2007;104(19):7904–7909.

107. Tao X, Lee A, Limapichat W, Dougherty. A gating charge transfer center in voltage sensors. *Science (80-)*. 2010;328(5974):67–73.

108. Skerritt MR, Campbell DL. KV4.3 expression and gating: S2 and S3 acidic and S4 innermost basic residues. *Channels (Austin)*. 2009;3(6):413–26.

109. Pless SA, Galpin JD, Niciforovic AP, Ahern CA. Contributions of counter-charge in a potassium channel voltage-sensor domain. *Nat Chem Biol*. 2011;7(9):617–23.

110. Jiang Y, Ruta V, Chen J, Lee A, MacKinnon R. The principle of gating charge movement in a voltage-dependent K+ channel. *Nature*. 2003;423(6935):42–8.

111. Chanda B, Asamoah O, Blunck R, Roux B, Bezanilla F. Gating charge displacement in voltage-gated ion channels involves limited transmembrane movement. *Nature*. 2005;436(7052):852–856.

112. Villalba-Galea CA, Sandtner W, Starace DM, Bezanilla F. S4-based voltage sensors have three major conformations. *Proc Natl Acad Sci U S A*. 2008;105(46):17600–7.

113. Logothetis DE, Movahedi S, Satler C, Lindpaintner K, Nadal-Ginard B. Incremental reductions of positive charge within the S4 region of a voltage-gated K+ channel result in corresponding decreases in gating charge. *Neuron*. 1992;8(3):531–40.

114. Papazian DM, Timpe LC, Jan YN, Jan LY. Alteration of voltage-dependence of Shaker potassium channel by mutations in the S4 sequence. *Nature*. 1991;349(6307):305–10.

115. Stühmer W, Conti F, Suzuki H, et al. Structural parts involved in activation and inactivation of the sodium channel. *Nature*. 1989;339(6226):597–603.

116. Gonzalez C, Rebolledo S, Perez ME, Larsson HP. Molecular mechanism of voltage sensing in voltage-gated proton channels. *J Gen Physiol*. 2013;141(3):275–85.

117. Tombola F, Ulbrich MH, Isacoff EY. Architecture and gating of Hv1 proton channels. *J Physiol*. 2009;587(Pt 22):5325–9.

118. Chamberlin A, Qiu F, Rebolledo S, Wang Y, Noskov SY, Larsson HP. Hydrophobic plug functions as a gate in voltage-gated proton channels. *Proc Natl Acad Sci U S A*. 2013;111(2):E273–82.

119. Yang N, Horn R. Evidence for voltage-dependent S4 movement in sodium channels. *Neuron*. 1995;15(1):213–8.

120. Yang N, George AL, Horn R. Molecular Basis of Charge Movement in Voltage-Gated Sodium Channels. *Neuron*. 1996;16(1):113–122.

121. Starace DM, Bezanilla F. Histidine scanning mutagenesis of basic residues of the S4 segment of the Shaker K+ channel. *J Gen Physiol*. 2001;117(5):469–490.

122. Starace DM, Bezanilla F. A proton pore in a potassium channel voltage sensor reveals a focused electric field. *Nature*. 2004;427(6974):548–553.

123. Starace DM, Stefani E, Bezanilla F. Voltage-dependent proton transport by the voltage sensor of the Shaker K+ channel. *Neuron*. 1997;19(6):1319–27.

124. Schow E V, Freites JA, Gogna K, White SH, Tobias DJ. Down-State Model of the Voltage-Sensing Domain of a Potassium Channel. *Biophys J*. 2010;98(12):2857–2866.

125. Tombola F, Ulbrich MH, Isacoff EY. The voltage-gated proton channel Hv1 has two pores, each controlled by one voltage sensor. *Neuron*. 2008;58(4):546–56.

126. Kulleperuma K, Smith SME, Morgan D. Construction and validation of a homology model of the human voltage-gated proton channel hHV1. *J Gen*. 2013;141(4):445–65.

127. Schow E V, Freites JA, White SH, Tombola F, Wood ML, Tobias DJ. Water wires in atomistic models of the Hv1 proton channel. *Biochim Biophys Acta - Biomembr*. 2012;1818(2):286–293.

128. Pathak MM, Yarov-Yarovoy V, Agarwal G, et al. Closing in on the resting state of the Shaker K(+) channel. *Neuron*. 2007;56(1):124–40.

129. Tombola F, Pathak MM, Gorostiza P, Isacoff EY. The twisted ion-permeation pathway of a resting voltage-sensing domain. *Nature*. 2007;445(7127):546–9.

130. Gonzalez C, Koch HP, Drum BM. Strong cooperativity between subunits in voltage-gated proton channels. *Nat Struct*. 2009.

131. Koch HP, Kurokawa T, Okochi Y. Multimeric nature of voltage-gated proton channels. *Proc*. 2008;105(26):9111–9116.

132. Lee S-Y, Letts JA, MacKinnon R. Functional reconstitution of purified human Hv1 H+ channels. *J Mol Biol*. 2009;387(5):1055–60.

133. Musset B, Smith SME, Rajan S. Zinc inhibition of monomeric and dimeric proton channels suggests cooperative gating. *J*. 2010;588(Pt 9):1435–1449.

134. Musset B, Smith SME, Rajan S, Cherny V V. Oligomerization of the voltage gated proton channel. 2010;4(4):9–14.

135. Tombola F, Ulbrich MH, Isacoff EY. The voltage-gated proton channel Hv1 has two pores, each controlled by one voltage sensor. *Neuron*. 2008;58(4):546.

136. Tombola F, Ulbrich MH, Kohout SC, Y IE. The opening of the two pores of the Hv1 voltage-gated proton channel is tuned by cooperativity. *Nat Struct*. 2009;17(1):44–50.

137. Sakata S, Kurokawa T, Nørholm MHH. Functionality of the voltage-gated proton channel truncated in S4. *Proc*. 2010;107(5):2313–2318.

138. Li SJ, Zhao Q, Zhou Q, Unno H, Zhai Y, Sun F. The role and structure of the carboxyl-terminal domain of the human voltage-gated proton channel Hv1. *J Biol Chem*. 2010;285(16):12047–54.

139. Fujiwara Y, Kurokawa T, Takeshita K. The cytoplasmic coiled-coil mediates cooperative gating temperature sensitivity in the voltage-gated H+ channel Hv1. *Nat Commun*. 2012;3:816.

140. Lee S-Y, Letts JA, Mackinnon R. Dimeric subunit stoichiometry of the human voltage-dependent proton channel Hv1. *Proc Natl Acad Sci U S A*. 2008;105(22):7692–5.

141. Fujiwara Y, Kurokawa T, Takeshita K, Nakagawa A, Larsson HP, Okamura Y. Gating of the designed trimeric/tetrameric voltage-gated H+ channel. *J Physiol*. 2013;591(Pt 3):627–40.

142. Musset B, Capasso M, Cherny V V, et al. Identification of Thr29 as a critical phosphorylation site that activates the human proton channel Hvcn1 in leukocytes. *J Biol Chem*. 2010;285(8):5117–21.

143. Cukierman S. The transfer of protons in water wires inside proteins. *Front Biosci a J virtual Libr*. 2003;8:s1118–s1139.

144. Voth GA. The computer simulation of proton transport in biomolecular systems. *Front Biosci a J virtual Libr*. 2003;39(2):143–150.

145. Nagle JF, Morowitz HJ. Molecular mechanisms for proton transport in membranes. *Proc Natl*. 1978;75(1):298–302.

146. Swanson JMJ, Maupin CM, Chen H, et al. Proton solvation and transport in aqueous and biomolecular systems: insights from computer simulations. *J Phys Chem B*. 2007;111(17):4300–14.

147. DeCoursey TE, Cherny V V. Voltage-activated hydrogen ion currents. *J Membr Biol*. 2003;141(3):203–223.

148. Deamer DW. Proton permeation of lipid bilayers. *J Bioenerg Biomembr*. 1987;19(5):457–79.

149. Paula S, Volkov AG, Van Hoek AN, Haines TH, Deamer DW. Permeation of protons, potassium ions, and small polar molecules through phospholipid bilayers as a function of membrane thickness. *Biophys J*. 1996;70(1):339–48.

150. Deamer DW, Nichols JW. Proton flux mechanisms in model and biological membranes. *J Membr Biol*. 1989;107(2):91–103.

151. DeFelice LJ, Goswami T. Transporters as channels. *Annu Rev Physiol*. 2007;69:87–112.

152. Gadsby DC. Ion channels versus ion pumps: the principal difference, in principle. *Nat Rev Mol Cell Biol*. 2009;10(5):344–52.

153. Rakowski RF, Gadsby DC, De Weer P. Voltage dependence of the Na/K pump. *J Membr Biol*. 1997;155(2):105–12.

154. Gadsby DC. Steady-state current-voltage relationship of the Na/K pump in guinea pig ventricular myocytes. *J Gen Physiol*. 1989;94(3):511–537.

155. Grewer C, Gameiro A, Mager T, Fendler K. Electrophysiological characterization of membrane transport proteins. *Annu Rev Biophys*. 2013;42:95–120.

156. Bezanilla F. The voltage sensor in voltage-dependent ion channels. *Physiol Rev*. 2000;80(2):555–92.

157. Perozo E, MacKinnon R, Bezanilla F, Stefani E. Gating currents from a nonconducting mutant reveal open-closed conformations in Shaker K+ channels. *Neuron*. 1993;11(2):353–8.

158. Hoshi T, Zagotta WN, Aldrich RW. Biophysical and molecular mechanisms of Shaker potassium channel inactivation. *Science*. 1990;250(4980):533–8.

159. Nagle JF. Theory of passive proton conductance in lipid bilayers. *J Bioenerg Biomembr*. 1987;19(5):413–26.

160. Brewer ML, Schmitt UW, Voth GA. The formation and dynamics of proton wires in channel environments. *Biophys J*. 2001;80(4):1691–702.

161. Pomès R, Roux B. Structure and dynamics of a proton wire: a theoretical study of H+ translocation along the single-file water chain in the gramicidin A channel. *Biophys J*. 1996;71(1):19–39.

162. Eigen M. Proton Transfer, Acid-Base Catalysis, and Enzymatic Hydrolysis. Part I: ELEMENTARY PROCESSES. *Angew Chemie Int Ed English*. 1964;3(1):1–19.

163. Markovitch O, Chen H, Izvekov S, Paesani F, Voth GA, Agmon N. Special pair dance and partner selection: elementary steps in proton transport in liquid water. *J Phys Chem B*. 2008;112(31):9456–66.

164. Cukierman S. Proton mobilities in water and in different stereoisomers of covalently linked gramicidin A channels. *Biophys J*. 2000;78(4):1825–34.

165. Bernèche S, Roux B. A gate in the selectivity filter of potassium channels. *Structure*. 2005;13(4):591–600.

166. Berger TK, Isacoff EY. The pore of the voltage-gated proton channel. *Neuron*. 2011.

167. Musset B, Smith SME, Rajan S, Morgan D, Cherny V V, DeCoursey TE. Aspartate 112 is the selectivity filter of the human voltage-gated proton channel. *Nature*. 2011;480(7376):273–7.

168. Hong L, Pathak MM, Kim IH, Ta D, Tombola F. Voltage-Sensing Domain of Voltage-Gated Proton Channel Hv1 Shares Mechanism of Block with Pore Domains. *Neuron*. 2013;77(2):274–87.

169. White MM, Bezanilla F. Activation of squid axon K+ channels. Ionic and gating current studies. *J Gen Physiol*. 1985;85(4):539–54.

170. Sigg D, Bezanilla F. Total charge movement per channel. The relation between gating charge displacement and the voltage sensitivity of activation. *J Gen Physiol*. 1997;109(1):27–39.

171. Gandhi CS, Clark E, Loots E, Pralle A, Isacoff EY. The Orientation and Molecular Movement of a K+ Channel Voltage-Sensing Domain. *Neuron*. 2003;40(3):515–525.

172. Sokolov S, Scheuer T, Catterall WA. Gating pore current in an inherited ion channelopathy. *Nature*. 2007;446(7131):76–8.

173. Struyk AF, Markin VS, Francis D. Gating pore currents in DIIS4 mutations of NaV1. 4 associated with periodic paralysis: saturation of ion flux and implications for disease pathogenesis. *J Gen*. 2008;132(4):447–464.

174. Gosselin-Badaroudine P, Delemotte L, Moreau A, Klein M, Chahine M. Gating pore currents and the resting state of Nav1.4 voltage sensor domains. *Proc Natl Acad Sci*. 2012;109(47):19250–19255.

175. Jurkat-Rott K, Groome J, Lehmann-Horn F. Pathophysiological role of omega pore current in channelopathies. *Front Pharmacol*. 2012;3:112.

176. El-Din TMG, Heldstab H, Lehmann C, Greeff NG. Double gaps along Shaker S4 demonstrate omega currents at three different closed states. *Channels*. 2010;4(2):93–100.

177. Klassen T, Spencer A, Gallin W, systemadmin. A naturally occurring omega current in a Kv3 family potassium channel from a platyhelminth. *BMC Neurosci*. 2008;9(1):52.

178. Tarek M, Delemotte L. Omega currents in voltage-gated ion channels: what can we learn from uncovering the voltage-sensing mechanism using MD simulations? *Acc Chem Res*. 2013;46(12):2755–62.

179. Struyk AF, Cannon SC. A Na+ channel mutation linked to hypokalemic periodic paralysis exposes a proton-selective gating pore. *J Gen Physiol*. 2007;130(1):11–20.

180. Cannon SC. Voltage-sensor mutations in channelopathies of skeletal muscle. *J Physiol*. 2010;588(Pt.11):1887–1895.

181. Sokolov S, Scheuer T, Catterall WA. Ion permeation and block of the gating pore in the voltage sensor of NaV1. 4 channels with hypokalemic periodic paralysis mutations. *J Gen*. 2010;136(2):225–236.

182. Sokolov S, Scheuer T, Catterall WA. Ion permeation through a voltage-sensitive gating pore in brain sodium channels having voltage sensor mutations. *Neuron*. 2005;47(2):183–189.

183. Bezanilla F, Villalba-Galea CA. The gating charge should not be estimated by fitting a two-state model to a Q-V curve. *J Gen Physiol*. 2013;142(6):575–8.

184. Almers W. Gating currents and charge movements in excitable membranes. *Rev Physiol Biochem Pharmacol*. 1978;82:96–190.

185. Ramsey IS, Villalba-Galea CA. Voltage-Sensor Relaxation in Hv1 Proton Channels. *Biophys J*. 2011;100(3, Supplement 1):28a – 29a.

186. Hodgkin AL, Huxley AF. A quantitative description of membrane current and its application to conduction and excitation in nerve. *J Physiol*. 1952;117(4):500–44.

187. Alvarez O, Gonzalez C, Latorre R. Counting channels: a tutorial guide on ion channel fluctuation analysis. *Adv Physiol Educ*. 2002;26(1-4):327–41.

188. Armstrong CM, Bezanilla F. Inactivation of the sodium channel. II. Gating current experiments. *J Gen Physiol*. 1977;70(5):567–590.

189. Ledwell JL, Aldrich RW. Mutations in the S4 region isolate the final voltage-dependent cooperative step in potassium channel activation. *J Gen Physiol*. 1999;113(3):389–414.

190. DeCoursey TE, Cherny V V. Deuterium isotope effects on permeation and gating of proton channels in rat alveolar epithelium. *J Gen Physiol*. 1997;109(4):415–34.

191. Paldi T. Deprotonation of Arginines in S4 is Involved in NaChBac Gating. *J Membr Biol*. 2012;245(11):761–771.

192. Doering C, McRory J. Effects of extracellular pH on neuronal calcium channel activation. *Neuroscience*. 2007;146(3):1032–1043.

193. Zhou W, Jones SW. The effects of external pH on calcium channel currents in bullfrog sympathetic neurons. *Biophys J*. 1996;70(3):1326–34.

194. Prole D. Mechanisms Underlying Modulation of Neuronal KCNQ2/KCNQ3 Potassium Channels by Extracellular Protons. *J Gen Physiol*. 2003;122(6):775–793.

195. Zhang X. Slo3 K+ Channels: Voltage and pH Dependence of Macroscopic Currents. *J Gen Physiol*. 2006;128(3):317–336.

196. Schreiber M, Wei A, Yuan A, Gaut J, Saito M. Slo3, a Novel pH-sensitive K+ Channel from Mammalian Spermatocytes. *J Biol Chem*. 1998;273(6):3509–3516.

197. Armstrong CM, Cota G. Modification of sodium channel gating by lanthanum. Some effects that cannot be explained by surface charge theory. *J Gen Physiol*. 1990;96(6):1129–40.

198. Gilly WF, Armstrong CM. Divalent cations and the activation kinetics of potassium channels in squid giant axons. *J Gen Physiol*. 1982;79(6):965–96.

199. Qiu F, Rebolledo S, Gonzalez C, Larsson HP. Subunit Interactions during Cooperative Opening of Voltage-Gated Proton Channels. *Neuron*. 2013;77(2):288–98.

200. Ahern CA, Horn R. Focused electric field across the voltage sensor of potassium channels. *Neuron*. 2005;48(1):25–9.

201. Zagotta WN, Hoshi T, Aldrich RW. Shaker potassium channel gating. III: Evaluation of kinetic models for activation. *J Gen*. 1994;103(2):321–362.

202. Koren G, Liman ER, Logothetis DE, Nadal-Ginard B, Hess P. Gating mechanism of a cloned potassium channel expressed in frog oocytes and mammalian cells. *Neuron*. 1990;4(1):39–51.

203. Schoppa NE, Sigworth FJ. Activation of Shaker potassium channels I. Characterization of voltage-dependent transitions. *J Gen Physiol*. 1998;111(2):271–294.